NASA CONTRACTOR REPORT

NASA CR-959

NASA CR-959

EXPERIMENTAL INVESTIGATION OF TURBULENCE IN THE MIXING REGION BETWEEN COAXIAL STREAMS

by Thomas S. Zawacki and Herbert Weinstein

Prepared by
ILLINOIS INSTITUTE OF TECHNOLOGY
Chicago, Ill.
for Lewis Research Center

NATIONAL AERONAUTICS AND SPACE ADMINISTRATION • WASHINGTON, D. C. • FEBRUARY 1968

NASA CR-959

EXPERIMENTAL INVESTIGATION OF TURBULENCE IN THE MIXING REGION BETWEEN COAXIAL STREAMS

By Thomas S. Zawacki and Herbert Weinstein

Prepared under Grant No. NsG-694 by
ILLINOIS INSTITUTE OF TECHNOLOGY
Chicago, Ill.

for Lewis Research Center

NATIONAL AERONAUTICS AND SPACE ADMINISTRATION

For sale by the Clearinghouse for Federal Scientific and Technical Information
Springfield, Virginia 22151 – CFSTI price $3.00

FOREWORD

Research related to advanced nuclear rocket propulsion is described herein. This work was performed under NASA Grant NsG-694 with Mr. Maynard F. Taylor, Nuclear Systems Division, NASA Lewis Research Center as Technical Manager.

ABSTRACT

An experimental study is made of axially symmetric, turbulent, incompressible, co-flowing streams.

Hot wire anemometry techniques are used to make measurements in three systems, the homogeneous system with a resultant density ratio of 1, and two hetreogeneous systems, one with an inner to outer stream density ratio of 4 to 1, and another with an inner to outer stream density ratio of 7 to 1.

The outer stream velocity was varied from 12 to 50 ft/sec. and the inner stream was changed to provide outer stream to inner stream velocity ratios of from 1 to 40.

Data is presented for the relative axial turbulence intensity, the relative radial turbulence intensity, and the turbulent shear stress for various velocity ratios in the homogeneous system, in both the initial mixing region and the downstream or similar region. The maximum relative turbulence intensity found was 0.40.

For the 4 to 1 density case, data is presented for average velocity, the average density, and the relative velocity turbulence intensity for various velocity ratios in both the initial mixing region and the downstream or similar region. The maximum relative turbulence intensity found was 0.70.

Average density and velocity profiles are presented for the 7 to 1 density ratio in the near and downstream regions.

Comparisons are made regarding the effect of the initial velocity and density ratios.

TABLE OF CONTENTS

LIST OF ILLUSTRATIONS

LIST OF ILLUSTRATIONS cont.

NOMENCLATURE

a - Tollmien solution variable related to Prandtl's mixing length theory.

A - Intercept term for linear hot film relationship.

b - Width of mixing region for velocity.

B - Slope term for linear hot film relationship.

C - Prandtl's mixing length constant.

C_p - Heat capacity of the gas.

D - Diameter of the hot film.

k - Thermal conductivity of the gas.

l - Prandtl's mixing length .

Nu - Nusselt number.

Pe - Pressure.

P - Power dissapation from the hot film.

r_o - Radius of inner stream orifice.

$r_{u\,1/2}$ - Half-radius with respect to velocity.

$r_{\rho\,1/2}$ - Half-radius with respect to density.

Re - Reynolds number.

S - Sensitivity of hot film to density and velocity.

T_w - Temperature of the hot film.

T_g - Temperature of the gas.

U - Axial velocity components.

U_e - Effective cooling velocity for the hot film.

V - Radial velocity components.

X - Rectangular coordinate .

Y - Rectangular coordinate .

Z - Axial coordinate.

ε - Eddy kinematic viscosity.

γ - Conversion factor.

Λ - Reichardt's factor

T_o - Time interval for time averaging process.

T_{zr} - Laminar shearing stress, z, r, plane .

T^t_{zr} - Turbulent shearing stress, z, r plane .

μ - Molecular viscosity.

ρ - Density.

δ - Small increment in the density.

Superscripts

$\overline{}$ - Time average component.

' - Fluctuating component.

Subscripts

o - Free stream.

i - Initial inner stream valve.

$\mathcal{C}_L$ - Center line.

I INTRODUCTION

There are many physical applications that involve the mixing of coaxial turbulent streams of similar and dissimilar fluids. These applications include ejectors, afterburners, jet engine combustion chambers, and the more advanced concept of a gaseous core nuclear rocket. In relating the general set of equations for continuity, momentum, diffusion, and energy to any particular problem, many assumptions must be made regarding the nature of these flows in order to obtain a set of equations that are solvable.

Since Prandtl[1] first developed his mixing length theory, investigators such as Tollmien[7], Keuthe[13], and Squire and Trouncer[14], have provided theoretical solutions for the velocity profiles in a homogeneous system. These solutions were based on the assumption of a point source of the fluid or the assumption that the initial profile was flat. In both cases, these solutions did not adequately represent the velocity field in the initial mixing region.

Kabashi and Tani[16,17] have given experimental results for the velocity profiles and turbulence quantities far downstream of the initial mixing region, for a coaxial homogeneous system. Forstall and Shapiro,[18] and Boehman[30] made experimental studies of the coaxial system by injecting small amounts of an inert gas into the inner stream. Again they made measurements far downstream of the initial region. Alpinieri reported average concentration and velocity data for the coaxial system far downstream, where the inner stream was a different gas than the outer stream.

In view of the small amount of experimental data available, the purpose of this work is to make an experimental study of the mixing characteristics of a turbulent coaxial flow system.

The objectives of the work will be to obtain velocity and turbulence data in the near and far downstream regions of a homogeneous system and to obtain velocity, composition, and turbulence data in the near and far regions of a coaxial heterogeneous system, where in one case the inner stream to outer stream density ratio is 4 to 1. and another case where the inner stream to outer stream density ratio is 7 to 1.

II BACKGROUND

Turbulent flows are characterized by a random fluctuating flow superimposed on a time smoothed mean flow. The instantaneous velocity components, pressure and composition (for heterogeneous systems) can be expressed in terms of a time smoothed mean quantity and a fluctuating quantity in the following manner.

$$U = \overline{U} + u', \; V = \overline{V} + v', \; W = \overline{W} + w', \; \rho = \overline{\rho} + \rho',$$

$$P_e = \overline{P}_e + p'_e$$

The average term, denoted as the barred quantity is defined by taking a time average of the instantaneous component over a time interval T_o, large with respect to any slow variations or unsteady nature of the mean flow. Denoting Q as the generalized term of interest then,

$$\overline{Q} = \frac{1}{T_o} \int_t^{t+T_o} Q \, dt$$

From the definitions stated, the time average of the fluctuating term is zero.

$$\overline{Q'} = \frac{1}{T_o} \int_t^{t+T_o} Q' \, dt = 0$$

Many times the product of two terms appears in the equations that describe the fluid motion. Let the two terms be Q and R, with each containing a time smoothed term and a fluctuating term, $Q = \overline{Q} + Q'$ and $R = \overline{R} + R'$. Multiplying the two terms together the result becomes,

$$(\overline{Q} + Q')(\overline{R} + R') = \overline{Q}\,\overline{R} + \overline{R}\,Q' + \overline{Q}\,R' + Q'\,R'.$$

Applying the time averaging process to the equation it becomes (using a bar to

denote the time average).

$$\overline{(\bar{Q} + Q')(\bar{R} + R')} = \overline{\bar{Q}\bar{R} + \bar{R}Q' + \bar{Q}R' + Q'R'}.$$

By using the properties of the time averaging process, that $\overline{\bar{Q} + \bar{R}} = \bar{\bar{Q}} + \bar{\bar{R}} = \bar{Q} + \bar{R}$, and that the time average of the fluctuating terms are zero, the final equation for the product of two terms can be given as,

$$\overline{(\bar{Q} + Q')(\bar{R} + R')} = \bar{Q}\bar{R} + \overline{Q'R'}.$$

Even though the terms $\bar{Q}'$ and $\bar{R}'$ are equal to zero, in the general case $\overline{Q'R'}$ is not necessarily equal to zero. In fact, $\overline{Q'R'}$ is zero only if Q and R are linearly independent of each other.

With this brief description of the definition of the terms used in describing turbulent flows, these definitions can be applied to the equations of conservation of mass and momentum. It has been shown experimentally that in highly turbulent flows, the turbulent transport of heat, momentum, and matter is much greater than that of molecular transport. Previous investigators have tried to formulate concepts of the turbulent motion, and its contribution to the transport mechanism.

II - 1 Concepts

The simplified equation of motion for an axially symmetric, steady, isobaric, essentially parallel flow of a homogeneous fluid can be represented in the following form,

$$U \frac{\partial U}{\partial z} + V \frac{\partial U}{\partial r} = \frac{1}{r\rho} \frac{\partial r}{\partial r} T_{zr}$$

For the case of pure viscous laminar motion the shear stress $T_{zr} = \mu \left(\frac{\partial U}{\partial r}\right)_z$. T. V. Boussinesq[12] in 1877 was the first to work on the problem of the form of the shearing stress in turbulent flow. In analogy with the coefficient of viscosity for laminar flow he introduced a turbulent transport coefficient A_t. The turbulent

shearing stress was then given as the product of the so called apparent turbulent viscosity or eddy viscosity A_t, and the radial time smooth velocity gradient, $\tau^t_{zr} = A_t \left(\frac{\partial \overline{U}}{\partial r}\right)_z$. This turbulent viscosity is not a property of the fluid, as is the molecular viscosity, but instead is dependent upon local nature of the flow. In the same manner as the kinematic viscosity is defined for a fluid, an apparent or eddy kinematic viscosity can be defined for turbulent flow, $\varepsilon = \frac{At}{\rho}$. Using this definition the turbulent shearing stress in the $r - z$ plane becomes $\tau^t_{zr} = \rho \varepsilon \left(\frac{\partial \overline{U}}{\partial r}\right)_z$. The idea of the apparent or eddy viscosity was not readily usable since the relationship of the turbulent viscosity with the mean properties of the flow system was not known. Since the mechanism of turbulent transport was not well understood, emperical relationships had to be developed between the apparent or eddy kinematic viscosity ε and the flow field.

Four basic concepts of turbulent mixing which had been most widely used are Prandtls old mixing length theory[1], Prandtls new mixing length theory[3], Taylors hypothesis[2] and Reichardts theory of turbulence[4].

The equations of continuity and momentum for a homgeneous incompressible, axially symmetric system at steady state can be written,

$$\frac{\partial (Ur)}{\partial z} + \frac{\partial (Vr)}{\partial r} = 0 \quad \text{(continuity)}, \qquad \text{II - 1 - 1}$$

$$U \frac{\partial U}{\partial z} + V \frac{\partial U}{\partial r} = \frac{\kappa}{r \rho} \frac{\partial}{\partial r} \left(r \frac{\partial U}{\partial r}\right) \quad \text{(momentum)}. \qquad \text{II - 1 - 2}$$

Using the definitions previously stated that the velocity components are composed of a time mean average term and a fluctuating term the equations become,

$$\frac{\partial (\overline{U} + u')r}{\partial z} + \frac{\partial (\overline{V} + v')r}{\partial r} = 0 \qquad \text{II - 1 - 3}$$

$$(\bar{U}+u')\frac{\partial(\bar{U}+u')}{\partial z}+(\bar{V}+v')\frac{\partial(\bar{U}+u')}{\partial r}=\frac{\mu}{r\rho}\frac{\partial}{}(r\frac{\partial(\bar{U}+u')}{\partial r}) \qquad \text{II-1-4}$$

By expanding the equations, and using the time average procedure the following equations are obtained.

$$\frac{\partial(\bar{U}r)}{\partial z}+\frac{\partial}{\partial r}(\bar{V}r)=0, \qquad \text{II-1-5}$$

$$\bar{U}\frac{\partial\bar{U}}{\partial z}+\bar{V}\frac{\partial\bar{U}}{\partial r}+\overline{u'\frac{\partial u'}{\partial z}}+\overline{v'\frac{\partial u'}{\partial r}}=\frac{\mu}{r\rho}\frac{\partial(r\frac{\partial\bar{U}}{\partial r})}{}. \qquad \text{II-1-6}$$

Subtracting equation II-5 from equation II-2 shows the continuity equation holds for the fluctuating terms also.

$$\frac{\partial(u'r)}{\partial z}+\frac{\partial(v'r)}{\partial r}=0 \qquad \text{II-1-7}$$

By applying equation II-1-7 to equation II-1-6 the following momentum equation results.

$$\bar{U}\frac{\partial\bar{U}}{\partial z}+\bar{V}\frac{\partial\bar{U}}{\partial r}+\frac{1}{r}\frac{\partial\overline{u'^2}}{\partial z}+\frac{1}{r}\frac{\partial}{\partial r}r\,\overline{u'v'}=\frac{\mu}{r\rho}\frac{\partial(r\frac{\partial\bar{U}}{\partial r})}{\partial r} \qquad \text{II-1-8}$$

Assuming that $\overline{u'^2}$ and $\overline{u'v'}$ are of the same order of magnitude, the final boundary layer assumption can be made, that in comparison with the other terms, the term $\frac{1}{r}\frac{\partial\overline{u'^2}}{\partial z}$ can be neglected.

$$\bar{U}\frac{\partial\bar{U}}{\partial z}+\bar{V}\frac{\partial\bar{U}}{\partial r}=-\frac{1}{r}\frac{\partial r}{\partial r}\overline{u'v'}+\frac{1}{r\rho}\frac{\partial}{\partial r}(r\,T_{zr}) \qquad \text{II-1-9}$$

Comparison of the two terms on the right hand side of equation II-1-9, gives rise to the idea of the apparent turbulent shearing stress or the Reynolds stress, $\tau^t_{zr} = \rho\overline{u'v'}$. Then the equation II-1-9 can be rewritten to include the sum of the turbulent and molecular terms.

$$\bar{U}\frac{\partial \bar{U}}{\partial z} + \bar{V}\frac{\partial \bar{U}}{\partial r} = \frac{1}{r\rho}\frac{\partial}{\partial r}\, r\,(\tau^t_{zr} + \tau_{zr}) \qquad \text{II - 1 - 10}$$

Previously it has been stated that for high turbulent flows, the contribution of the laminar shearing stress is negligible, $\tau^t_{zr} \gg \tau_{zr}$.

Prandtl[1] first established the concept of the mixing length theory. If an eddy moving in a turbulent stream has a mean free path of l (mixing length), the change in velocity caused by this eddy moving in a tranverse or radial direction from its layer to a layer of a different velocity is given by $\Delta U = l\frac{\partial U}{\partial r}$, assuming only the first term of the Taylors series expansion is necessary. The eddy maintains its original velocity until it reaches the next layer, whereupon it suddenly changes to the velocity of that layer. The emergence of this particle in the new layer should give rise to a fluctuation in the velocity $u' = \Delta U$. Prandtl assumed the radial velocity fluctuations are proportional to the axial velocity fluctuations, $v' \sim \mp u'$. The sign of the proportionality depends upon the slope of the radial velocity profile. If $\frac{\partial \bar{U}}{\partial r} > o$ then $v' \sim -u'$, anf if $\frac{\partial \bar{U}}{\partial r} < o$ then $v' \sim u'$. Combining the difinitions of u' and v' the turbulent shearing stress is given as follows in terms of the mixing length,

$$\tau^t_{zr} = \pm\, \rho l^2 \frac{\partial \bar{U}}{\partial r}\left|\frac{\partial \bar{U}}{\partial r}\right| .$$

In the case of an unbounded stream, where there are no boundaries to damp out the oscillations of the fluid particles, Prandtl assumed that the mixing length could be held constant at any cross section, $l(r)$ = constant. Taking

for example, in this argument, the case of jet issuing into a stagnant field, Experiment shows that by plotting the dimensionless velocity $\frac{\bar{U}}{\bar{U}_c}$ where $\bar{U}_c$ is the centerline velocity at the particular cross-section, against the dimensionless coordinate $\frac{r}{b}$, where b is the width of the jet, the profiles coincide regardless of the axial position. The similarity of the velocity profiles implies the similarity between geometric dimensions, or that the dimensionless mixing length defined $\frac{l}{b}$, is independent of the axial position.

Prandtl assumed that the rate of growth of the jet is controlled by the fluctuations in the radial velocity,

$$\frac{db}{dt} \sim v' \sim - l \frac{\partial \bar{U}}{\partial r}$$

Because of the similarity of the profiles across the jet,

$$\frac{\partial \bar{U}}{\partial r} = \frac{\bar{U}_c}{b}$$

therefore,

$$\frac{db}{dt} \sim \frac{l \bar{U}_c}{b} \sim \bar{U}_c .$$

It is also possible to write,

$$\frac{db}{dt} = \frac{db}{dz} \frac{dz}{dt} \sim \bar{U}_c \frac{db}{dz} .$$

From this series of equations it is possible to set down the equations governing the increase in thickness and variation of the mixing length in the direction of the flow.

$$\frac{db}{dz} = \text{constant}, \quad b = z \cdot \text{constant}, \quad l = c z .$$

Substituting the mixing length into the turbulent shearing stress, the shear stress

becomes,

$$\tau_{zr}^{t} = \rho c^2 z^2 \frac{\partial \bar{U}}{\partial r} \left| \frac{\partial \bar{U}}{\partial r} \right|,$$

where c is a single emperical constant of free turbulence.

The basic idea of Prandtls mixing length can be extended to the case where mass transfer is involved[6]. Assuming that molecular diffusion can be neglected the equations for continuity and diffusion can be written as follows in terms of the density.

$$\frac{\partial(\rho U r)}{\partial z} + \frac{\partial(\rho V r)}{\partial r} = 0 \quad \text{(continuity)},$$

$$U \frac{\partial \rho}{\partial z} + V \frac{\partial \rho}{\partial r} = 0 \quad \text{(diffusion)}.$$

Applying the concept of turbulence that the density and velocity components have a time mean average term and a fluctuating term, and time averaging, the diffusion equation becomes,

$$\bar{U} \frac{\partial \rho}{\rho r} + \bar{V} \frac{\partial \rho}{\partial r} + \overline{u' \frac{\partial \rho'}{\partial z}} + \overline{v' \frac{\partial \rho'}{\partial r}} = 0 \qquad \text{II - 1 - 15}$$

With the aid of the continuity equation, and assuming that the term $\overline{u' \partial \rho' / \partial z}$ can be neglected in comparison with the rest of the terms, the equation II-1-15 becomes,

$$\bar{U} \frac{\partial \bar{\rho}}{\partial z} + \bar{V} \frac{\partial \bar{\rho}}{\partial r} = -\frac{1}{r} \frac{\partial}{\partial r} r \overline{\rho' v'}. \qquad \text{II - 1 - 16}$$

The fluctuation in density is its change of magnitude during transfer of a fluid particle from one layer to another by a distance of one mixing length l, $\rho' = l \frac{\partial \bar{\rho}}{\rho r}$.

From the previous case, $v' \sim \overline{+}\ l \frac{\partial U}{\partial r}$. The mixing length for the density fluctuations and the velocity fluctuations are the same and the mixing length is proportional to the axial position. The governing equation for mass transfer becomes, in terms of density,

$$\overline{U}\frac{\partial \overline{\rho}}{\partial z} + \overline{V}\frac{\partial \overline{\rho}}{\partial r} = \pm \frac{c^2 z^2}{r}\frac{\partial}{\partial r}\left(r \frac{\partial \overline{U}}{\partial r}\frac{\partial \overline{\rho}}{\partial r}\right)$$

On further analysis, it can be reasoned that the velocity profile $\frac{\overline{U}}{\overline{U}_c}$ and the density profile $\frac{\overline{\rho} - \rho_o}{\overline{\rho}_c - \rho_o}$, where ρ_o, is the external medium density and ρ_c is the density at the centerline, should coincide. However, measurements show that profiles do not coincide.

Taylor[2] developed a theory of turbulence by assuming that the tangential stresses in turbulent flow were caused by vorticity transfer and not by momentum transfer. For two dimensional case the mean vorticity $\overline{\omega}$ is given by,

$$\overline{\omega} = \frac{1}{2}\left(\frac{\partial \overline{U}}{\partial y} - \frac{\partial \overline{V}}{\partial x}\right).$$

The usual boundary layer assumption is made that $\frac{\partial \overline{V}}{\partial x} \ll \frac{\partial \overline{U}}{\partial y}$, therefore the equation reduces to $\overline{\omega} = \frac{1}{2}\frac{\partial \overline{U}}{\partial y}$. Assuming the mean free path of a particle or eddy is given by Taylor's mixing length l_T, a particle will have an excess or deficiency of vorticity during a traverse movement from one layer to another equal to, $\Delta \overline{\omega} = l_T \frac{\partial \overline{\omega}}{\partial y} = \frac{1}{2} l_T \frac{\partial^2 \overline{U}}{\partial y^2}$. The loss of the individuality of the particle in the new layer should result in a fluctuation in the vorticity, $\overline{\omega}'$. The fluctuation in the vorticity ω' can be set equal to $\frac{1}{2}\frac{\partial u'}{\partial y}$. Consequently, $\frac{\partial u'}{\partial y} = l_T \frac{\partial^2 \overline{U}}{\partial y^2}$, and

$$\overline{U}\,\frac{\partial \overline{U}}{\partial z} + \overline{V}\,\frac{\partial \overline{U}}{\partial r} = -\overline{v' l_T}\,\frac{\partial^2 \overline{U}}{\partial y^2} \qquad \text{II - 1 - 18}$$

The quantity $\overline{v' l_T}$ must be determined in the same manner as in Prandtl's old mixing length theory. Assuming that the transverse fluctuations of velocity have the same order of magnitude as the longitudinal fluctuations $\pm\ v' \sim u' \sim l\,\frac{\partial \overline{U}}{\partial y}$ equation II-1-18 reduces to,

$$\overline{U}\,\frac{\partial \overline{U}}{\partial x} + \overline{V}\,\frac{\partial \overline{U}}{\partial y} = \pm\ 2\ l_T^2\,\frac{\partial \overline{U}}{\partial y}\,\frac{\partial^2 \overline{U}}{\partial y^2}. \qquad \text{II - 1 - 19}$$

The corresponding equation deduced from Prandtl's old theory is,

$$\overline{U}\,\frac{\partial \overline{U}}{\partial x} + \overline{V}\,\frac{\partial \overline{U}}{\partial y} = \pm\ 2\ l^2\,\frac{\partial \overline{U}}{\partial y}\,\frac{\partial^2 \overline{U}}{\partial y^2}$$

Comparison of the right hand side of the two previous equations II-1-18 and II-1-19 shows that if Taylor's mixing length l_T is taken as the $\sqrt{2}$ times Prandtl's mixing lentth l, the equations become identical. Taylor's hypothesis was derived for the case of plane flow, and can only be applied as an approximation to the axially symmetric system.

The use of Taylor's hypothesis in the diffusion equation does not predict the same equation as does Prandtl's old theory, but predicts a faster spread of mass then momentum.

In 1942, Prandtl[3] proposed a new theory of turbulence. From Prandtl's old mixing length theory the apparent or eddy kinenatic viscosity is given as, $\varepsilon = l^2\,\frac{\partial U}{\partial r}$. Prandtl's new theory assumes that ε can be kept constant across a cross-section. Defining $\overline{U}_o$ as the free stream velocity, $\overline{U}_c$ the centerline velocity at the particular cross-section, and b the width of the mixing region, the dimensionless velocity profiles are similar at various axial positions and at a given value of $\frac{r}{b}$,

$$\frac{\partial\left(\frac{\overline{U}-\overline{U}_o}{\overline{U}_c-\overline{U}_o}\right)}{\partial(r/b)} = \text{constant}$$, and because of the velocity similarity, the geometrical dimensions of the system are similar, $\frac{l}{b}$ = constant, $\frac{y}{b}$ = constant. Making the proper substitutions into the definition of the eddy kinematic viscosity,

$$\epsilon = \left(\frac{l^2}{b^2}\right) \quad b^2 \left(\overline{U}_c - \overline{U}_o\right) \quad \frac{\partial\left(\frac{\overline{U}-\overline{U}_o}{\overline{U}_c-\overline{U}_o}\right)}{\partial\left(\frac{r}{b}\right)} \quad .$$

From the previous statements, the combination of terms

$$\left(\frac{l^2}{b^2}\right) \cdot \frac{\partial\left(\frac{\overline{U}-\overline{U}_o}{\overline{U}_c-\overline{U}_o}\right)}{\partial\left(\frac{r}{b}\right)} = \text{constant}.$$

Therefore, the eddy kinematic viscosity can be written as proportional to maximum difference of the velocity at any particular cross-section. $\epsilon = K\, b\, (\overline{U}_c - \overline{U}_o)$

The fourth and last theory of turbulence to be considered is Reichardt's theory of turbulence. Reichardt assumed that the lateral transport of momentum is proportional to the transverse gradient of the horizontal component of momentum. Given that $\overline{UV}$ represents the lateral transport of momentum and $\overline{U^2}$ represents the axial component of momentum then Reichardt's assumption can be written.

$$\overline{UV} = -\Lambda(z)\frac{\partial\overline{U^2}}{\partial r}$$

The coefficient Λ is assumed to be constant along the radial direction but varies in the axial direction. In this manner it is analogous to Prandtl's mixing length, but unlike it, has no physical interpretation. The equation of motion for an axially symmetric system, assuming no pressure gradient in the axial direction, and neglecting molecular viscosity, can be written, as

$$\frac{\partial \overline{U^2}}{\partial z} + \frac{\partial}{\partial r}\ \overline{UV} + \frac{\overline{UV}}{r} = 0$$

(note $\overline{UV}$ may not be taken as $\bar{U}\bar{V}$ in this case).

Using Peichardt's assumption for turbulent mixing the following equation is obtained.

$$\frac{\partial \overline{U^2}}{\partial z} = \quad (z)\ \left(\frac{\partial^2 \overline{U^2}}{\partial r^2} + \frac{1}{r}\ \frac{\partial \overline{U^2}}{\partial r} \right).$$

II - 2 Applications of concepts

The turbulent mixing concepts as presented in the previous section were necessary to provide representative forms for the turbulent shear stress, so the equation of motion might be solved for specific turbulent flow situations.

Tollmien[7] applied Prandtl's old theory of free turbulence to the equation of motion to obtain a solution for the free circular jet. His solution assumes the jet originates from a point source. The solution therefore is not valid close to the origin of the jet, but at large values of the ratio of the axial position to the initial jet diameter. The solution predicts the similar profiles that are found in experiment. In the final form the velocity ratio $\frac{\bar{U}}{\bar{U}_c}$, is plotted versus $\frac{r}{a z}$ where $a = \sqrt[3]{c^2}$, and c is Prandtl's mixing length constant. By comparing the solution with experimental data of Trupel and Gottinger[8], Zimm[9] and Turbus and Syrkin[10], Tollmien obtained values of a that brought agreement between the solution and the experimental data. It is interesting to note that the value of a depended upon the initial configuration of the velocity profile. In the Trupel and Gottinger[8] experiments the initial profile was flat and an a of 0.066 was determined. However in the Turkus and Syrkin experiments where the initial profile was that of a well developed turbulent flow in a pipe, an a of 0.076 was determined.

Gortler[5,6] solved the equation of motion for a plane jet using Prandtl's new

theory. The extension of the problem to the circular jet problem is not difficult. Choosing the free jet where the external stream velocity is taken to be zero, the eddy kinematic viscosity reduces to $\varepsilon = c b \overline{U}_c$. With the proper transfor-fation of coordinates the solution is readily obtained. While Tollmien's solution of the velocity profile agreed quite well with the experimental data almost over the entire cross-section of the jet, Gortlers did not.

In 1935, Keuthe[13] used Prandtl's old mixing length theory to solve the case of two parallel streams of the same composition, moving in the same direction, but having different velocities. In the same work he made an analytical study of the initial region of an axially symmetric jet discharging into a fluid at rest. Unlike Tollmien's solution which assumed a point source, Keuthe's set orifice had a finite radius. He assumed that the velocity profile in the initial region could be represented by the form $\underline{U} = \left[1 - \left(\frac{r}{b}\right)^{3/2} \right]^2$. Where $\underline{U}$ is the normalized velocity $\frac{\overline{U}}{\overline{U}_c}$, and r is the radial coordinate. Using Prandtl's old mixing length theory and Van Karmen's integral method, he mapped out the velocity field in the initial region of the jet, showing that the potential core disappeared at about 4.5 orifice diameters. Kuethe also performed a series of experiments and mapped the velocity profiles for the free jet case. By comparing his analytical solution with the experimental data, he found that a $c^2 = 0.00496$, or $c = 0.0705$, gave good agreement between the theory and the experiment. Kuethe also plotted data he had obtained far downstream of the orifice with Tollmien's solution. The experimental points deviated only a small amount near the centerline from Tollmien's solution, otherwise good agreement was obtained.

Squire and Trouncer[14], in 1944, studied the axially symmetric round jet in a general stream of the same composition but of different velocities. They divided the jet into two regions, the initial region, up to the point where the potential core vanished, and the second or general mixing region. Velocity profiles in both regions

were approximated by cosine profiles $\underline{U} = \frac{1}{2}\left(1 + \cos\frac{r\pi}{b}\right)$, where $\underline{U}$ is the dimensionless velocity $\frac{\overline{U} - \overline{U}_o}{\overline{U}_c - \overline{U}_o}$ and b the width of the mixing region. Using Prandtl's old mixing length theory they obtained a numerical solution for the spread of the jet in the near and downstream regions for outer stream to inner stream ratios from 0 to 1. A value of $c^2 = 0.0067$ was calculated. Their limiting case of no external flow agreed well with the solution of Kuethe.

In each study presented the initial profile at the orifice was assumed to be flat, constant velocity across the initial face. In 1954 T. R. Torda, W. J. Thompson and B. K. Genetti [15] presented an analysis in the initial mixing region for two dimensional parallel jets and for co-flowing axially symmetric jets, assuming that a boundary layer was present on the dividing plate for the two dimensional case, and on the pipe separating the flows of the coaxial case, for laminar flow.

The most extensive experimental investigations of the coaxial flow system was done in two works of Tani and Kobashi [16]. Their experimental apparatus consisted of a 9 mm jet exhausting into a tunnel 60 cm by 60 cm. Velocity profiles were measured with a pilot tube at various axial positions, and different initial velocity ratios. Their experimental results showed that plotting the dimensionless velocity $\frac{\overline{U} - \overline{U}_o}{\overline{U}_c - \overline{U}_o}$ versus $\frac{r}{r_{1/2}}$ the profiles were similar, where $r_{1/2}$ is termed the half radius, the radial position where $\overline{U} = {}^1/_2\,(\overline{U}_c + \overline{U}_o)$. The velocity decay along the centerline was linear with axial distance when the axial point of origin was shifted to the end of the potential core. Their experiments provided information about the spread of the half radius of the jet. For a pure jet where the external velocity $\overline{U}_o$ is zero, the half radius increases linearly with axial position, and for the wake flow, the half radius increases as the square root of the axial position. For the case where there is flow in both streams, the half radius asymptotically approaches the square root value.

An important contribution was their measurement of the turbulent quantities

of the system. Using a single hot wire annemometer, they measured turbulence intensity in the axial direction, defined as $\frac{\sqrt{\overline{u'^2}}}{\overline{U}}$, the turbulence intensity in the radial direction, $\frac{\sqrt{\overline{v'^2}}}{\overline{U}}$ and the turbulent Reynold's stress $\overline{u'v'}$. They present typical curves for each quantity. They noted that the maximum turbulence intensity occurred at the maximum turbulent shear.

The second work[17] provided more information on the determination of ϵ, the eddy kinematic viscosity. Kobashi took a typical profile of the turbulent shear stress and found the position of maximum shear. At this same position of maximum shear he found the slope of the velocity profile with respect to the radius. From this he calculated an,

$$\epsilon_c = \frac{-\overline{u'v'}_{max}}{\left(\frac{d\overline{U}}{dr}\right)_{\text{max shear}}}$$

Assuming that this value of the eddy kinematic viscosity held constant across the radius, he back calculated the shear stress profile, $\overline{u'v'} = \epsilon_c \left(\frac{\partial \overline{U}}{\partial r}\right)_z$. The curve calculated from this procedure in most cases feel through the experimental points. He further stated that ϵ did not vary significantly from one axial position to the next. This indicates that the eddy or apparent kinematic viscosity can be held constant throughout the entire mixing region as a good approximation.

There have been only a few experimental investigations of the coaxial system where the external and internal streams were of differing composition. Forstall and Shapiro[18] provided experimental data for the case where a small amount of helium was injected into internal stream. The resultant density ratio was still 1. They mapped the concentration and velocity field. Their data showed the concentration and velocity profiles were similar, and that the mass spread faster than momentum. Both the cosine profile used by Squire and Trouncer and the 3/2 power profile used by Kuethe matched the experimental data. They found that the turbulent Schmidt number

did not vary by 10% from 0.7 and is essentially independent of the experiment.

A similar experiment was performed by L. Boehman[30]. He was concerned with near sonic, sonic and super sonic flows and injected small amounts of argon into the inner jet. Again, the density ratio remained unity. Boehman developed expressions for ε, the eddy kinematic viscosity, in a constant density coaxial flow field with a constant external flow, using three simplified mathematical expressions for the velocity field. His analysis showed that the proper radial variation of ε was one that is nearly constant over the central portion of the mixing region, and which decreases to zero at the outer edge of the mixing zone, while the axial variation was shown to be proportional to $\frac{(r_{1/2})^2 \overline{U}_c}{z}$ and approaches a constant at large values of z as Macynski[19] had predicted in 1962. Prandtl's new form which is proportional to the difference in velocity predicts a value of zero at large values of the axial position.

Using his actual velocity and concentration profile data, Boehman obtained values of ε in the potential core region of the jet by working back through the equations of motion. Further downstream experimental error became too great to perform any significant calculations. By making a transformation into the von Mises plane, he obtained values of ε on the centerline further downstream.

In the coaxial case, Prandtl's theory predicts an eddy kinematic viscosity of zero at equal inner and outer stream velocities and suggests a point where no mass transfer between streams occurs, excluding an infinite Schmidt No. Boehman showed that at equal velocities, even more mixing was obtained than the case where the two streams were of different velocities.

For the heterogeneous system, where large density differences were present, different forms for the eddy kinematic viscosity were proposed based on the difference of the momentum of the two streams, or the difference in the mass flow of both streams, $\varepsilon = K_1 (\rho \overline{U}_{max} - \rho \overline{U}_{min})$, $\varepsilon = K_2 (\rho \overline{U}^2_{max} - \rho \overline{U}^2_{min})$.

These forms were extended from Prandtl's new theory and have no fundamental basis for being a valid representation for the eddy kinematic viscosity.

Alpinieri[20] made a study of the heterogeneous system, using hydrogen and carbon dioxide in the inner jet. His purpose was to study the cases where the mass flow rates were equal, and the velocities were equal. Using an analysis of Libby and Ferri and Zakay, Alpinieri showed the eddy kinematic viscosity could be taken as constant across the radial position, and is only a function of the axial position. His radial and velocity profiles were insensitive to a change in Schmidt number from 0.6 to 1.0. He proposed the following form for a possible representation of the eddy kinematic viscosity.

$$\frac{(\rho\varepsilon)_c}{\rho_o \overline{U}_o r_o} = 0.025 \frac{b_{1/2}}{r_o} \left(\frac{\rho_o \overline{U}_c}{\rho_i U_i} + \frac{\rho_o \overline{U}_o^2}{\rho_i U_i^2} \right)$$

He showed the centerline decay of concentration and velocity obtained by using this formulation agreed quite well with the experimental data. This form with the external velocity, U_o, set equal to zero reduces to the classical form for the free jet.

Alpinieri argued that the amount of the central jet that is entrained by the external stream must depend on the external mass flow and momentum. Similarly the amount of the external stream entrained by the internal stream must depend upon the mass flow and momentum of the inner stream. Thus it seemed reasonable that the eddy kinematic viscosity, which is a measure of the momentum change, must depend upon the momentum and mass flow of both jets.

Relatively few experiments have been made on the measurements of turbulent quantities in coaxial flows. Kobashi used only one hot wire, and changed the position of the wire each time to obtain turbulence data, and no one has ever checked his data. No one has reported turbulence data in heterogeneous coaxial

flows. Conger[31] used hot wires to measure velocity and concentration turbulence behind a grid. He assumed for flow behind the grid, the velocity fluctuations had no correlation with the concentration fluctuations, $\overline{u'c'} = 0$. This is not true for the coaxial flow system.

III HOT WIRE ANEMOMETRY

III - 1 Background

Many techniques have been devised and used in the experimental investigations of fluid flow. Most of these devices have been used for measuring the average velocity and concentration in flows that are assumed to be non-turbulent. The main difficulty in the measurement of turbulence is caused by the fact that turbulent flows have a three dimensional, random, fluctuating component. It is difficult to obtain a device that has a fast enough response to the high frequency fluctuations that are part of the flow.

The most widely used instrument for instantaneous measurements in turbulent flow is the hot wire anemometer. The detecting element is a short fine wire, usually made from tungsten or platinum, heated by an electric current. For good turbulence measurements the diameter of the wire should be about 0.00015 inches. A newer probe, called a hot film, was constructed by coating a thin film of platinum over a quartz cylinder. Although this probe has a diameter of 0.001 to 0.002 inches, it is more stable and durable than the hot wire, without much loss in the frequency response range.

There are two types of systems that are used to control whe wire or film, the constant current method, and the constant temperature method. In the constant current method, the current through the wire is kept constant and the resistance of the wire changes with the fluctuations in the flow fluid. In the constant temperature method, the temperature (resistance) of the wire is kept constant and the current changes according to the fluctuations.

Even though the constant temperature system has basic advantages over the constant current type, all the early investigators used the constant current system due to the instability of the electronics associated with the constant temperature system.

Due to increased knowledge in electronic feedback systems in recent years, constant temperature systems can be made which provide an excellent means of measuring turbulence quantities.

The total heat transfer of a heated wire to a surrounding fluid, depends on the velocity of the fluid, the temperature difference between the wire and the fluid, the physical properties of the fluid, and the dimensions and physical properties of the wire.

King[27] derived the relationship that was originally used to describe the cooling of a heated cylinder. He derived it on a basis of potential flow around the wire, and obtained the following relationship:

$$P = K_g L (T_w - T_g) \left[1 + \left(\frac{2\pi \rho_g c_p DU}{k_g} \right)^{1/2} \right] \qquad III - 1 - 1$$

The relationship is valid for $\frac{\rho_g c_{pg} DU}{k_g} > 0.08$. Kings equation predicted a linear relationship between the heat loss P, and the square root of the velocity.

Heat is transferred from the wire to the surroundings by heat conduction, free and forced connection, and radiation. In general the effect of radiation can be neglected, and except for lower velocities, below 1 foot per second, free connection can be neglected.

Empirically the heat transfer from a cylinder to a flowing gas may be obtained in terms of the dimensionless groups of Nusselt Nu, Prandtl Pr, and Reynolds Re.

$$Nu = \frac{hD}{K}, \quad Pr = \frac{c_p \nu}{K}, \quad Re = \frac{\rho UD}{\nu}$$

Kramer [26] obtained the following emperical relationship which gave satisfactory results for liquids and gases.

$$Nu = 0.42\ Pr^{1/5} + 0.57\ Pr^{1/3}\ Re^{1/2} \qquad III - 1 - 2$$

The heat transferred per unit time to the flowing gas from a wire of length L and temperature T is given by,

$$g = h \pi D L (T_w - T_g) \qquad III - 1 - 3$$

Solving for h in equation III-1-3 and substituting this value of h into the Nusselt number of equation III-1-2 the following reault is obtained.

$$g = \pi k L (T_w - T_g) \left[0.42\ (Pr)^{1/5} + 0.57\ (Pr)^{1/3}\ (Re)^{1/2}\right] \qquad III - 1 - 4$$

The heat transfer rate g can be related to the power dissapation in watts P by a conversion factor γ . The physical properties of the gas that occur in the dimensionless groups are evaluated at the mean film temperature T_f , where

$$Tf = (Tw + Tg) / 2$$

Finally Kramer's equation can be written in the following form:

$$P = \gamma \pi K_f L (T_w - T_g) \left[0.42 \left(\frac{c_p \mu}{k}\right)_f^{1/5} + 0.57 \left(\frac{c_p \mu}{k}\right)_f^{1/3} \left(\frac{\rho D}{\mu}\right)_f^{1/2} U^{1/2}\right] \qquad III - 1 - 5$$

Kramer's equation, as does King's predicts a linear relationship between the power dissapation and the square root of velocity.

$$P - A + BU^{1/2} \qquad III - 1 - 6$$

$$A = L \pi K_f (T_w - T_g)(0.42)\left(\frac{c_p \mu}{k}\right)^{1/5} \qquad III - 1 - 7$$

$$B = L \pi K_f (T_w - T_g)(0.57)\left(\frac{c_p \mu}{K}\right)_f^{1/3}\left(\frac{\rho D}{\mu}\right)_f^{1/2} \qquad \text{III - 1 - 8}$$

Collis and Williams[32] also developed an equation that predicted the heat dissipation as a function of velocity for air, $Nu\left(\frac{T_w}{T_e}\right) - 0.17 = A + B\ Re^n$, where for a Reynolds number of less than 44, based on the diameter of the wire, the coefficients A, B, and n, are 0.24, 0.56, and 0.45 respectively.

Baid[33] showed none of the equations predict the power dissipation of gaseous mixtures, and in actual practice the coefficients A and B are not calculated from either King's, Kramer's or Collis and William's equation, but are experimentally determined by a calibration technique. From equations III-1-7 and III-1-8, the coefficients A and B are noted to be functions of the composition of the gas, since thermal conductivity, heat capacity, and viscosity are functions of composition. In using the hot wire or film in a heterogeneous system, the output of the wire versus concentration must also be known.

III - 2 Fluctuations in a Homogeneous System

The hot wire or film is sensitive to the velocity components in the plane perpendicular to it. The velocity component parallel to the wire is usually neglected. If u' represents a turbulent fluctuation in the axial velocity component U, and v' a turbulent fluctuation in the radial velocity component, the effective cooling velocity U_e, for a hot film placed normal to the radial plane r, and the axial plane z, is given by,

$$U_e = \left[(\overline{U} + u')^2 + v'^2 \right]^{1/2} \qquad \text{III - 2 - 1}$$

The value obtained in the hot wire equation is $U_e^{1/2}$ not U_e, so the square root of equation III-2-1 is taken and the result is expanded in a Taylor series.

$$U_e^{1/2} = \overline{U}^{1/2}\left(1 + \frac{u'}{\overline{U}} - \frac{1}{8}\frac{u'^2}{\overline{U}^2} + \frac{1}{4}\frac{v'^2}{\overline{U}^2} + \cdots\right). \qquad \text{III - 2 - 2}$$

Time averaging equation III-2-2 produces the following result :

$$\overline{U_e^{1/2}} = \overline{U}^{1/2}\left(1 - \frac{1}{8}\frac{\overline{u'^2}}{\overline{U}^2} + \frac{1}{4}\frac{\overline{v'^2}}{\overline{U}^2} + \cdots\right). \qquad \text{III - 2 - 3}$$

Squaring equation III-2-3 gives the apparent velocity measured by the wire as a function of the axial velocity and various turbulence quantities[25].

$$\left[\overline{U_e^{1/2}}\right] = \overline{U}\left(1 - \frac{1}{4}\frac{\overline{u'^2}}{\overline{U}^2} + \frac{1}{2}\frac{\overline{v'^2}}{\overline{U}^2} + \cdots\right). \qquad \text{III - 2 - 4}$$

A correction factor must be applied to the velocity measured by the wire to obtain true velocity $\overline{U}$. Since the signs of the turbulence quantities of the correction factor of equation III-2-4 are opposite, the correction can be neglected if $u'^2 \sim v'^2$. If P' represents a fluctuation in the power due to a fluctuation in the velocity the equation for the power dissapation becomes,

$$\overline{P} + P' = A + B\left[(\overline{U} + u')^2 + v'^2\right]^{1/2} \qquad \text{III - 2 - 5}$$

or,

$$\overline{P} + P' = A + B\,\overline{U}^{1/2}\left[1 + \frac{u'}{2\overline{U}} - \frac{1}{8}\frac{u'^2}{\overline{U}^2} + \frac{1}{4}\frac{v'^2}{\overline{U}^2} + \cdots\right) \qquad \text{III - 2 - 6}$$

The instantaneous equation for the power dissi pation can also be time averaged.

$$\overline{P} = A + B\,\overline{U_e^{1/2}}. \qquad \text{III - 2 - 7}$$

If the correction factor is neglected, then from equation III-2-3, $\overline{U_e^{1/2}}$ is approximately $\overline{U}^{1/2}$. Substituting for $\overline{U_e^{1/2}}$ the term $\overline{U}^{1/2}$ into equation

III-2-7, the time average power can be given as,

$$\overline{P} = A + B\overline{U}^{1/2} \qquad \text{III - 2 - 8}$$

Subtracting equation III-2-8 from III-2-6 and neglecting the second order terms, the fluctuating power is related the fluctuating velocity.

$$P' = B\overline{U}^{1/2}\ \frac{u'}{2U}\ .$$

Squaring, time averaging, taking the square root, and rearranging the final result for the turbulence intensity is obtained as a function of the root mean square value of the power.

$$\frac{\sqrt{\overline{u'^2}}}{\overline{U}} = 2\frac{\sqrt{\overline{P'^2}}}{\overline{P} - A}\ . \qquad \text{III - 2 - 9}$$

Thus axial turbulence intensities may be obtained in a homogeneous system.

Another method of obtaining turbulence intensities in both the axial and radial direction is by the use of an X-array probe, as shown below.

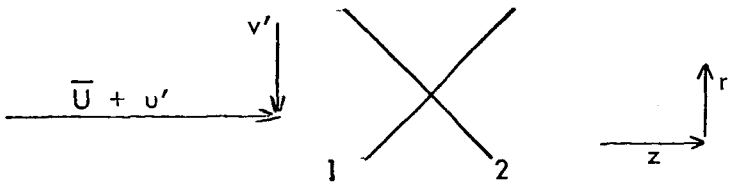

The subscript 1 will denote the characteristics of the wire in position 1, and the superscript 2 will refer to the wire in position 2. The cooling velocity is given by the normal velocity past the wire. For the wire in position 1, the cooling velocity will be,

$$U_{e_1} = (\overline{U} + u')\sin\theta - v'\cos\theta$$

and for the wire in position 2,

$$U_{e_2} = (\overline{U} + u')\sin\theta - v'\cos\theta$$

The cooling velocity deviates slightly from the sine law and is usually represented by the sine of the angle raised to the 1.1 power. Given that P′ represents the fluctuation in the power, the two equations for the power dissapation can be written.

$$\overline{P}_1 + P'_1 = A_1 + B_1 \left[(\overline{U} - u') \sin\theta + v' \cos\theta \right]^{1/2}$$

$$\overline{P}_2 + P'_2 = A_2 + B_2 \left[(\overline{U} + u') \sin\theta - v' \cos\theta \right]^{1/2} .$$

Rearranging,

$$\overline{P}_1 + P'_1 = A_1 + B_1 (\overline{U} \sin\theta)^{1/2} \left[1 + \frac{u'}{\overline{U}} + \frac{v'}{\overline{U}} \cot\theta \right]^{1/2} \qquad \text{III - 2 - 10}$$

$$\overline{P}_2 + P'_2 = A_2 + B_2 (\overline{U} \sin\theta)^{1/2} \left[1 + \frac{u'}{\overline{U}} - \frac{v'}{\overline{U}} \cot\theta \right]^{1/2} . \qquad \text{III - 2 - 11}$$

Expanding the function under the square root side of equation's III-2-10 and III-2-11 they become,

$$\overline{P}_1 + P'_1 = A_1 + B_1 (\overline{U} \sin\theta)^{1/2} \left[1 + \frac{u'}{2\overline{U}} + \frac{v'}{2\overline{U}} \cot\theta \right] \qquad \text{III - 2 - 12}$$

$$\overline{P}_2 + P'_2 = A_2 + B_2 (\overline{U} \sin\theta)^{1/2} \left[1 + \frac{u'}{2\overline{U}} - \frac{v'}{2\overline{U}} \cot\theta \right] \qquad \text{III - 2 - 13}$$

The time average of the instantaneous power equation yields,

$$\overline{P}_1 = A_1 + B_1 \overline{(U_e \sin\theta)^{1/2}}$$

$$\overline{P}_2 = A_2 + B_2 \overline{(U_e \sin\theta)^{1/2}}$$

As was shown for the single wire case, $\overline{U_e^{1/2}}$ may be approximated by $\overline{U}^{1/2}$.

Therefore

$$\overline{P}_1 = A_1 + B_1 \left(\overline{U} \sin\theta\right)^{1/2} , \qquad \text{III - 2 - 14}$$

$$\overline{P}_2 = A_2 + B_2 \left(\overline{U} \sin\theta\right)^{1/2} . \qquad \text{III - 2 - 15}$$

Subtracting equation III-2-14 from III-2-12, and equation III-2-15 from III-2-13, the fluctuating power P′ is related to the fluctuating velocity components u′ and v′.

$$P'_1 = \left(P_1 - A_1\right) \left(\frac{u'}{2\overline{U}} + \frac{v'}{2\overline{U}} \cot\theta\right) , \qquad \text{III - 2 - 16}$$

$$P'_2 = \left(\overline{P}_2 - A_2\right) \left(\frac{u'}{2\overline{U}} - \frac{v'}{2\overline{U}} \cot\theta\right) . \qquad \text{III - 2 - 17}$$

The sum and difference of the fluctuating powers can also be formed.

$$\left(P'_1 + P'_2\right) = \frac{u'}{2\overline{U}} \left[\left(\overline{P}_1 - A_1\right) + \left(\overline{P}_2 - A_2\right)\right] +$$

$$\frac{v'}{2U} \left[\left(\overline{P}_1 - A_1\right) - \left(\overline{P}_2 - A_2\right)\right] \qquad \text{III - 2 - 18}$$

$$\left(P'_1 - P'_2\right) = \frac{u'}{2\overline{U}} \left[\left(\overline{P}_1 - A_1\right) - \left(\overline{P}_2 - A_2\right)\right] +$$

$$\frac{v'}{2\overline{U}} \left[\left(\overline{P}_1 - A_1\right) + \left(\overline{P}_2 - A_2\right)\right] . \qquad \text{III - 2 - 19}$$

Squaring and time averaging equations III-2-16 through 19, and denoting $P_1 - A_1$ as X, and $P_2 - A_2$ as Y, the following four equations are obtained.

$$\frac{4\overline{P'^2_1}}{X^2} = \frac{\overline{u'^2}}{\overline{U}^2} + \frac{2\overline{u'v'}}{\overline{U}^2}\cot\theta + \frac{\overline{v'^2}}{\overline{U}^2}(\cot\theta)^2 \qquad \text{III - 2 - 20}$$

$$4\overline{P'^2_2} = \frac{\overline{u'^2}}{U^2} - \frac{2\overline{u'v'}}{U^2}\cot\theta + \frac{\overline{v'^2}}{U^2}(\cot\theta)^2 \qquad \text{III - 2 - 21}$$

$$4\overline{(P'_1 + P'_2)^2} = (X+Y)^2 \frac{\overline{u'^2}}{\overline{U}^2} - +$$

$$2(X+Y)(X-Y)\frac{\overline{u'v'}}{\overline{U}^2}\cot\theta + (X-Y)^2\frac{\overline{v'^2}}{\overline{U}^2}(\cot\theta)^2 \qquad \text{III - 2 - 22}$$

$$4\overline{(P'_1 - P'_2)^2} = (X-Y)^2\frac{\overline{u'^2}}{\overline{U}^2} +$$

$$2(X+Y)(X-Y)\frac{\overline{u'v'}}{\overline{U}^2}\cot\theta + (X+Y)^2\frac{\overline{v'^2}}{\overline{U}^2}(\cot\theta)^2 . \qquad \text{III - 2 - 23}$$

Adding equations III-2-20 and III-2-21, and subtracting equation III-2-23 from III-2-22 and rearranging gives two equations and two unknowns.

$$\frac{4\overline{P'^2_1}}{X^2} + \frac{4\overline{P'^2_2}}{Y^2} = \frac{\overline{u'^2}}{\overline{U}^2} + \frac{\overline{v'^2}}{\overline{U}^2}(\cot\theta)^2 \qquad \text{III - 2 - 24}$$

$$\frac{\overline{(P'_1 + P'_2)^2} - \overline{(P'_1 - P'_2)^2}}{XY} = \frac{\overline{u'^2}}{\overline{U}^2} + \frac{\overline{v'^2}}{\overline{U}^2}(\cot\theta) . \qquad \text{III - 2 - 25}$$

Equations III-2-24 and III-2-25 can be solved simultaneously for the turbulence intensities in the axial and radial direction.

$$\frac{\sqrt{\overline{u'^2}}}{\overline{U}} = \frac{1}{2}\left[\frac{4\overline{P'^2_1}}{(\overline{P}_1 - A_1)^2} + \frac{4\overline{P'^2_2}}{(\overline{P}_2 - A_2)^2} + \frac{\overline{(P'_1+P'_2)^2} - \overline{(P'_1-P'_2)^2}}{(\overline{P}_1 - A_1)(\overline{P}_2 - A_2)}\right]^{1/2} \qquad \text{III - 2 - 26}$$

$$\frac{\sqrt{\overline{v'^2}}}{\overline{U}} = \frac{1}{2}\left[\frac{4\overline{P'^2_1}}{(\overline{P}_1 - A)^2_1} + \frac{4\overline{P'^2_2}}{(\overline{P}_2 - A)^2_2} - \frac{\overline{(P'_1 + P'_2)^2} - \overline{(P'_1 - P'_2)^2}}{(\overline{P}_1 - A_1)(\overline{P}_2 - A_2)}\right]^{1/2} \qquad \text{III - 2 - 27}$$

Subtracting equation III-2-21 from equation III-2-20 gives the turbulent shear stress $\overline{u'v'}$.

$$\frac{\overline{u'v'}}{\overline{U}^2} = \frac{1}{4\cot\theta}\left[\frac{4\overline{P'^2_1}}{(\overline{P}_1 - A)^2_1} - \frac{4\overline{P'^2_2}}{(\overline{P}_2 - A)^2_2}\right]. \qquad \text{III - 2 - 28}$$

Thus the turbulence quantities in a homogeneous system can be measured with an X array probe, even though the wire may have different characteristics. A and B, the intercept in the power equations, are obtained by extrapolating the power versus square root of velocity calibration curve to zero velocity.[29]

III - 3 Heterogeneous Systems

In the previous section methods have been described to make turbulence measurements in a homogeneous system. In a heterogeneous system the power dissipation is related to the composition of the flowing fluid, $P = P(\rho, u)$, or

$$P = A(\rho) + B(\rho)\, U^{1/2}. \qquad \text{III - 3 - 1}$$

This means in order to calculate the velocity the coefficients must be calibrated against composition.

Turbulent measurements become much more difficult in this case. The power dissipation can be expanded in a total differential. For small fluctuations dP, $d\rho$, and du may be replaced by P', ρ' and u' respectively.

$$P' = \left(\frac{\partial P}{\partial \rho}\right)_U \rho' + \left(\frac{\partial P}{\partial U}\right)_\rho U' . \qquad \text{III - 3 - 2}$$

From equation III-3-1 the partial derivities may easily be obtained.

$$\left(\frac{\partial P}{\partial \rho}\right)_U = \frac{\partial (A(\rho))}{\partial \rho} + U^{1/2} \frac{\partial (B(\rho))}{\partial \rho}$$

A and B must be known functions of the density, ρ . Another method of finding the partial derivitive $\left(\frac{\partial P}{\partial \rho}\right)_U$ is to take a small density increment δ, and calculate the power dissapation at $\rho + \delta$, and $\rho - \delta$ and divide by the increment 2δ .

$$\left(\frac{\partial P}{\partial \rho}\right)_U \cong \frac{P(\rho + \delta) - P(\rho - \delta)}{2\delta}$$

where

$$P(\rho + \delta) = A(\rho + \delta) + B(\rho + \delta) U^{1/2}$$

$$P(\rho - \delta) = A(\rho - \delta) + B(\rho - \delta) U^{1/2}$$

Denoting the partial

$$\left(\frac{\partial P}{\partial \rho}\right)_U \quad \text{as} \quad S_1$$

and

$$\left(\frac{\partial P}{\partial U}\right)_\rho \quad \text{as} \quad S_2 ,$$

the fluctuating power is given by,

$$P' = S_1 \rho' + S_2 U' \qquad \text{III - 3 - 3}$$

Squaring and time averaging equation III-3-2 gives,

$$\overline{P'^2} = S_1^2 \overline{\rho'^2} + 2 S_1 S_2 \overline{\rho' u'} + S_2^2 \overline{u'^2} \qquad \text{III - 3 - 4}$$

This equation applies to a single wire. Two more equations must be obtained to satisfy the condition of three unknowns. From equations III-1-7 and III-1-8, it can be noted that the term B contains the diameter of the wire and A does not. Since the diameter is not a linear term, another equation can be obtained by changing the diameter of the wire[28].

$$\overline{P'^2_2} = S_2^2 \overline{\rho'^2} + 2 S_3 S_4 \overline{\rho' u'} + S_4^2 \overline{u'^2} \qquad \text{III - 3 - 5}$$

where P'^2_2 is the fluctuative power of the new wire and S_3 and S_4 are the partial derivitives

$$\left(\frac{\partial P}{\partial \rho}\right)_u , \quad \left(\frac{\partial P}{\partial U}\right)_\rho ,$$

respectively. A third equation can be obtained by taking the root mean square value of the sum of the fluctuating powers.

$$\overline{(P'_1 + P'_2)^2} = (S_1 + S_2)^2 \overline{\rho'^2} + 2 (S_1 + S_3)(S_2 + S_4) \overline{\rho' u'} + (S_3 + S_4) \overline{u'^2} \qquad \text{III - 3 - 6}$$

The three equations can be solved simultaneously for

$$\overline{\rho'^2}, \quad \overline{\rho' u'}, \quad \text{and} \quad \overline{u'^2}.$$

An X-array probe can also be used in a heterogeneous system. Given that a fluctuation in the density causes a fluctuation A' in the intercept term and a fluctuation B' in the slope term of equation III-3-1, the fluctuating power can be related to fluctuations in density and velocity.

$$\overline{P}_1 + P'_1 = (\overline{A}_1 + A'_1) + (\overline{B}_1 + B'_1)\left[(\overline{U} + u')\sin\theta + v'\cos\theta\right]^{1/2}$$

$$\overline{P}_2 + P'_2 = (\overline{A}_2 + A'_2) + (\overline{B}_2 + B_2)\left[(\overline{U} + u')\sin\theta + v'\cos\theta\right]^{1/2}$$

Rearranging, expanding the square root function in a Taylor series, neglecting second order terms, and assuming that time averaged instantaneous power may be written as

$$\overline{P} = \overline{A} + \overline{B}\,(\overline{U}\sin\theta)^{1/2},$$

the following two equations are obtained.

$$P'_1 = A'_1 + (\overline{U}\sin\theta)^{1/2} B'_1 + B_1 (\overline{U}\sin\theta)^{1/2}\left[\frac{u'}{\overline{U}} + \frac{v'}{\overline{U}}\cot\theta\right] \qquad \text{III - 3 - 7}$$

$$P'_2 = A'_2 + (\overline{U}\sin\theta)^{1/2} B'_2 + B_2 (\overline{U}\sin\theta)^{1/2}\left[\frac{u'}{\overline{U}} - \frac{v'}{\overline{U}}\cot\theta\right] \qquad \text{III - 3 - 8}$$

The A_i terms and B_i terms must be related to the fluctuations in the density. Assuming that a small fluctuation in the density ρ' causes a small fluctuation in A and B, the following relationships are assumed to hold.

$$A_i' = \left(\frac{d\overline{A_i}}{d\rho}\right)\rho', \qquad B_i' = \left(\frac{d\overline{B_i}}{d\rho}\right)\rho'$$

Substituting the A_i and B_i terms into equations III-3-7 and III-3-8, the fluctuating power is related to the fluctuating density and velocity.

$$P_1' = \overline{\rho}\left[\frac{d\overline{A}_1}{d\rho} + (\overline{U}\sin\theta)^{1/2}\frac{d\overline{B}_1}{d\rho}\right]\frac{\rho'}{\overline{\rho}} +$$

$$B_1\,(\overline{U}\sin\theta)^{1/2}\left[\frac{u'}{\overline{U}} + \frac{v'}{\overline{U}}\cot\theta\right] \qquad \text{III - 3 - 9}$$

$$P_2' = \overline{\rho}\left[\frac{d\overline{A}_2}{d\rho} + (\overline{U}\sin\theta)^{1/2}\frac{d\overline{B}_2}{d\rho}\right]\frac{\rho'}{\overline{\rho}} +$$

$$\overline{B}_2\,(\overline{U}\sin\theta)^{1/2}\left[\frac{u'}{\overline{U}} - \frac{v'}{\overline{U}}\cot\theta\right] \qquad \text{III - 3 - 10}$$

The coefficients of the ρ', u', v' terms respectively can be defined in the following manner.

$$R_{i_1} = \overline{\rho}\left[\frac{d\overline{A}_i}{d\rho} + (\overline{U}\sin\theta)^{1/2}\frac{d\overline{B}_i}{d\rho}\right]$$

$$R_{i_2} = \overline{B}_i\,(\overline{U}\sin\theta)^{1/2}$$

$$R_{i_3} = \overline{B}_i\,(\overline{U}\sin\theta)^{1/2}\cot\theta$$

Substituting the coefficients into equations III-3-9 and III-3-10 gives,

$$P'_1 = R_{11}\frac{\rho'}{\rho} + R_{12}\frac{u'}{U} + R_{13}\frac{v'}{U} \qquad \text{III - 3 - 11}$$

$$P'_2 = R_{21}\frac{\rho'}{\rho} + R_{22}\frac{u'}{U} + R_{23}\frac{v'}{U} \qquad \text{III - 3 - 12}$$

Squaring equations III-3-11 and III-3-12, and time averaging, the root mean square power is obtained.

$$\overline{P'^2_1} = R_{11}\frac{\overline{\rho'^2}}{\overline{\rho}^2} + 2R_{11}R_{12}\frac{\overline{\rho'u'}}{\overline{\rho}\,\overline{U}} + 2R_{11}R_{13}\frac{\overline{\rho'u'}}{\overline{\rho}\,\overline{U}} +$$

$$R^2_{12}\frac{\overline{u'^2}}{\overline{U}^2} + 2R_{12}R_{13}\frac{\overline{u'v'}}{\overline{U}^2} + R^2_{13}\frac{\overline{v'^2}}{\overline{U}^2}$$

$$\overline{P'^2_2} = R_{21}\frac{\overline{\rho'^2}}{\overline{\rho}} + 2R_{21}R_{22}\frac{\overline{\rho'u'}}{\overline{\rho}\,\overline{U}} + 2R_{21}R_{23}\frac{\overline{\rho'v'}}{\overline{\rho}\,\overline{U}} +$$

$$R^2_{22}\frac{\overline{u'^2}}{\overline{U}^2} + 2R_{22}R_{23}\frac{\overline{u'v'}}{\overline{U}^2} + R^2_{23}\frac{\overline{v'^2}}{\overline{U}^2}$$

There are two equations and six unknowns. Two more equations can be obtained by adding and subtracting equations III-3-11 and III-3-12 squaring and time averaging. That still leaves four equations and six unknowns. Another Xarray probe of a different diameter may be used to obtain another set of independent

equations, or the three quantities $\overline{\rho'^2}$, $\overline{\rho' u'}$, $\overline{u'^2}$, obtained from two single wires of different diameters (parallel wire probe) may be used in the solution.

III - 4 Measurement of Concentration

The composition of a flowing gas can be measured with a device called an aspirating probe. The principle involves the placement of a sonic nozzle in back of a hot film as shown below.

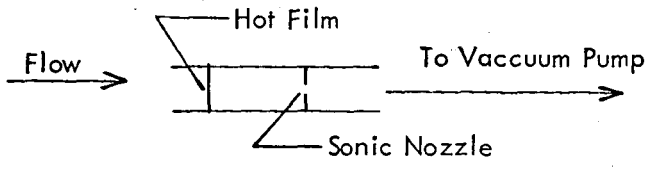

The heat dissapation from the wire can be given as the usual linear relationship, $P = A\ (\rho) + B\ (\rho)\ U_c^{1/2}$. The sonic velocity, for an ideal gas at the orifice is given by,

$$S = \left(\frac{g_c\, k\, R\, T}{M}\right)^{1/2},$$

where S is the sonic velocity, g_c is the gravitational constant, k is the ratio of specific heats, R is the gas constant, T is the temperature, and M is the molecular weight. The molecular weight of gaseous mixture can be defined as ρ / c_m, where ρ is the density of the mixture and c_m is the molar concentration, which for an ideal gas at constant pressure is a constant. The velocity past the wire can be related to the throat velocity by the ratio of the cross sectional areas,

$$\frac{U_c}{S} = \frac{A_t}{A},$$

where A_t is the area of the tube. The velocity U_c, can then be substituted

into the linear equation to obtain equation IV-3-1.

$$P = A(\rho) + B(\rho)\left(\frac{A_t}{A}\right)^{1/2}\left(\frac{g_c\, k\, R\, T\, C_m}{\rho}\right)^{1/4} \qquad \text{III - 3 - 13}$$

For an isothermal, constant pressure system, the power dissapation from the wire is only a function of the density ρ.

Equation III -3-13 is not used for determining the relationship between the power dissi pation and the density. The relationship is obtained by calibrating the probe for various compositions.

IV EXPERIMENTAL INVESTIGATION

IV - 1 Experimental Apparatus

The apparatus used in obtaining data for the coaxial flow system is shown in figure IV-1-1. The vertical test column had a square cross section of 8 inches, and was constructed of 3/4 inch thick plexiglass. The column was divided into three sections. The first was a 24 inch entrance region which was long enough to provide a parallel flow field without too much boundary layer buildup. The second section was a 36 inch long test section where mixing of the two streams took place. The third section was a short 12 inch section filled with cardboard honeycomb to prevent any swirling of the fluid due to exit efficts. The joints of each section were gasketed and clamped together with aluminum angle. The three sections were sealed from one another with O-rings to prevent any air from leaking into the system.

The bottom of the test section was connected to the inlet of the blower with 8 inch diameter sheet metal tubing. The blower, a Buffalo Forge type 6E low pressure drop, high capacity blower, was used to suck air through the outer stream of the system in order to obtain a flat flow profile and eliminate the turbulence and temperature effects caused by the blower. A large butterfly valve was placed between the column and the blower to provide a means of changing the outer air stream flow rate in the system.

The inner stream was introduced into the center of the column by a four foot long stainless steel tube, with an outer diameter of 3/4 inches and a wall thickness of 0.0135 inches. A four foot length of tubing was needed to insure fully developed turbulent profiles in the tube. The ratio of the tunnel cross section to the

tube diameter was made large, so that the assumption that wall effects could be neglected was valid. The vertical position of the tube in the column was secured with the use of a plumb bob.

A traversing mechanism, with both lateral and axial movement, designed by L. Boehman,[30] was constructed and mounted on the 36 inch test section of the column. A 24 inch slot milled through the mechanism and the plexiglass to provide access to any point in the mixing region. A four inch diameter port hole was drilled in the 36 inch test section to provide access to the inside of the test section.

The entire cross section of the square duct was probed at the initial mixing region, and at the furthest downstream point data was taken. The results showed the velocity profile of the outer stream was flat except near the walls of the square duct. The boundary layers on the outer walls were approximately 1/4" at the initial mixing plane, and 3/4" at the downstream plane. The corners were probed to make sure the circulation patterns in the corners did not affect the mixing pattern.

Three high precision Brooks rotameters were used to measure the volumetric flow of air and Freon to the inner stream. The three rotameters were selected to provide a continuous range of flow rates. The allowable air range was 0.1 standard cubic feet per minute to 90 standard cubic feet per minute. The air pressure was maintained at 40 pounds per square inch gauge at the outlet of the rotameters. For Freon -12, the flow rates ranged from 0.06 SCFM to 50 SCFM with the outlet rotameters pressure maintained at 65 psig. For Freon C-318, the flow rate ranged from 0.03 SCFM to 30 SCFM, with the pressure maintained at 20 psig. Four pressure gauges were provided to monitor the outlet pressure of the rotameters. Two Acme Cash high flow rate type pressure regulators were placed in line before the

rotameters to regulate the pressure at the outlet of the rotameters. Two needle valves placed in parallel at the outlet of each rotameter provided fine regulation for the flow rates to the inner stream.

The air for the inner stream was supplied by a small two stage compressor, with a maximum capacity of about 20 SCFM. A filter was put on the line between the compressor and the rotameters to remove oil and water that contaminated the air. Freon 12 and Freon C-318, for the inner stream, were supplied from 145 pound cylinders and 218 pound cylinders respectively. A large jacketed steam kettle, capable of holding three freon cylinders, was used to heat the cylinders and maintain the freon pressure. The external stream was room air sucked through the top of the column. An air conditioning filter was placed on the top of the column to remove large dust particles which might endanger the operation of the hot wire anenometer. No means was provided for measuring the valumetric flow rate of the outer stream.

The hot wire anenometry instrumentation needed for measurement of velocity, concentration, and turbulence quantities were supplied by Thermo Systems Incorporated of Minneapolis, Minnesota. Two independent channels were provided to control two wires at a constant temperature. Each unit was equipped with a linearizer that provided a direct measure of the power dissipation of the wire. A unit was provided to take the sum and difference of the outputs of the two channels. A Hewlitt-Packard root mean square voltmeter was supplied to measure the r.m.s. voltage of each signal. A Tektronix 502A dual beam oscilliscope was used to monitor the outputs of the two controlling channels. Four types of probes were supplied with the system. The first was single hot film, 0.002 inches in diameter and 0.04 inches in length.

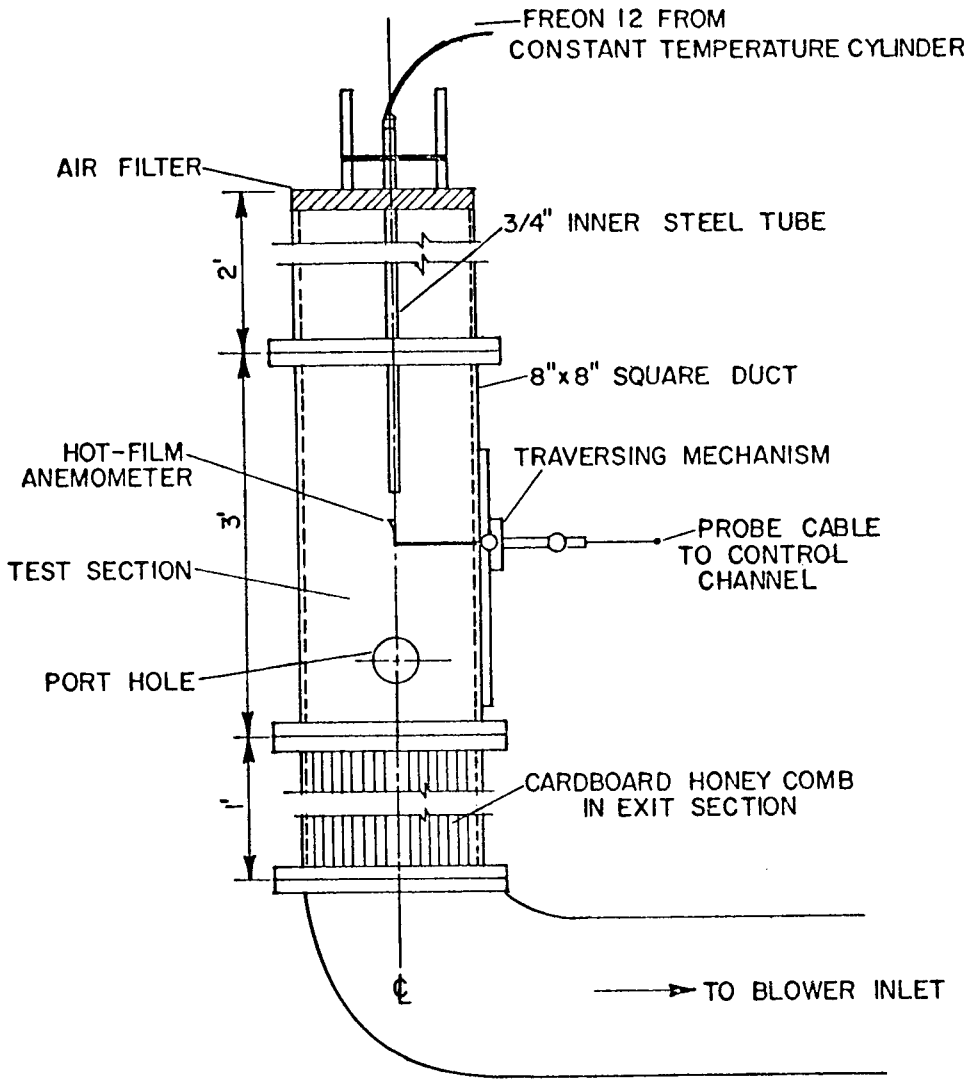

TEST SECTION

FIGURE IV - 1 - 1

A second type was an Xarray probe. This probe had two films, of the same dimensions as the film on the single probe, placed at right angles to each other and 45 degrees to the horizontal. To obtain correct measurements, the wires were mounted such that plane passing through the X formed by the wires was also r, z plane, of the flow geometry. A third type of probe was a parallel wire probe. This probe had two hot films, 0.002 inch diameter by 0.04 inch long film and a 0.001 inch diameter by 0.02 inch long film, mounted parallel to each other on the same probe base. The fourth type of probe was the aspirating probe. A 0.001 inch diameter hot film was mounted in a 0.08 inch inner diameter tube. A jewel bearing, with a 0.007-0.009 inch diameter hole drilled into it, was mounted in the tube in back of the wire. The hole in the bearing was made as small as possible so that a sample of minimum size would be withdrawn from the system. A cenco vacuum pump was used to withdraw the sample from the system, past the hot film and through the bearing. The vacuum pump provided sufficient pressure drop, so that there was sonic flow through the jewel bearing at all times.

IV - 2 Calibration of Instruments

Before making any measurements, calibration procedures were established to provide information about the output of the hot films versus concentration and velocity. Two different sections of pipe were invloved in the calibration, a fifteen foot length of schedule forty 2 inch pipe, and a fifteen foot length of 3/4 outer diameter stainless steel tubing. Each pipe was long enough to insure establishment of fully developed laminar and turbulent profits.

The three high precision rotameters were used to monitor the volumetric flow rates through the calibration system. The compressed air supply was used in all cases, in making air calibrations.

The end of the calibrating pipe was placed in specially constructed 6" by 6" cross section by 24" long plexiglass box. This prevented any stray air currents from affecting the hot film. The hot film probe was placed into the box through a hole drilled into the top of the box. The probe was secured on top by the lateral traversion section of the traversing mechanism.

A calibration for the homogeneous case was obtained first. In the laminar region the centerline, or maximum velocity, was taken to be twice the average velocity. The hot film was placed at the centerline of the two inch pipe, and the power dissipation, for various velocities in laminar flow, was measured by means of a digital voltmeter. The power dissipated from the hot film was plotted against the square root of velocity and a linear relationship was obtained. To check the assumption that the maximum velocity was twice the average velocity, a radial profile across the two inch pipe was taken in intervals of one tenth of an inch. The power dissipation obtained for the radial profile was converted into the radial velocity profile by means of the previously obtained calibration curve. The radial profile was then integrated to obtain the average velocity. The average integrated velocity was then compared to the average velocity predicted from the rotameter reading. These usually agreed within two or three percent.

The line obtained by the previous method was sufficient to describe the power versus velocity relationship in the velocity ranges of interest for air. However, for pure Freon 12, the maximum laminar bulk velocity obtainable was only about 2 feet per second. Information was then needed relating the maximum velocity to bulk velocity for turbulent profiles in the two inch pipe. It was assumed that the turbulence introduced into the flow stream had little affect on the average measurement. If the turbulence intensities in the axial and radial direction are of the same magnitude, the assumption is valid. For turbulent pipe flow this is approximately true.

Six turbulent Reynolds numbers were selceted ranging from 5,110 to 29,400.

The volumetric flow rate needed to obtain these Reynolds numbers were metered through the high precision rotameters. The power dissipation was measured at the centerline in each case. A check was made to verify that the maximum power dissipation occurs at the centerline. The probe was moved until a visual maximum was found by reading the output of the hot film on the digital voltmeter. This maximum was always close to or on the centerline.

The maximum power dissipation for each turbulent profile was converted into a corresponding velocity by using the straight line relationship that had been obtained using laminar profiles. The ratio of the average velocity, calculated from the volumetric flow rate and the cross sectional area of the pipe, to the maximum velocity was plotted versus the Reynolds number. This plot is shown in figure IV-2-1. It was assumed that this relationship was independent of the fluid, and could be applied to Freon 12, and Freon 12 - air mixtures.

Since the output of the hot film depends on both concentration and velocity, calibration curves had to be obtained for Freon 12 - air mixtures and Freon C-318-air mixtures. A mixing section was built from short sections of 2 inch pipe and couplings. The couplings were tightly packed with copper shreads to insure complete mixing.

The calibration of the Freon 12-air mixtures was based on the turbulent Reynolds numbers which were used in calculating the average to maximum velocity ratio for the calibration of the air system. For each mole fraction of Freon 12 of 0.2, 0.4, 0.6, 0.8, flow rates of Freon 12 and air were calculated to give the proper set of Reynolds numbers. In the calculation of the Reynolds number, the physical properties of the mixture was assumed to be a linear combination of the physical properties of each gas.

For each given Reynolds number the proper flow rates were metered through the rotameters and mixed in the mixing section. The maximum power dissipation

was measured at the outlet of the fifteen foot section of two inch pipe. The corresponding maximum velocity was calculated from the velocity ratio versus Reynolds number plot, which had been obtained for the air calibration. The power dissipation was then plotted versus the square root of the velocity for a constant composition. A straight line was drawn through the points in each case. Typical curves are presented in figures IV-2-2 and IV-2-3.

The composition measuring device, the aspirating probe was calibrated at mole fraction intervals of 0.1 for Freon 12. The flow rates were calculated such that the maximum velocity in the pipe was the same in each case. As in the single wire case the volumetric flow rates were metered, mixed and sent through the fifteen foot section of 2 inch pipe. The probe was placed at the centerline of the outlet of the pipe. The power dissipation was measured and plotted versus the composition. A typical curve is presented in figure IV-2-4.

The calibration of the Freon C-318-air system could not be done in the same manner as the Freon 12-air system. For the same set of Reynolds numbers used in the Freon 12 calibration, the same rotameter was needed to obtain the volumetric flow rates of both Freon C-318 and air. To avoid this problem the calibration was done in a 15 foot long, 3/4 inch diameter, section of stainless steel tubing. This also helped cut down the mass of Freon C-318 used in calibrations.

A bulk to maximum velocity ratio versus Reynolds number plot for air was obtained for 3/4 inch diameter tube. Again it was assumed that this plot was independent of the fluid, and could be applied to Freon C-318 and Freon C-318 - air mixtures.

Two Reynolds numbers were chosen for each mole fraction fo Freon C-318 of 0.2, 0.4, 0.6 and 0.8. The Reynolds numbers were chosen such that the volumetric flow rates for air and Freon C-318 could be metered through separate rotameters. For each Reynolds number the volumetric flow rates were metered through

the rotameters and mixed in the mixing section. The maximum power dissipation was measured at the outlet of the 15 foot section of stainless steel tubing. The corresponding maximum velocity was calculated from the velocity ratio versus Reynolds number plot for the 3/4 inch tube. The power dissipation was plotted versus the square root of velocity for a constant composition. A straight line was drawn through the points for a constant composition. Typical curves are presented in figures IV-2-6.

There was some difficulty in obtaining the calibration curve of the Freon C-318-air system for the aspirating probe. The molecular weight of Freon C-318 is about seven times that of air. This would indicate a good spread in power dissipation from one gas to the other. But the physical properties of the gases are such that not much change in the power dissipation was found with a change in the composition. In order to obtain a good spread in the power dissipation, the film had to be operated at a higher than normal temperature, which in turn caused the output of the film to drift as a function of time. A calibation curve was taken, as quickly as possible, in mole fraction intervals of 0.1 of Freon C-318. Figure IV-2-7 shows the calibration curve.

Calibration curves were obtained for the parallel film probe for both the Freon 12-air system, and Freon 12-air system, and Freon C-318-air system in the same way the calibration curve for the single film was obtained. Calibration curves for the Xarray probe were obtained for air only.

IV - 3 Experimental Procedure

For the homogeneous case, a single hot film sensor was placed in the test section. The probe was mounted in a vertical position and was connected to the horizontal probe holder by a right angle adapter. Setting the probe in this position minimized the interference caused by the probe and probe holder to the flow.

The sensor was aligned with the outer edge of the 3/4 inch diameter pipe with a cathometer. The sensor was then moved 3/8 inches to the centerline. The cathometer was also used to align the sensor with the end of the tube to indicate the origin of the system.

The volumetric flow rate needed for a particular run was set on one of the three precision rotameters, and the blower was turned on for external stream flow. The centerline value was checked by making a radial traverse until a visual maximum of the initial profile was obtained. If the visual centerline differed from the initial one, the visual centerline was used. A set of average readings were taken with a digital voltmeter at various radial and axial positions. The system was completely shut down, and the single hot film was replaced by the Xarray probe. The alignment procedure for the Xarray probe was the same as for the single sensor. The system was turned back on using the same flow settings that were used for the single sensor. Readings were taken at the same positions as the readings for the single probe. The average component of each wire was read on the digital voltmeter, and the root mean square voltage was read on the r.m.s. meter for each film, the sum of the outputs of the film, and the difference of the outputs of the films. These two traverses provided all the information needed for the calculation of velocity and the turbulence quantities.

Two separate traverses were used to obtain the data. The two traverses are not related to each other in the calculations, except in the calculation of the eddy kinematic viscosity, but for consistancy in the reportings of the data, the same conditions should exist in each case. A run was repeated two months after the original data had been taken, and the velocity profiles agreed within two percent. So it can be assumed that for the two traverses, even though there is a shut down period, the conditions are the same.

The heterogeneous case was more complicated. The power dissipation from the hot film is dependent on both the velocity and composition of the flowing fluid. Two separate traverses were made to calculate the velocity, first a traverse with the aspirating probe to determine the composition, and a traverse with a single hot film to determine the velocity. The calculation of the velocity depends on knowing the composition at the point of interest. Therefore, the traverses are related to each other in the calculations. Positioning and alignment of probes were carefully determined with precision rules within $\pm$ 0.005 inches, to make sure that for each separate traverse, the data points were taken at the same place. The average velocity and density data for the Freon 12 air runs and Freon C-318 runs were determined in this manner.

For four Freon 12-air runs, a third traverse was made with parallel film probe, in order to determine the velocity turbulence of the system. The calculation of the turbulence depends on both the velocity and the concentration, and therefore on two previous traverses. Again extra care was taken in aligning and positioning of the probe.

For the Freon C-318 runs, the aspirating probe wire tended to drift because it was operated at a high temperature. Before each traverse a check was made on the pure Freon C-318 reading and a pure air reading. If these checked readings were different than the original readings, a curve was drawn similar to the original calibration curve, using the new pure readings as the endpoints.

III - 4 Calculation Procedures

All the calculations for the homogeneous system were performed on an I.B.M. 7040 computer. The linear power versus square root of velocity relationship, and equations III-2-26, 27, and 28 were programmed to obtain the average velocity and the turbulence quantities in the homogeneous system. The slope and intercept characteristics of the single hot film, the intercept characteristics from the Xarray probe, the r.m.s. values of the power dissipation from the Xarray probe, and the average power readings from the single wire probe and the Xarray probe were used as inputs to the computer program. The average velocity, the axial turbulence intensity, the radial turbulence intensity, and the turbulent shear stress were obtained in tabular form as output from the computer.

For the heterogeneous system the output of the aspirating probe was converted into the corresponding density by using the calibration curve obtained for either the freon-12-air mixtures, or the freon C-318 - air mixtures (Figure IV-2-4, or IV-2-7). From the density the corresponding slope " B ", and intercept " A ", were obtained (Figure IV-2-3, or IV-2-6) for the linear power versus square root of velocity relationship. The velocities were then obtained on a desk calculater,

$$\overline{U} = \left[\frac{\overline{P} - \overline{A}(\rho)}{\overline{B}(\rho)} \right]^2 .$$

A computer program was written to solve equations III-3-4, 5, and 6, simultaneously for the turbulence quantities in a heterogeneous system. The slope and intercept versus density curves were approximated by a 20th order polynomial obtained from a special Illinois Institute of Technology computer center users program called Sinpak. The coefficients of the polynomial, the r.m.s. values of the power from the parallel probe, and the average velocity and density were used as inputs to the program. The experimental data was not sufficiently accurate to solve

the three equations simultaneously. The program was altered to solve two equations (III-3-4, and III-3-5) under the constraint that $\left| \frac{\overline{\rho' u'}}{\sqrt{\overline{\rho'^2}}\sqrt{\overline{u'^2}}} \right| \leq 1$, and the density and velocity fluctuations must be positive. The following table is a typical set of values obtained for

$$\frac{\overline{U}_o}{\overline{U}_i} = 5.4, \quad \frac{\rho_o}{\rho_i} = 0.25, \quad \frac{z}{r_o} = 5.6, \quad \frac{r}{r_o} = 0.56.$$

$\frac{\sqrt{\overline{\rho'^2}}}{\overline{\rho}}$	$\frac{\overline{\rho' u'}}{\sqrt{\overline{\rho'^2}}\sqrt{\overline{u'^2}}}$	$\frac{\sqrt{\overline{u'^2}}}{\overline{U}}$
0.23	-1.00	0.214
0.30	-0.86	0.216
0.40	-0.77	0.220
0.50	-0.74	0.226
0.60	-0.73	0.232

From the table it can be seen that there is a wide variation in the relative density fluctuations, $\frac{\sqrt{\overline{\rho'^2}}}{\overline{\rho}}$ while hardly any change occurred in the relative velocity fluctuations, $\frac{\sqrt{\overline{u'^2}}}{\overline{U}}$. Although one cannot predict a value of the relative density fluctuations, it might be assumed that $\frac{\sqrt{\overline{\rho'^2}}}{\overline{\rho}}$ lies between 0.23 and 0.60. Then the relative velocity fluctuations can be reported, with an accuracy of = 5%, as 0.220.

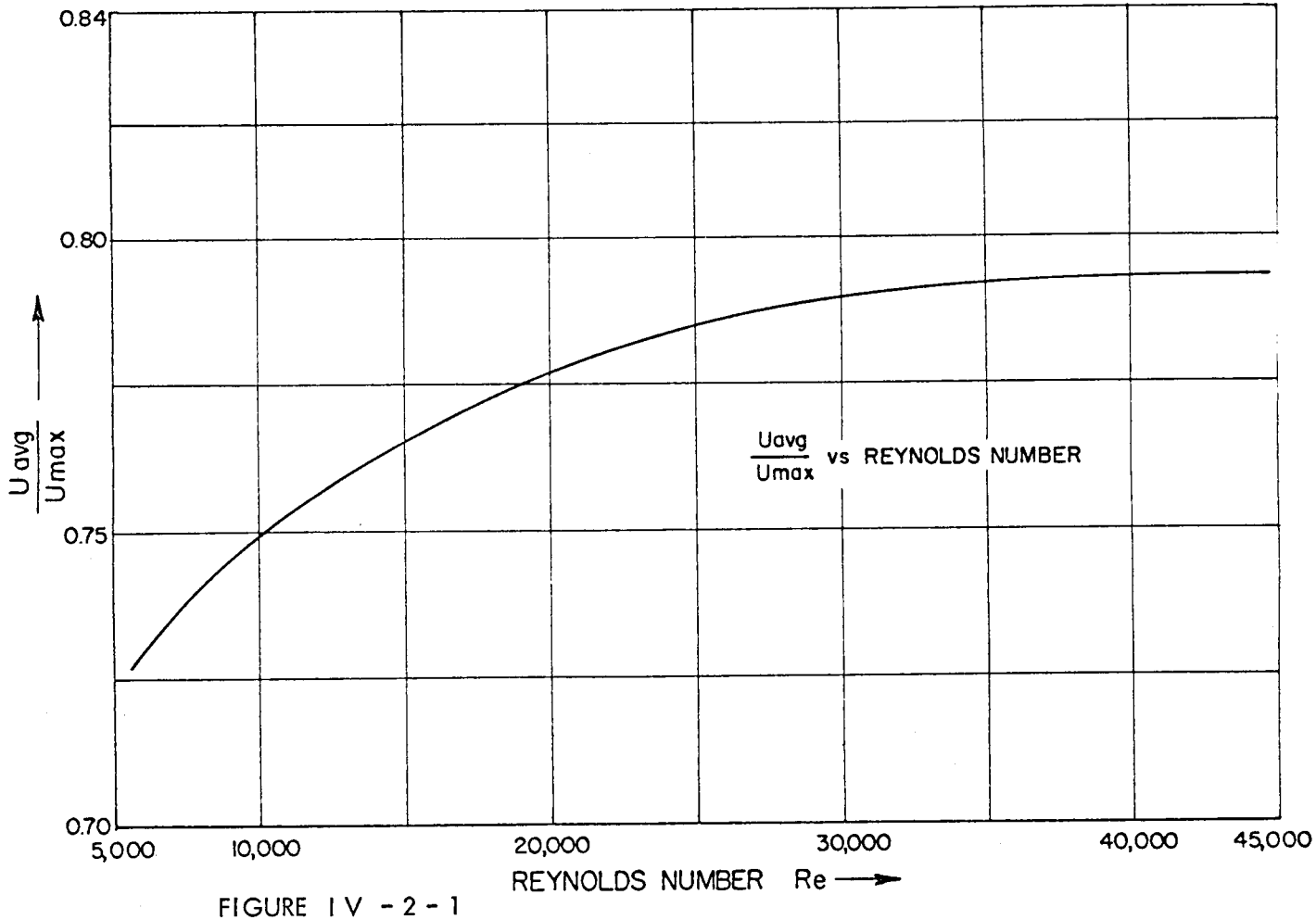

FIGURE IV - 2 - 1

MAXIMUM TO AVERAGE VELOCITY FOR SCHEDULE 40, 2" PIPE

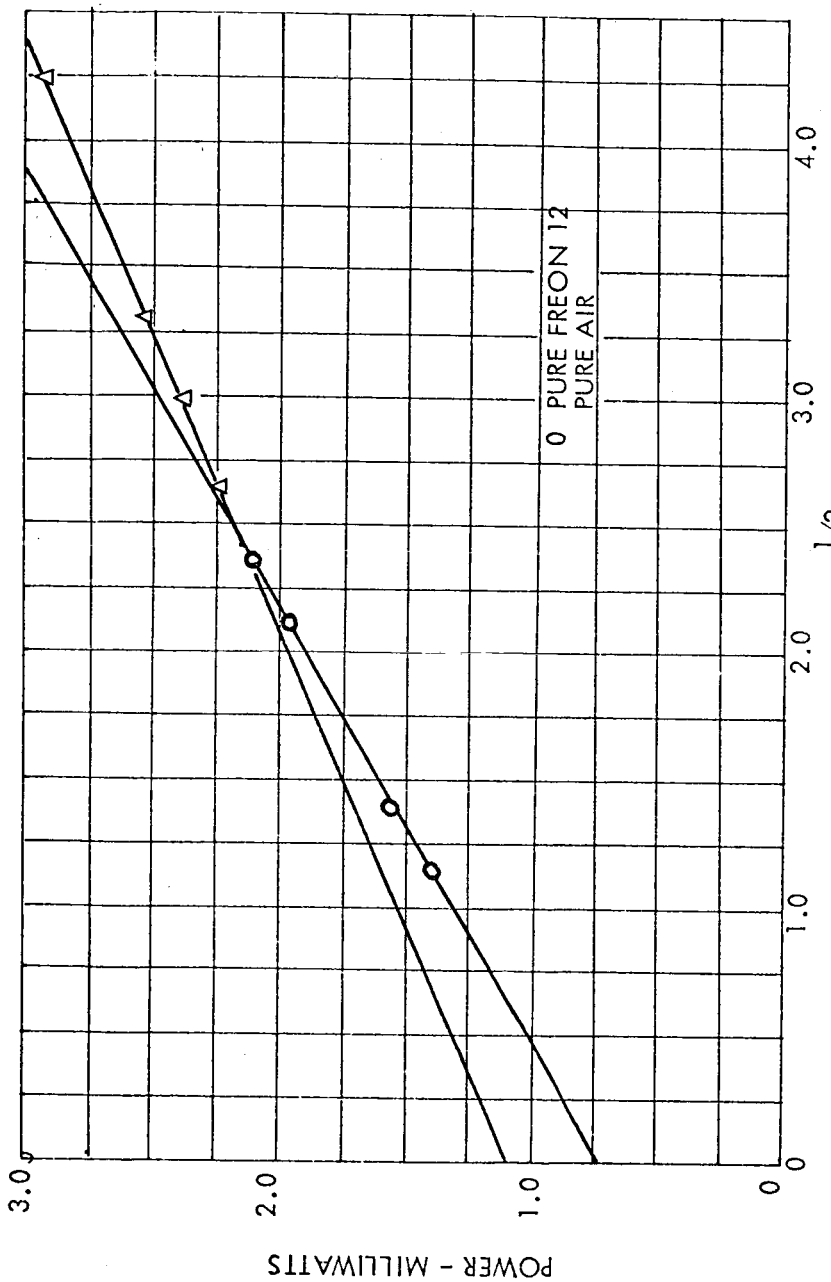

FIGURE IV - 2 - 2

CALIBRATION CURVES OF SINGLE WIRE PROBE

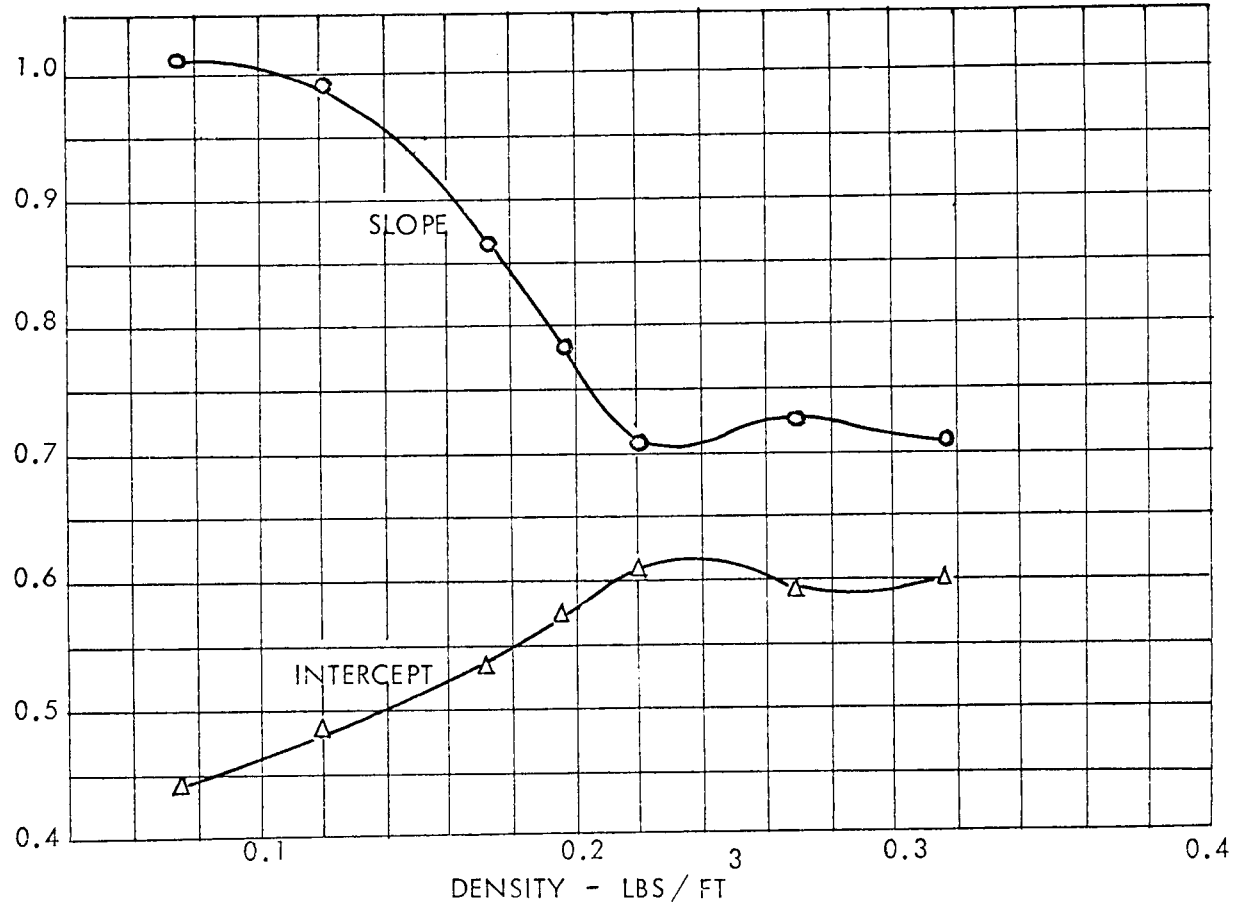

FIGURE IV - 2 -3

SLOPE "B" AND INTERCEPT "A" AS A FUNCTION OF DENSITY FOR FREON 12 AIR MIXTURES

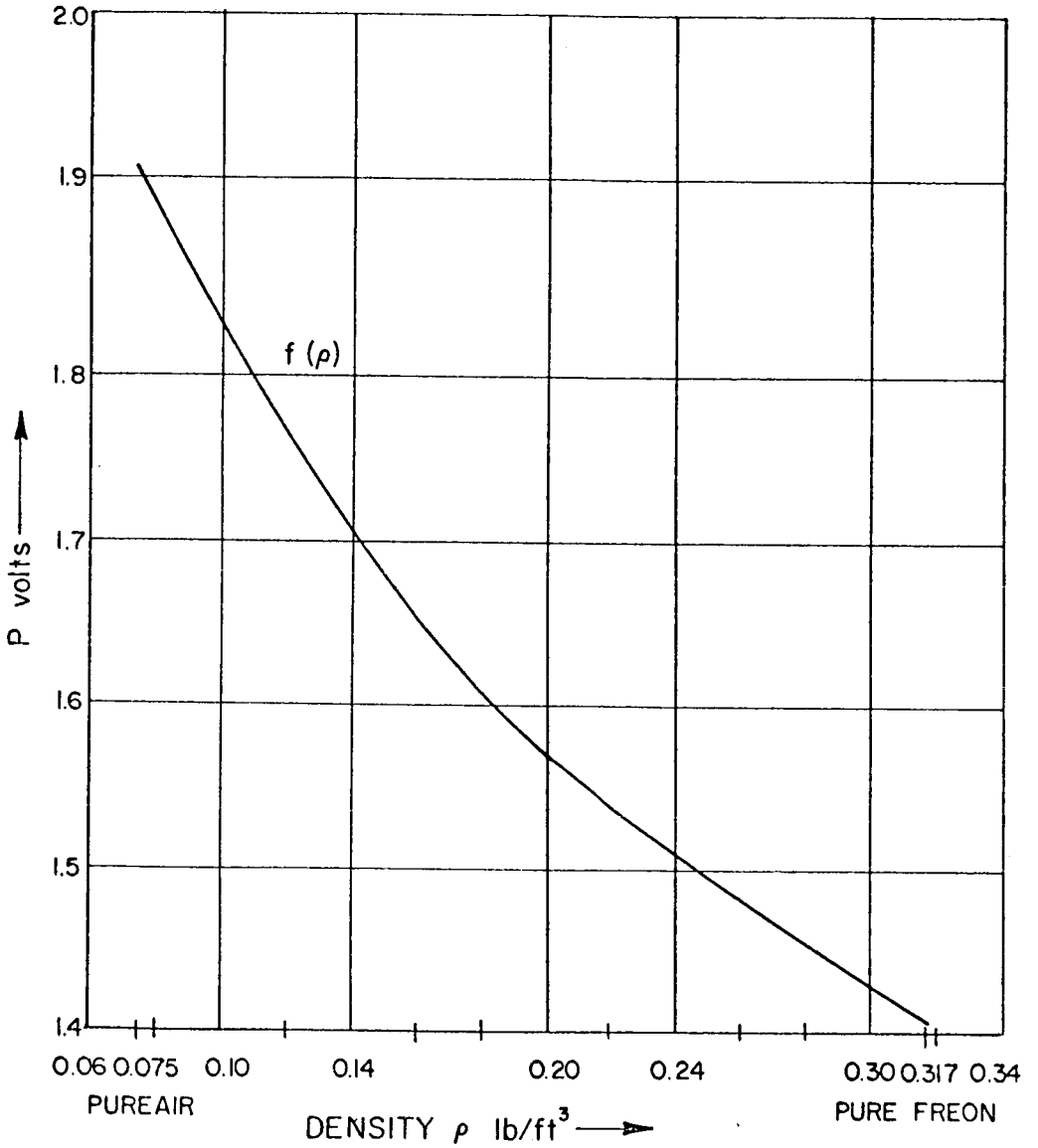

FIGURE IV - 2 - 4

ASPIRATING PROBE CALIBRATION CURVE FOR FREON - 12, AIR MIXTURES

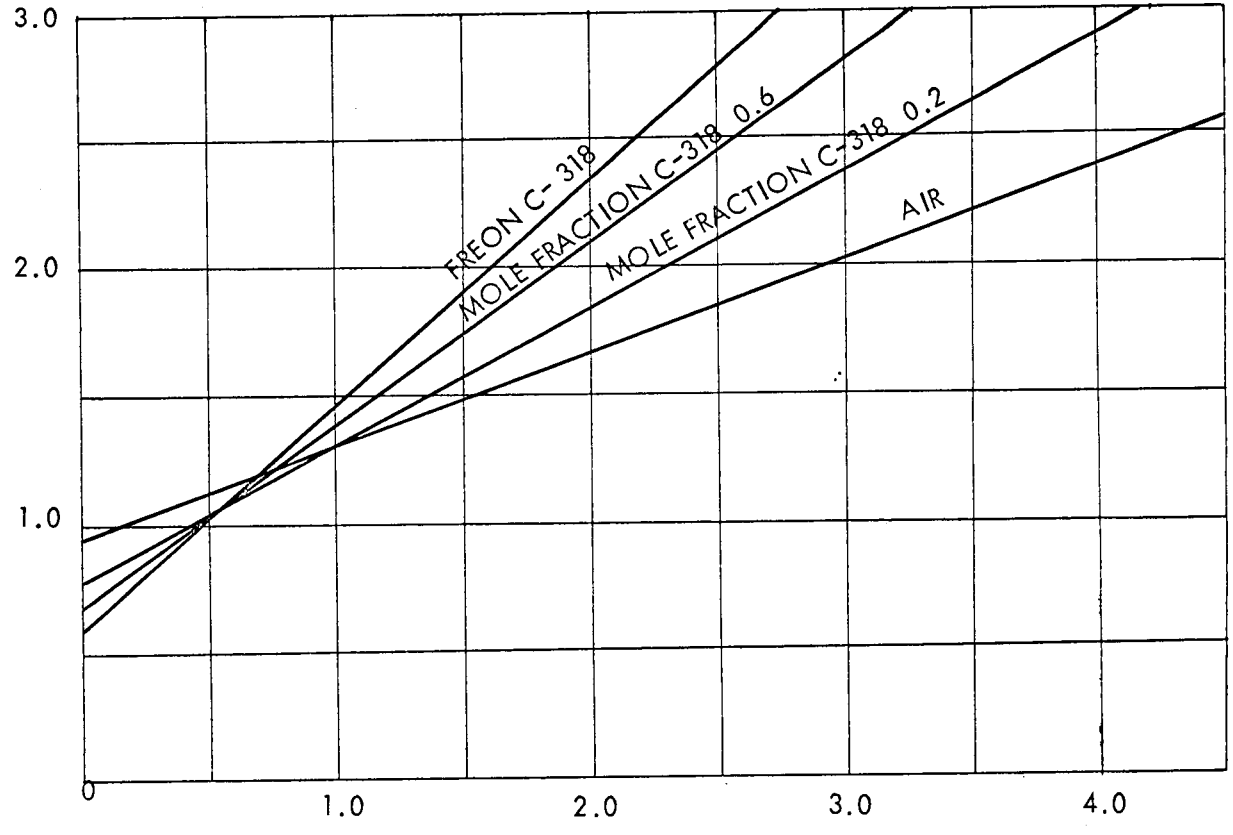

FIGURE IV - 2 - 5

CALIBRATION VURVE FOR SINGLE HOT FILM FOR FREON C - 318 - AIR MIXTURES

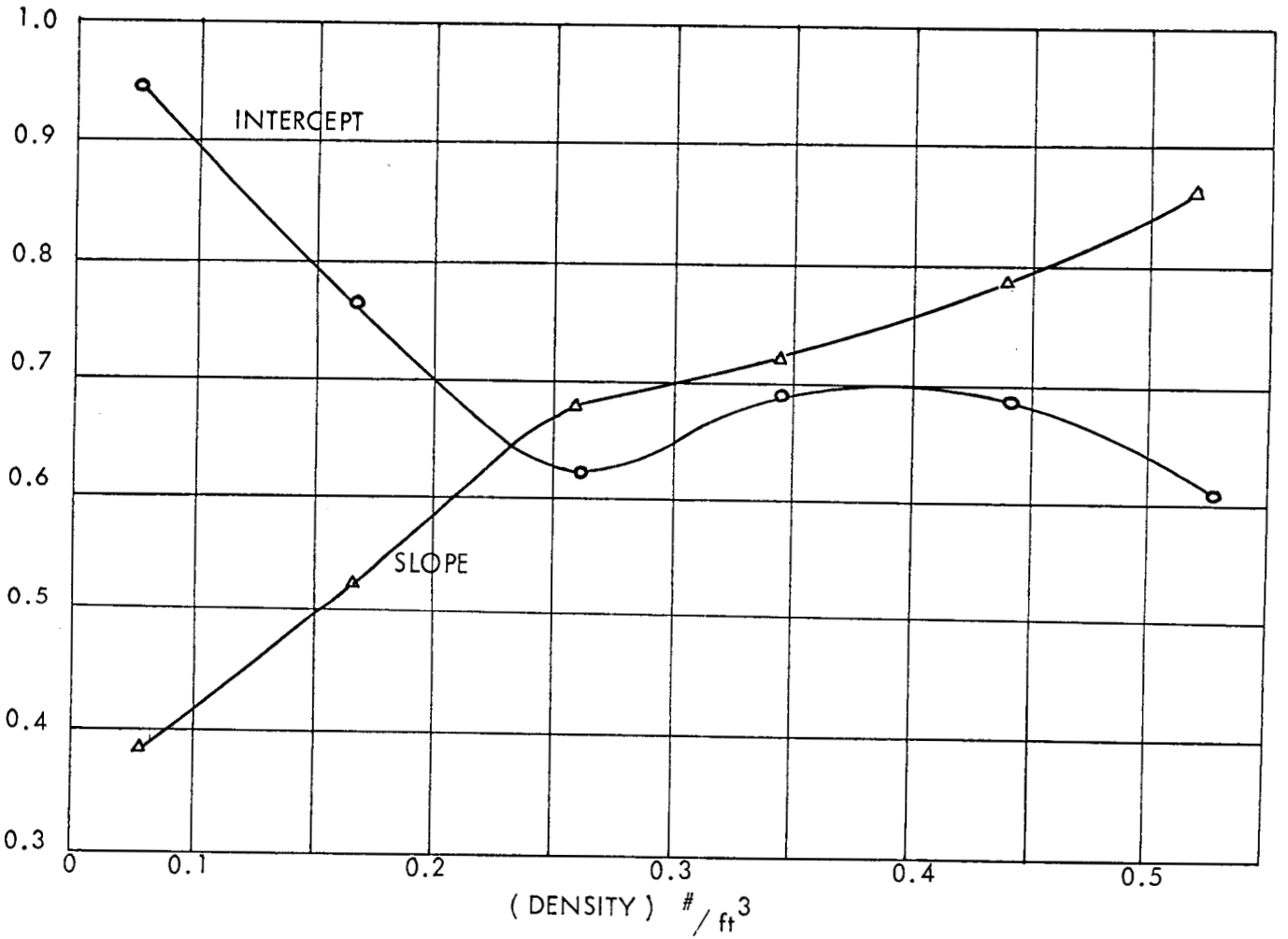

FIGURE IV - 2 - 6

INTERCEPT "A" AND SLOPE "B" VERSUS DENSITY FOR FREON C-318 - AIR MIXTURES

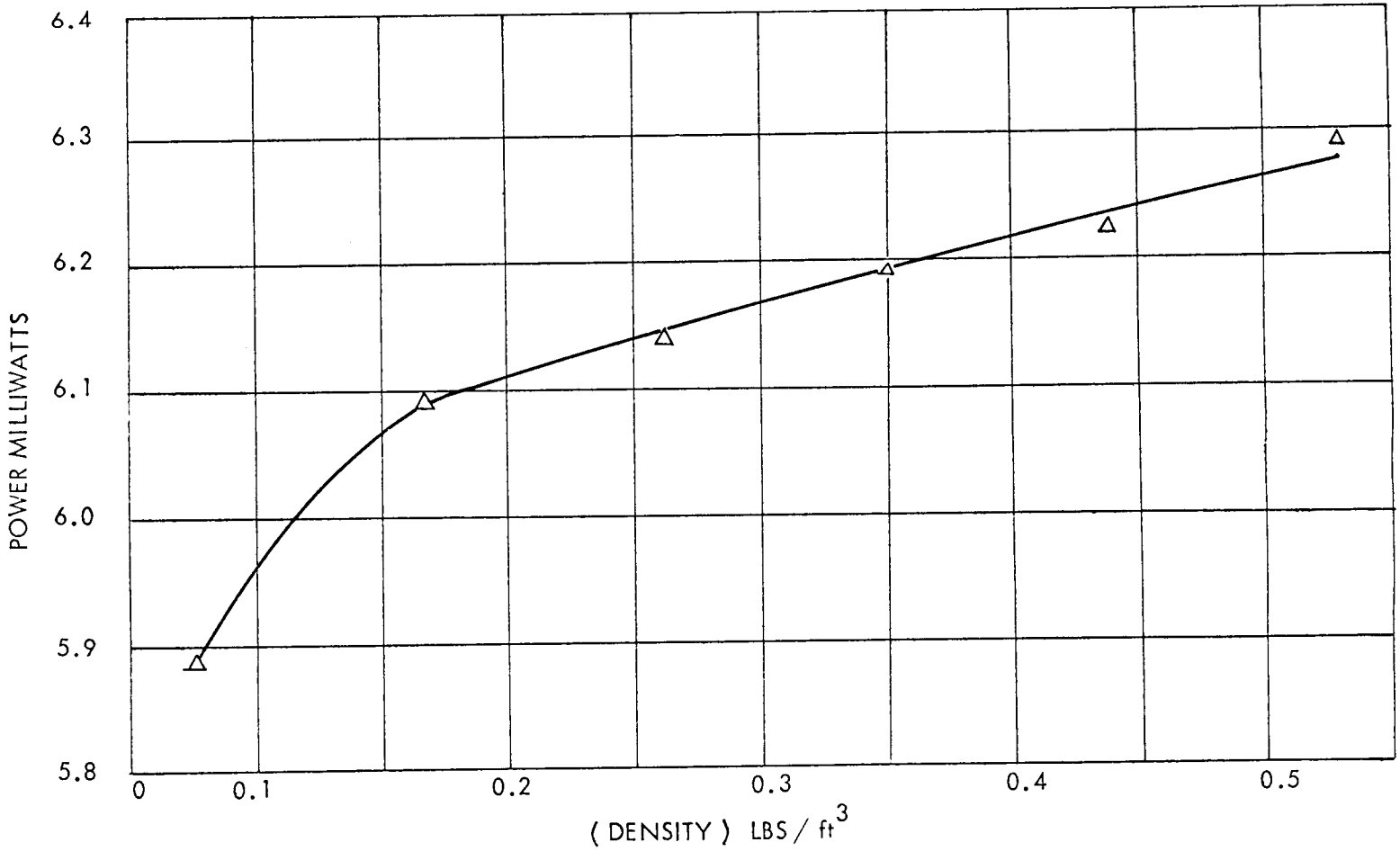

FIGURE IV - 2 - 7

ASPIRATING PROBE CALIBRATION CURVE FOR FREON C-318- AIR MIXTURES

V RESULTS AND DISCUSSION

V - 1 Homogeneous Case

Data is presented for six different outer stream to inner stream velocity ratios, 39.5, 28.5, 16, 8, 3.4 and 1. The dimensionless velocity profiles plotted as $\frac{\overline{U}}{\overline{U}_o}$ versus $\frac{r}{r_o}$, where $\overline{U}$ is the time averaged point velocity, and $\overline{U}_o$ is the free stream velocity, are shown in figures V-1-1 through V-1-6. Except for the three high velocity ratio cases, the velocity profiles behaved in the following manner. Initially a momentum trough is present caused by the boundary layer buildup on both the inside and outside of the dividing tube. While the flow in the trough is being accelerated, the velocity at the centerline decreases. Once this trough has been depleted, the velocity profile is represented by increasing continuous curve with the minimum at the centerline. At each succeeding axial position, the whole profile is accelerated, but still keeps the same shape. Figure V-1-5, the velocity profile for the equal bulk velocity case, illustrates the trough caused by the dividing tube. The trough is still present after an axial position of $\frac{z}{r_o} = 16.8$ has been reached for this case.

Figure V-1-7 is a similarity plot of the velocity profiles, plotted as $\frac{\overline{U} - \overline{U}_o}{\overline{U}_c - \overline{U}_o}$ versus $\frac{r}{r_{1/2}}$ where $\overline{U}$ is the time averaged velocity, $\overline{U}_o$ is the free stream velocity, $\overline{U}_c$ is the centerline velocity at the particular axial position the profile is being calculated, and $r_{1/2}$ is the half-radius, the point where the velocity $\overline{U}$, is one half the sum of the free stream velocity and the centerline velocity. The similarity curve was calculated using profiles from each velocity

ratio except the equal velocity case. The curve shows that for axial positions far downstream of the initial region, $\frac{z}{r_o} > 5.6$ the profiles are similar.

The Reynolds numbers for the velocity ratios of 39.5, 28.5, and 16 are correspondingly, 435, 583, and 1060, based on the diameter of the inner stream tube. These Reynolds numbers indicate that the flow in the tube should be laminar. With no external flow, the velocity profile was calculated at the outlet of the tube. The profile was laminar and no turbulence existed inside the tube. However, when the outer stream was turned on, large fluctuations were obtained at the outlet of the tube. Upon further investigation it was found that with no flow in the inner stream and full flow in the external stream, large fluctuations were found in the inner tube. An average component was found to exist, indicating that a circulation pattern existed inside the tube. The hot film was used to probe up to two inches inside of the tube. At two inches, the average component had dissipated, but small fluctuations, indicated by the oscilloscope used to monitor the output of the hot film, still existed.

For these high velocity ratios, or low inner stream velocities, these circulations and fluctuations are super-imposed on the mean flow. The nature of this phenomenon is not clear. No pressure profiles were taken around the entrance of the mixing region. This effect must be due to the sudden expansion of the outer stream around the solid boundary. The fluid moves in radially and converges at the centerline. From the centerline the fluid moves axially away from the tube, and since the tube is open the fluid moves into the tube setting up circulation patterns.

Figure V-1-8 shows the velocity profile along the centerline for the

three high velocity ratio flows. Due to the phenomenon of the high fluctuations in the tube, a peculiar profile is obtained between the axial positions $\frac{z}{r_o} = 0$ and $\frac{z}{r_o} = 2.8$. The velocity first decreases then increases and reaches a peak at $\frac{z}{r_o} = 1.4$, the velocity then decreases, reaching a minimum at $\frac{z}{r_o} = 2.8$. From this position the centerline velocity behaves as stated before, increasing with axial position.

Figure V-1-9 shows the centerline velocity profile for the velocity ratios of 8, 3.4 and 1. Although no data was recorded in the initial region, indicated by dotted lines, visual observation indicated that the peculiar double hump was not present. The behavior of these profiles were described and discussed earlier in this section.

Figure V-1-10 shows the centerline axial turbulence intensity, $\frac{\sqrt{\overline{u'^2}}}{\overline{U}}$ for all six velocity ratios. The dotted lines in the region very close to the tube entrance show the large fluctuations present in that area for the three high velocity ratios, 39.5, 28.5 and 16. For the three low velocity ratios, 8, 3.4 and 1, the initial turbulence level was that of a fully developed turbulent profile in a pipe. Also there was no difference detected in the initial turbulence level whether there was no flow in the external stream or full flow in the external stream. For the three high velocity runs the peak turbulence occurs at $\frac{z}{r_o} = 2.8$, this is the same position where the centerline velocity reaches its second minimum before behaving in a regular manner. As the velocity ratio is decreased this peak turbulence decreases. For the three lower velocity ratio runs the peak begins to move further downstream and decreases with decreasing velocity ratio.

Figures V-1-11 and V-1-12 represent the radial distributions of the

axial turbulence intensity $\frac{\sqrt{\overline{u'^2}}}{\overline{U}}$ and the radial turbulence intensity $\frac{\sqrt{\overline{v'^2}}}{\overline{U}}$, for the velocity ratio 39.5. From figure V-1-11, at an axial position $\frac{z}{r_o} = 1.4$, the peak axial turbulence intensity occurs at $\frac{r}{r_o} = 0.6$. At the next axial position $\frac{z}{r_o} = 2.8$, the peak has moved close to the centerline and is only slightly larger then the centerline value. The peak turbulence intensity at this position is about the same as it was at the previous axial position. There is a large decrease in the turbulence level in moving to the next axial position $\frac{z}{r_o} = 5.6$. It has been previously stated that after $\frac{z}{r_o} = 2.8$ the profiles began to behave as expected. Now it is seen that a marked decrease in turbulence occurs at this point. At each succeeding axial position the turbulence intensity decreases. Each radial profile is characterized by a maximum turbulence intensity, slightly larger than the centerline value. This maximum moves radially away from the centerline as the axial position is increased.

The radial turbulence intensities $\frac{\sqrt{\overline{v'^2}}}{\overline{U}}$, follows a somewhat similar pattern. At an axial position $\frac{z}{r_o} = 1.4$ the peak intensity occurs at approximately $\frac{r}{r_o} = 0.6$. At the next axial position $\frac{z}{r_o} = 2.8$, the peak has moved to the centerline. Then at each succeeding axial position the intensities decrease. Although there are inaccuracies in the data, there appears to be no maximum in the radial direction of the radial turbulence intensities.

Figure V-1-13 shows the turbulent shear stress distribution $\overline{u' v'}$ for the highest velocity ratio. It is typical of the rest of the shear stress distributions. The profiles begin at an axial position $\frac{z}{r_o} = 4.2$. The shear stress must be zero at both the centerline and in the free stream, and is negative in the mixing region. The absolute magnitude of the shear stress increases from the centerline and

reaches a maximum at $\frac{r}{r_o} = 0.6$, for $\frac{z}{r_o} = 4.2$. As the axial position is increased, the absolute magnitude of the shear stress decreases, and the maximum moves away from the centerline. Figures V-1-14 through V-1-22 show the turbulence quantites $\frac{\sqrt{\overline{u'^2}}}{\overline{U}}$, $\frac{\sqrt{\overline{v'^2}}}{\overline{U}}$, and $\overline{u'\ v'}$ for various velocity ratios.

From the turbulent shear stress and the velocity profiles, the eddy kinenatic viscosity can be calculated,

$$\epsilon = \frac{-\overline{u'\ v'}}{(\frac{\partial \overline{U}}{\partial r})_z}$$

Since both the turbulent shear stress and the velocity gradient have large errors near the centerline and near the free stream, a representative value of the eddy kinenatic viscosity was obtained by finding the greatest velocity gradient for a profile, then obtaining the turbulent shearing stress at the point of the maximum gradient,

$$\epsilon_c = \frac{-(\overline{u'v'})_{r_c}}{(\frac{\partial \overline{U}}{\partial r})_{z,\, r_c}}$$

The value, ϵ_c was thought to be the most reliable. Figure V-1-22 shows the axial variation of ϵ_c. The value of ϵ_c does not change much with axial position. The average value of ϵ_c indicates that the turbulent transport is about two orders of magnitude larger than molecular transport. The magnitude of ϵ_c 0.015 $ft^2/sec.$ agreed with the values obtained by Boehman. Because of the errors associated with $\overline{u'\ v'}$ and $(\frac{\partial \overline{U}}{\partial r})$ good radial profiles were unobtainable. Also data from two separate traverses had to be used to calculate ϵ_c thus compounding the error.

A run was taken of a turbulent jet issuing into a stagnant field. The half

radius was plotted versus the axial position. A straight line resulted, as is expected from Prandtl's theory for the free jet case, and an angle of 5^{o} was found for the slope of the straight line. This is the same angle Squire and Trouncer found that gave a Prandtl's mixing length constant, c^2, equal to 0.0067.

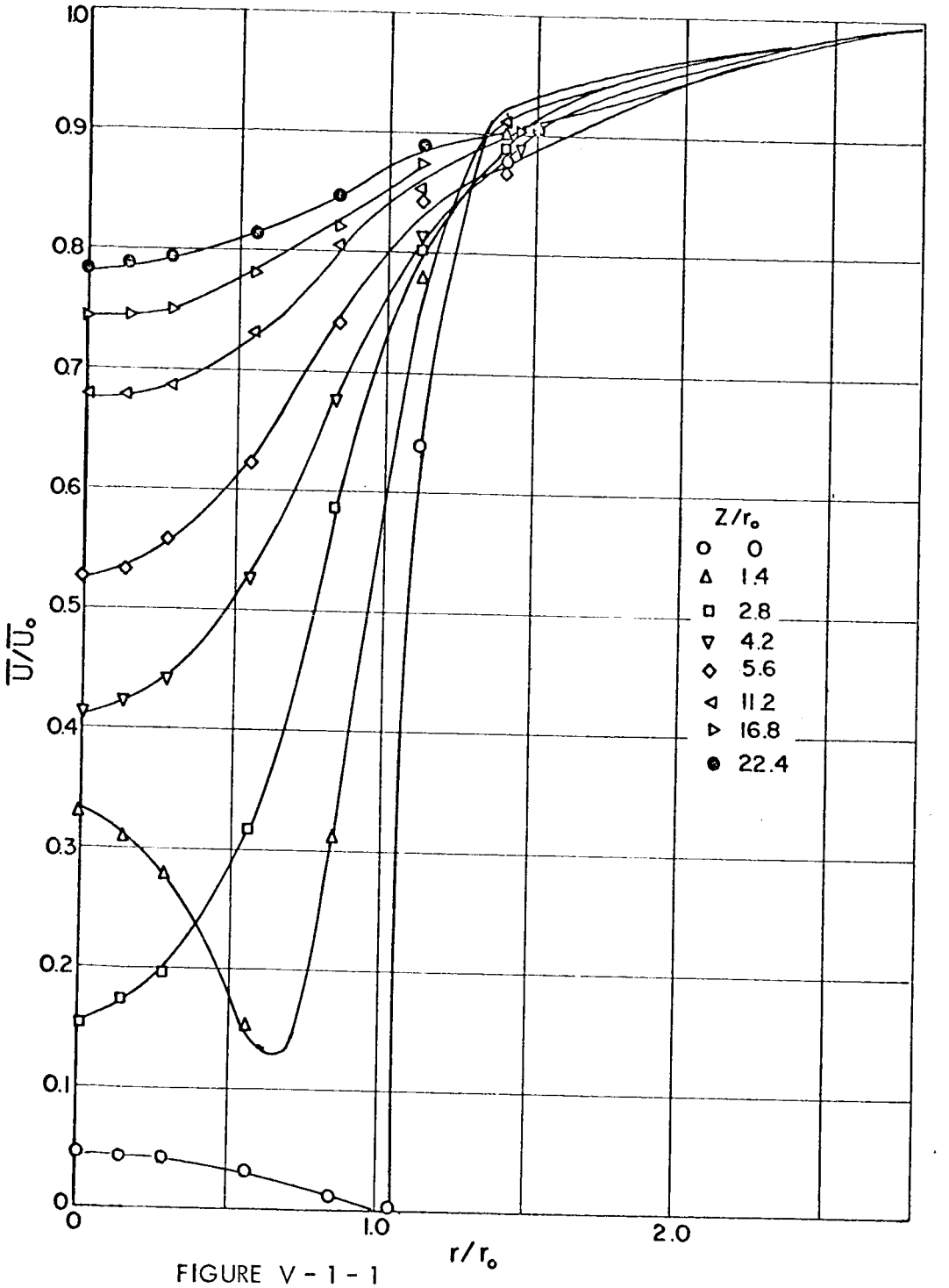

FIGURE V - 1 - 1

DIMENSIONLESS VELOCITY PROFILES, HOMOGENEOUS $\frac{\overline{U}_o}{\overline{U}_i} = 39.5$,

$\overline{U}_o = 48$ ft/sec.

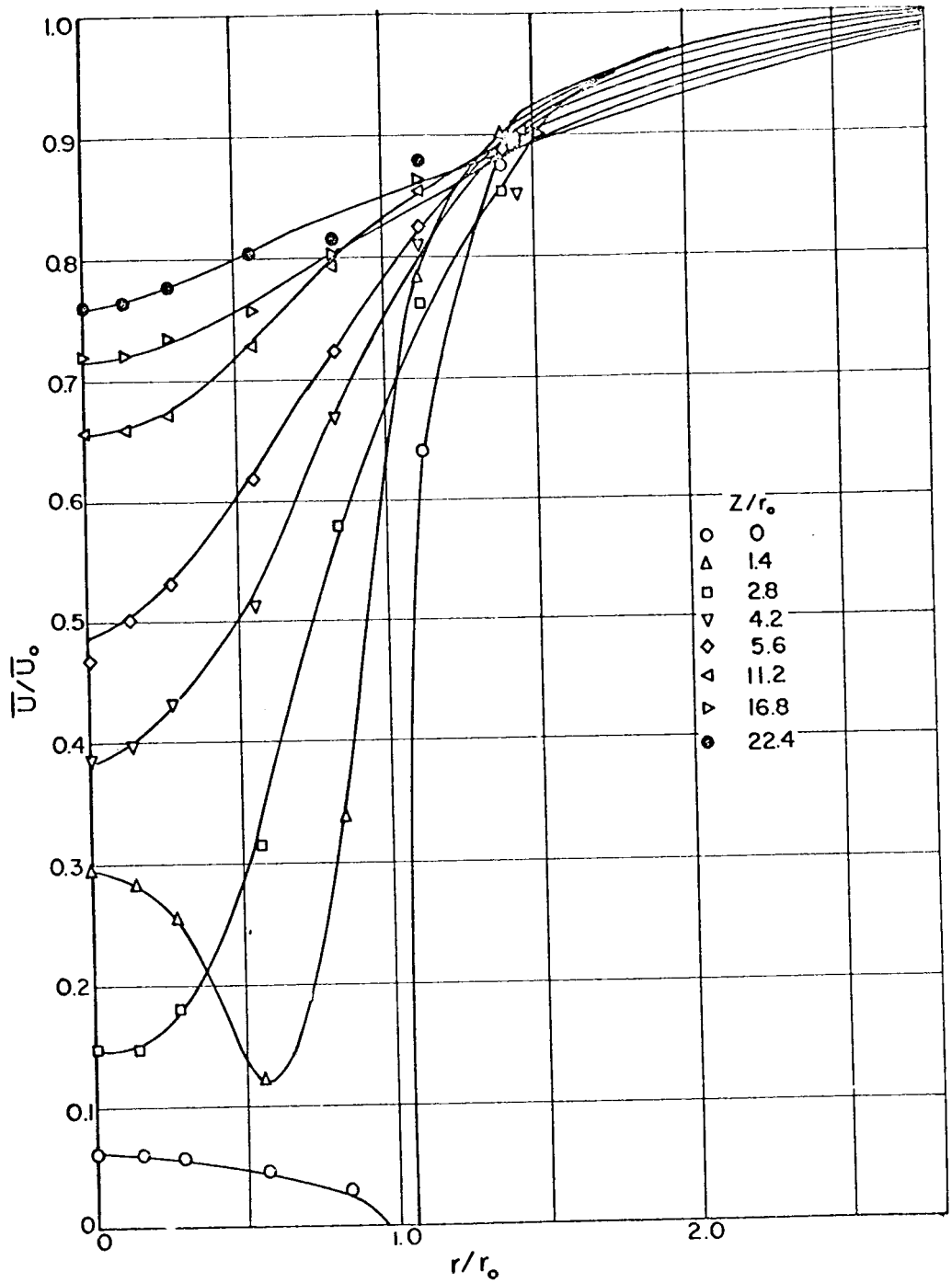

FIGURE V - 1 - 2

DIMENSIONLESS VELOCITY PROFILES, HOMOGENEOUS,

$\frac{U_o}{U_i} = 28.5$, $U_o = 48$ ft / sec.

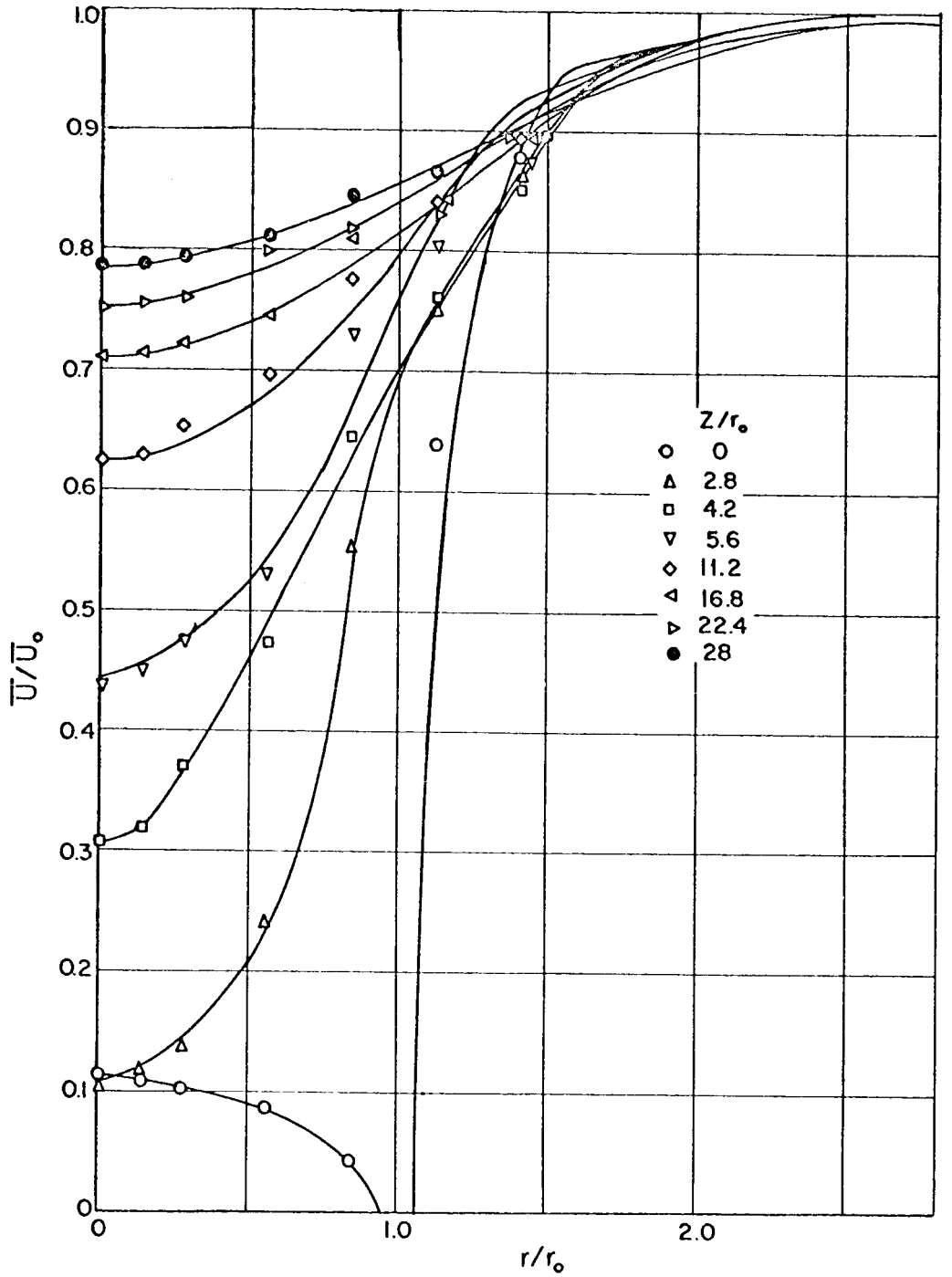

FIGURE V - 1 - 3

DIMENSIONLESS VELOCITY PROFILES HOMOGENEOUS,

$\frac{U_o}{U_i} = 16, \quad U_o = 48$ ft/sec

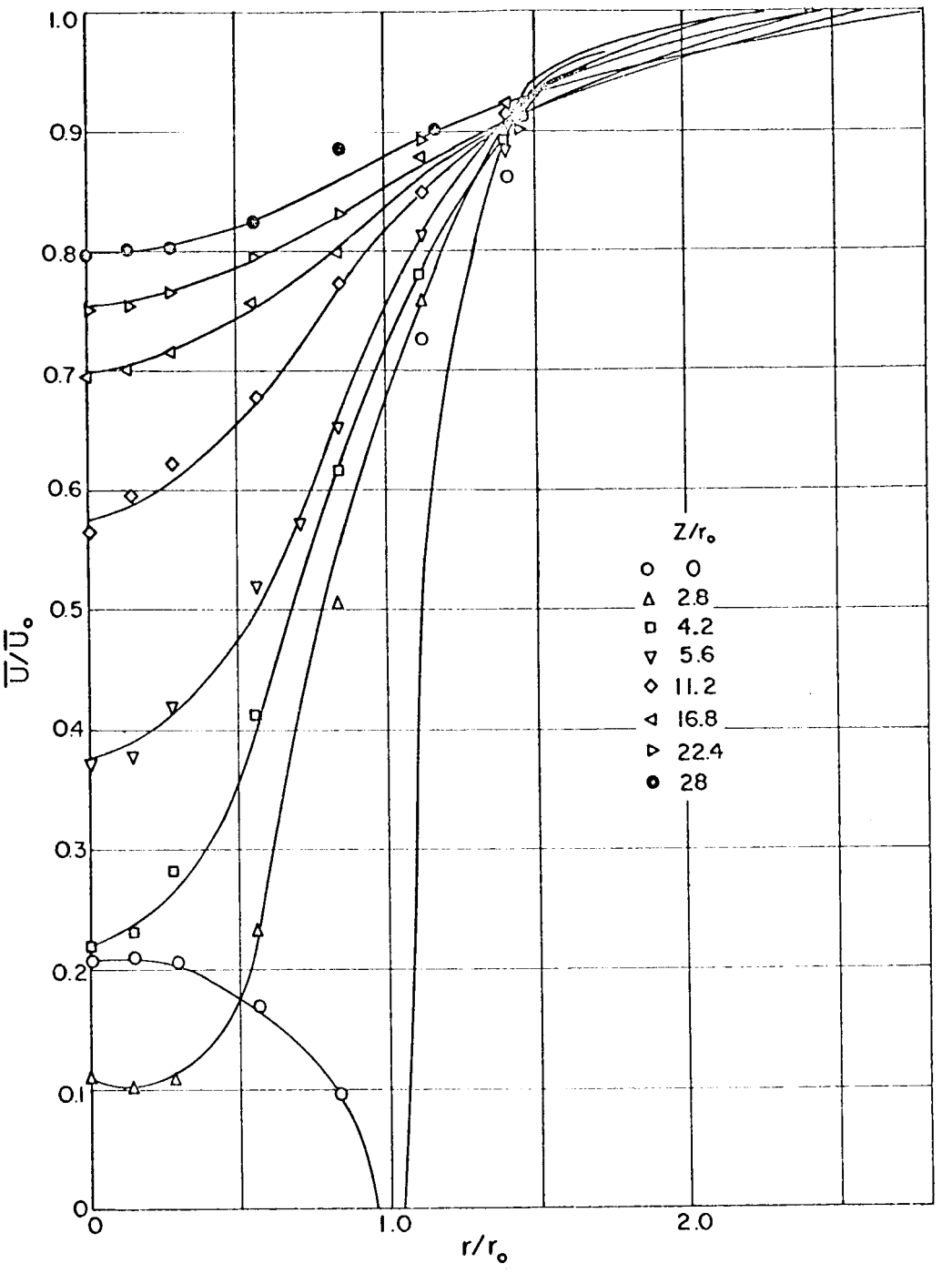

FIGURE V - 1 - 4

DIMENSIONLESS VELOCITY PROFILES, HOMOGENEOUS,

$\frac{U_o}{U_i} = 8, \quad U_o = 48 \text{ ft/sec.}$

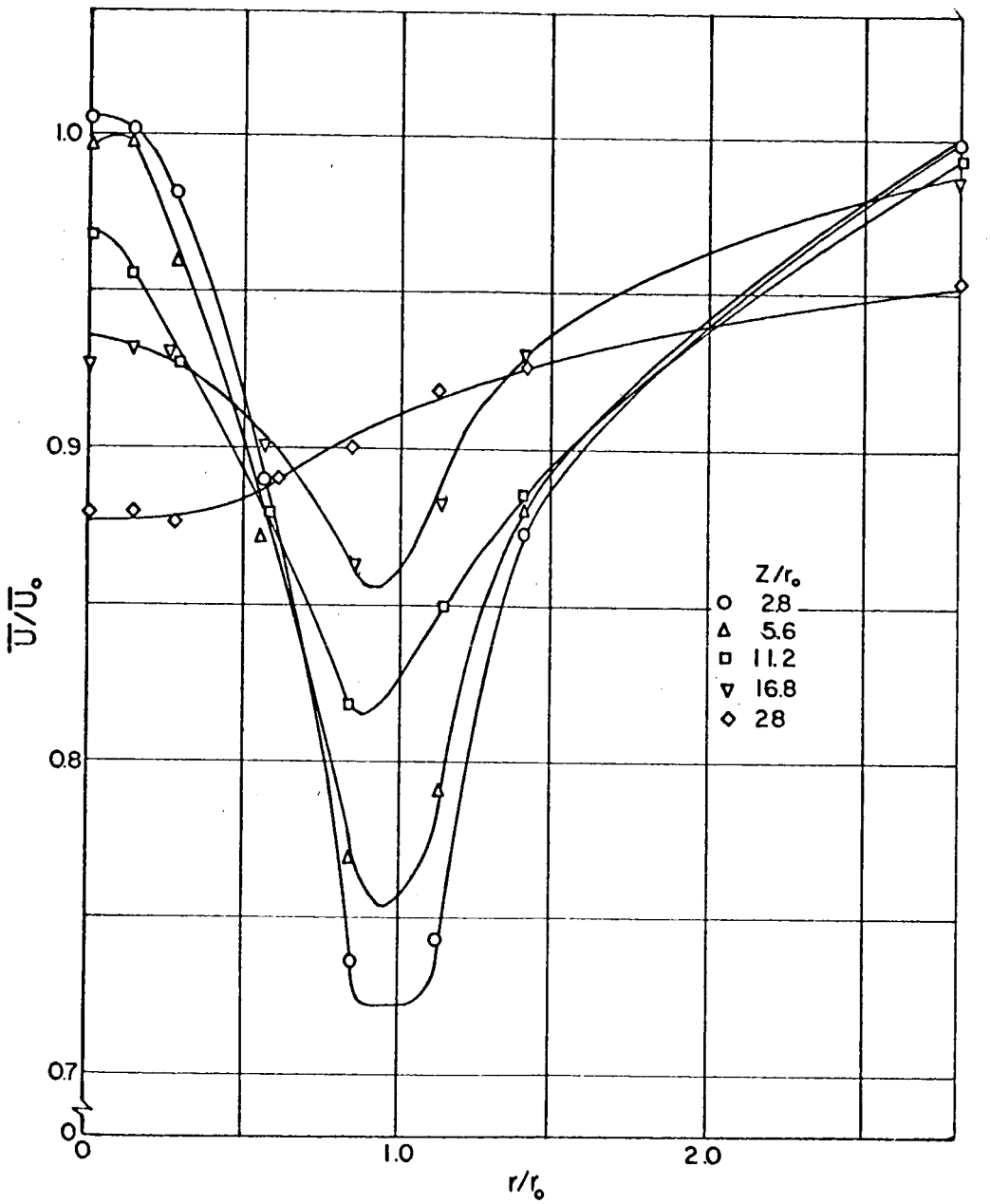

FIGURE V - 1 - 5

DIMENSIONLESS VELOCITY PROFILES, HOMOGENEOUS,

$\frac{U_o}{U_i} = 1, \; U_o = 48$ ft/sec.

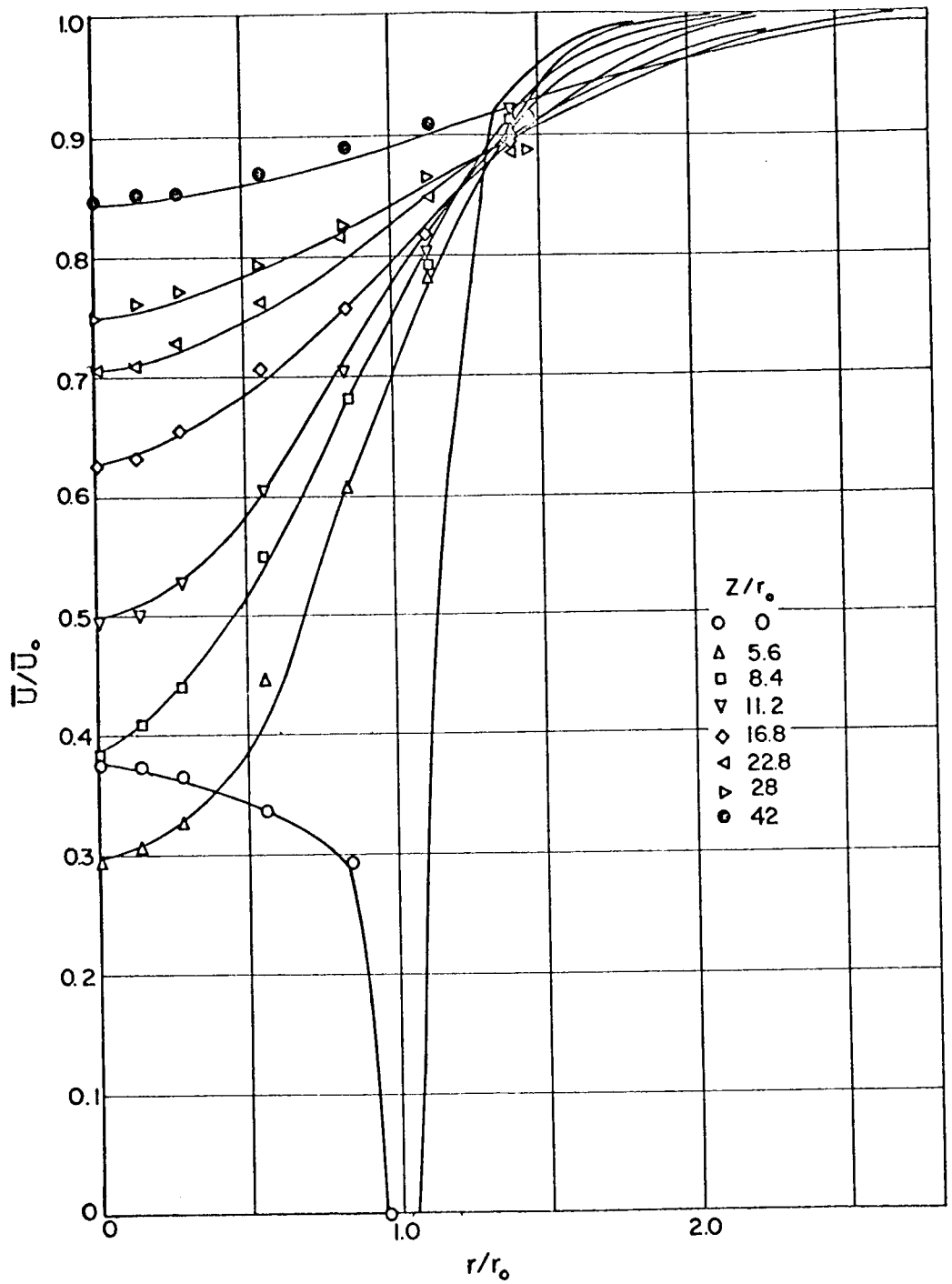

FIGURE V - 1 - 6

DIMENSIONLESS VELOCITY PROFILES, HOMOGENEOUS,

$\frac{U_o}{U_i} = 3.4$, $U_o = 48$ ft / sec

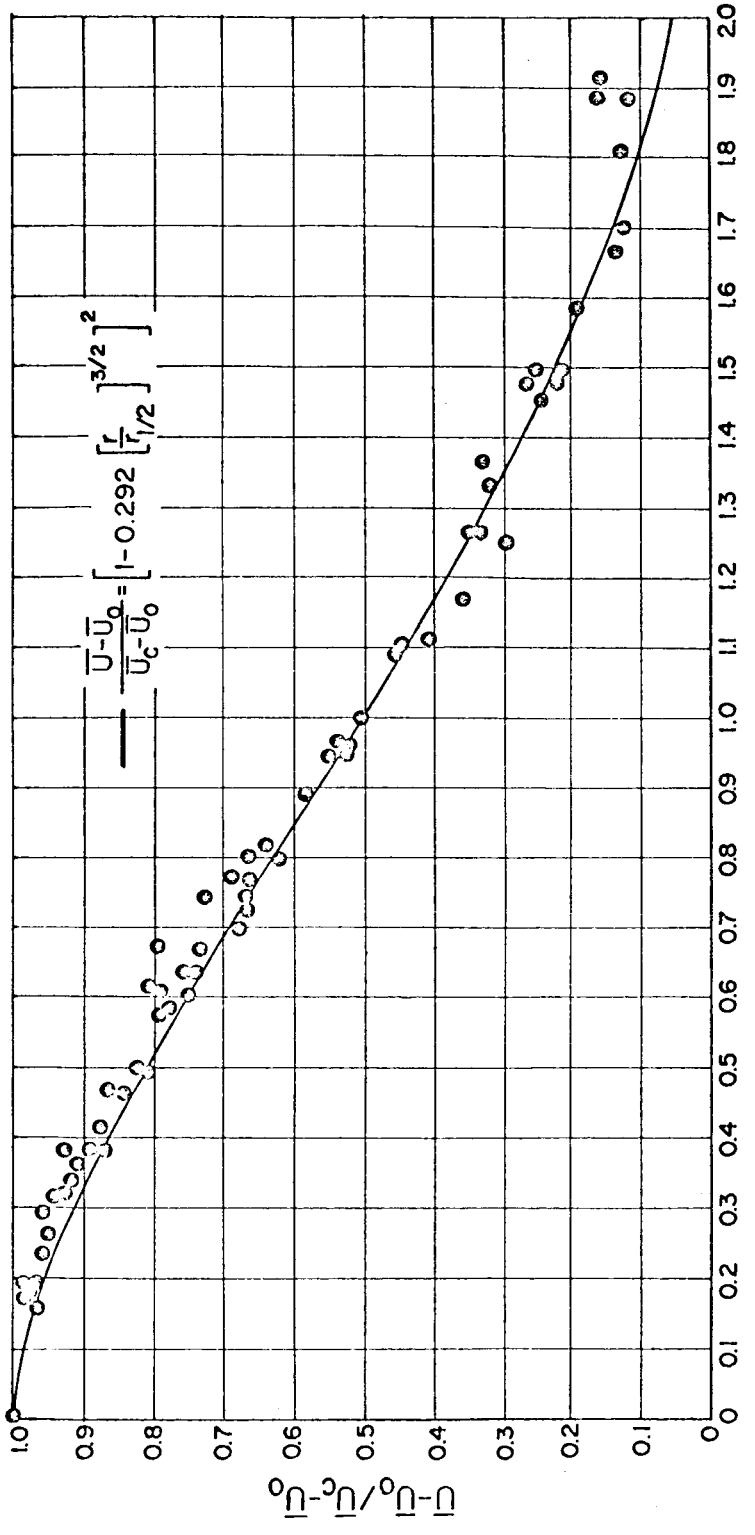

FIGURE V - 1 - 7

DIMENSIONLESS SIMILARITY PLOT OF ALL VELOCITY PROFILES, HOMOGENEOUS

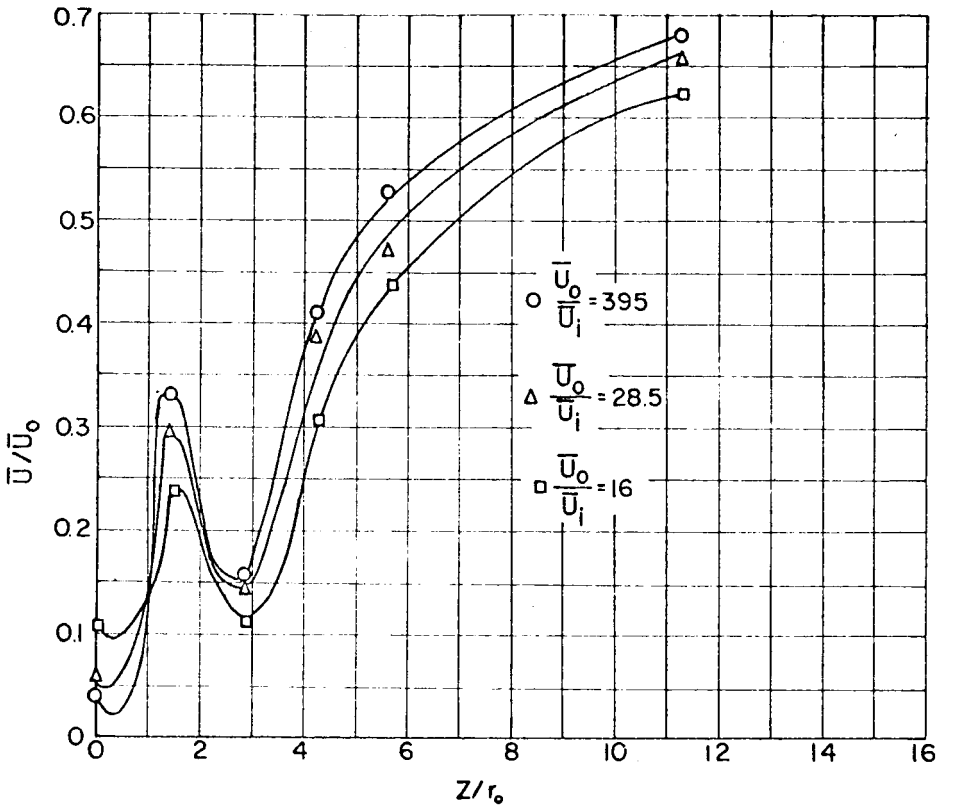

FIGURE V - 1 - 8

CENTERLINE VELOCITY PROFILES FOR $\frac{U_o}{U_i}$ = 39.5, 28.5, 16

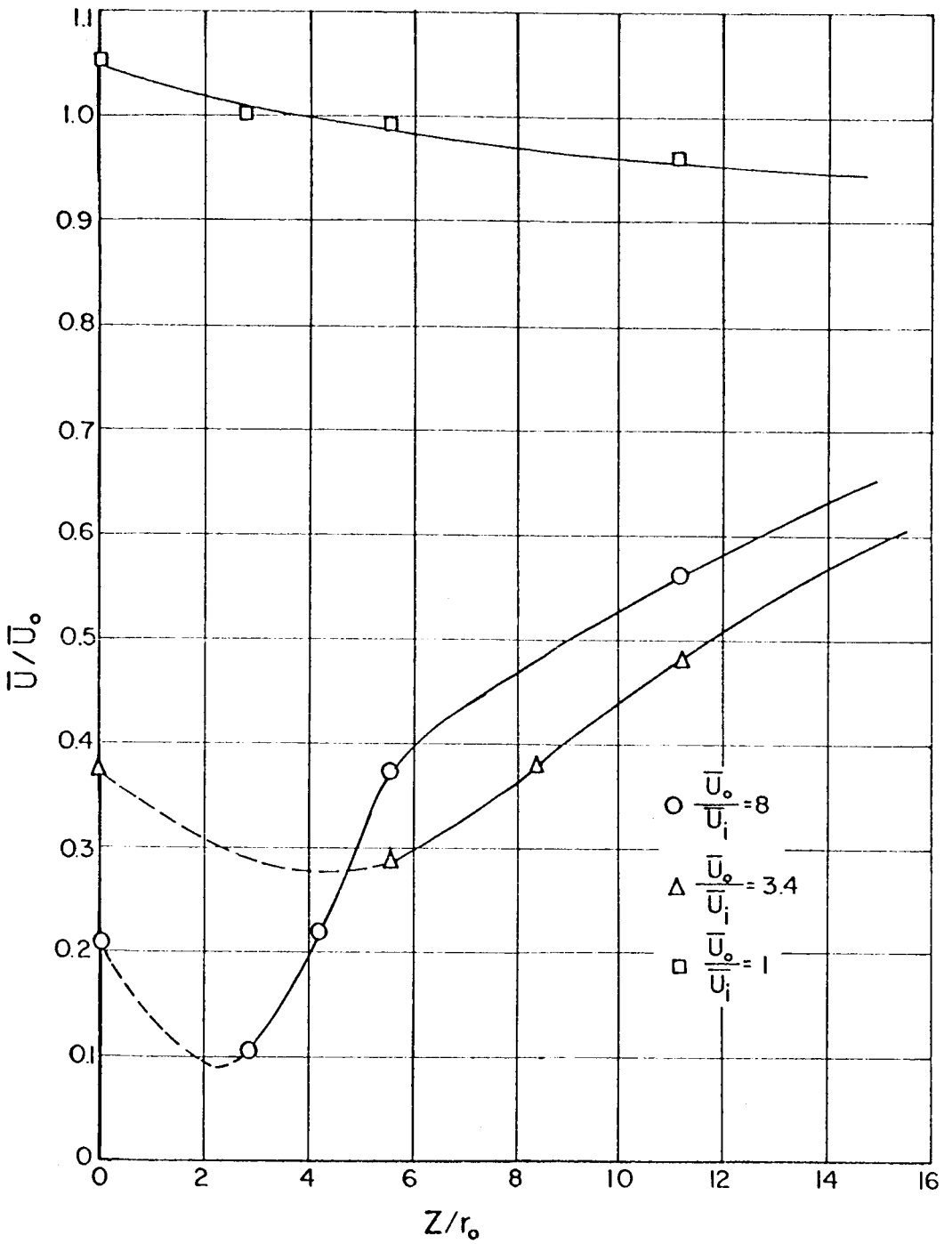

FIGURE V - 1 - 9

CENTERLINE VELOCITY PROFILES FOR $\frac{U_o}{U_i}$ = 8, 3.4, 1.

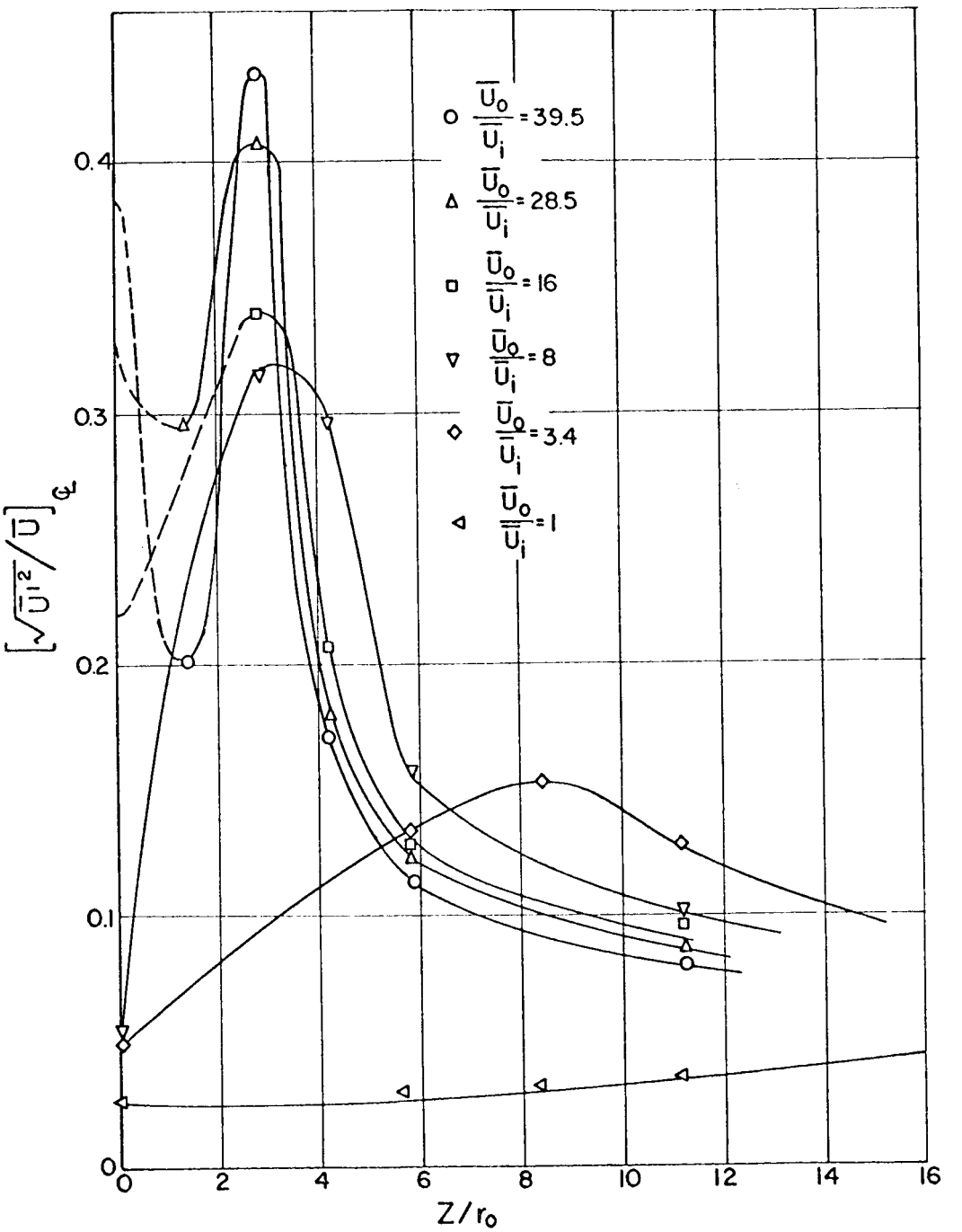

FIGURE V - 1 - 10

CENTERLINE AXIAL TURBULENCE INTENSITY

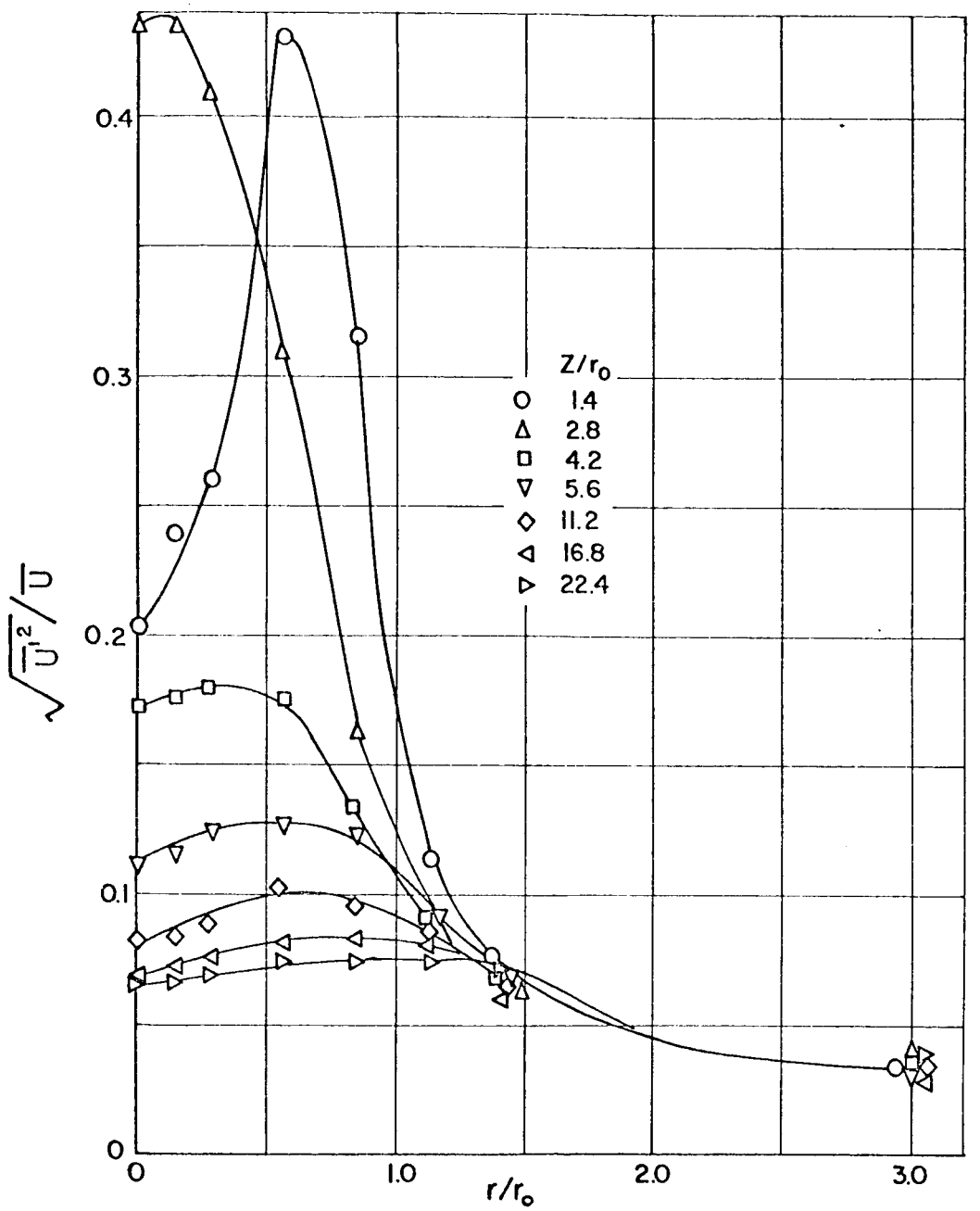

FIGURE V - 1 - 11

AXIAL TURBULENCE INTENSITY PROFILES FOR $\frac{U_o}{U_i} = 39.5$

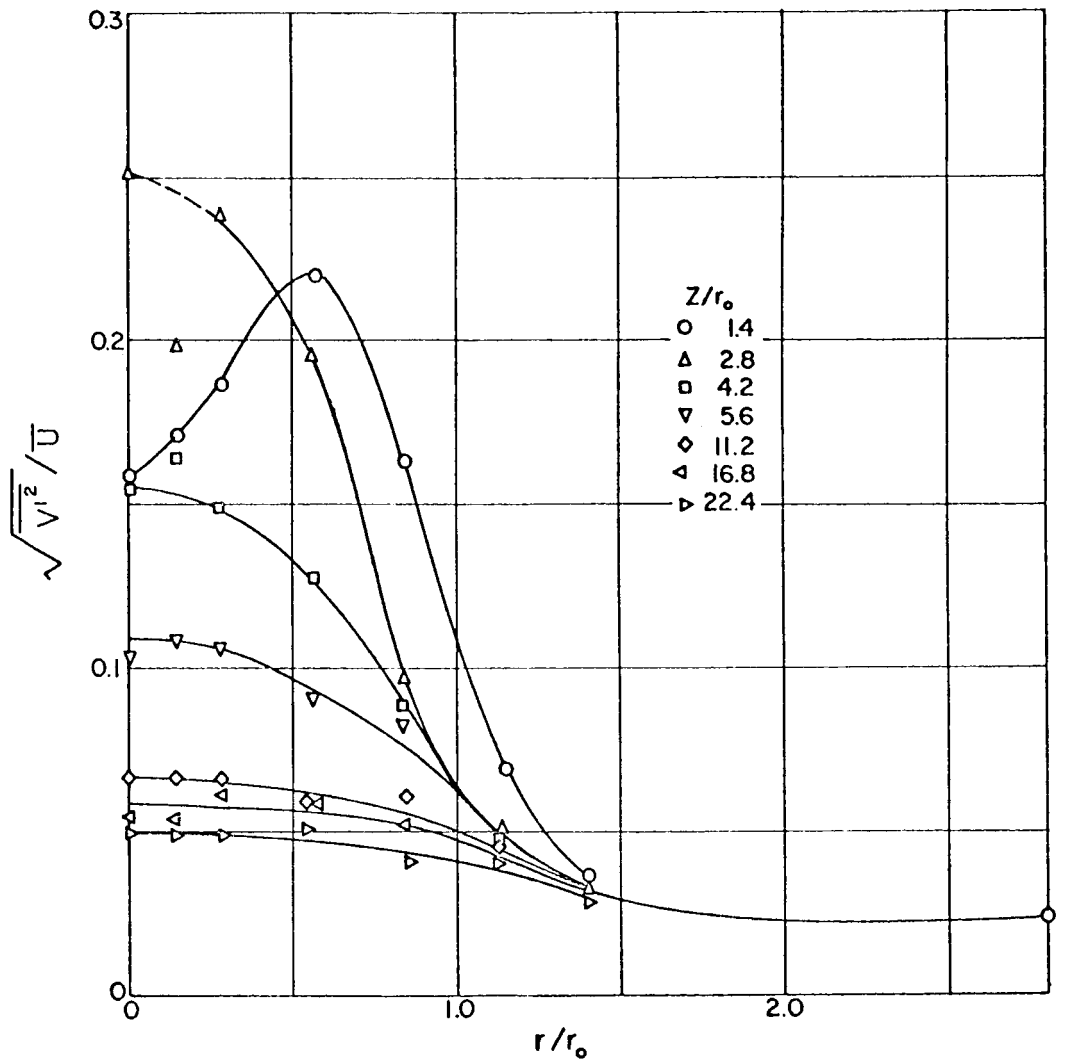

FIGURE V - 1 - 12

RADIAL TURBULENCE INTENSITY PROFILES FOR $\frac{U_o}{U_i} = 39.5$

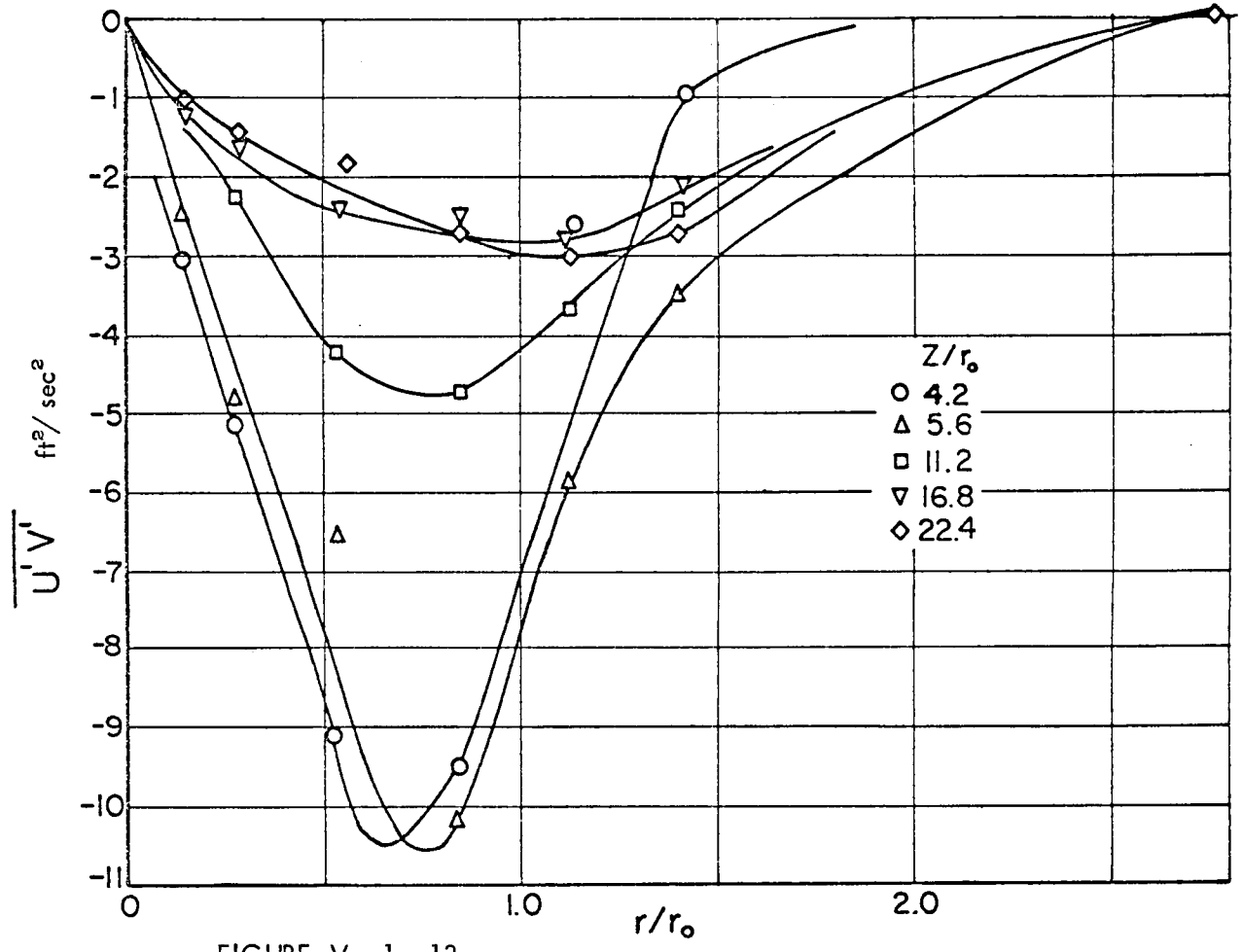

FIGURE V - 1 - 13

TURBULENT SHEAR STRESS DISTRIBUTION FOR $\frac{\overline{U}_o}{\overline{U}_i} = 39.5$

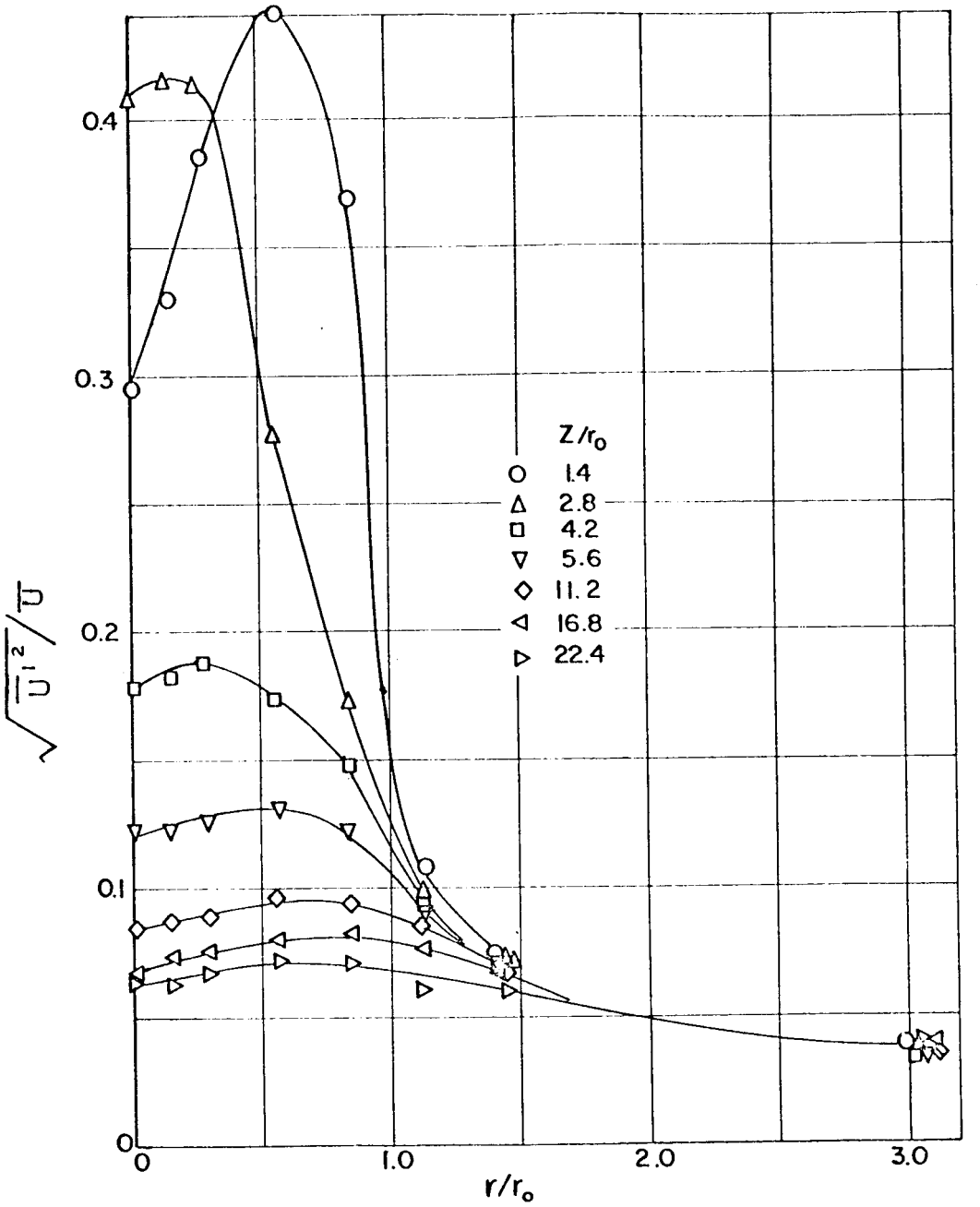

FIGURE V - 1 - 14

AXIAL TURBULENCE INTENSITY PROFILES FOR $\frac{U_o}{U_i} = 28.5$

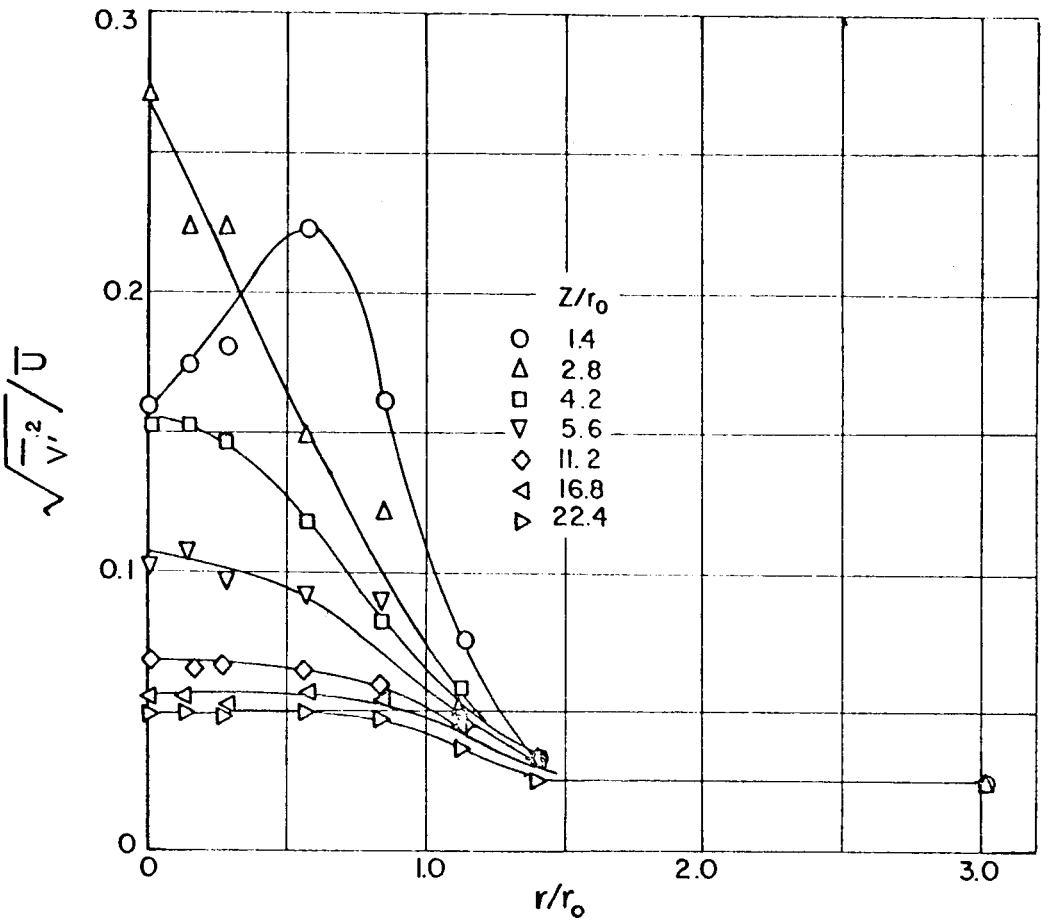

FIGURE V - 1 - 15

RADIAL TURBULENCE INTENSITY PROFILES FOR $\frac{\overline{U}_o}{\overline{U}_i} = 28.5$

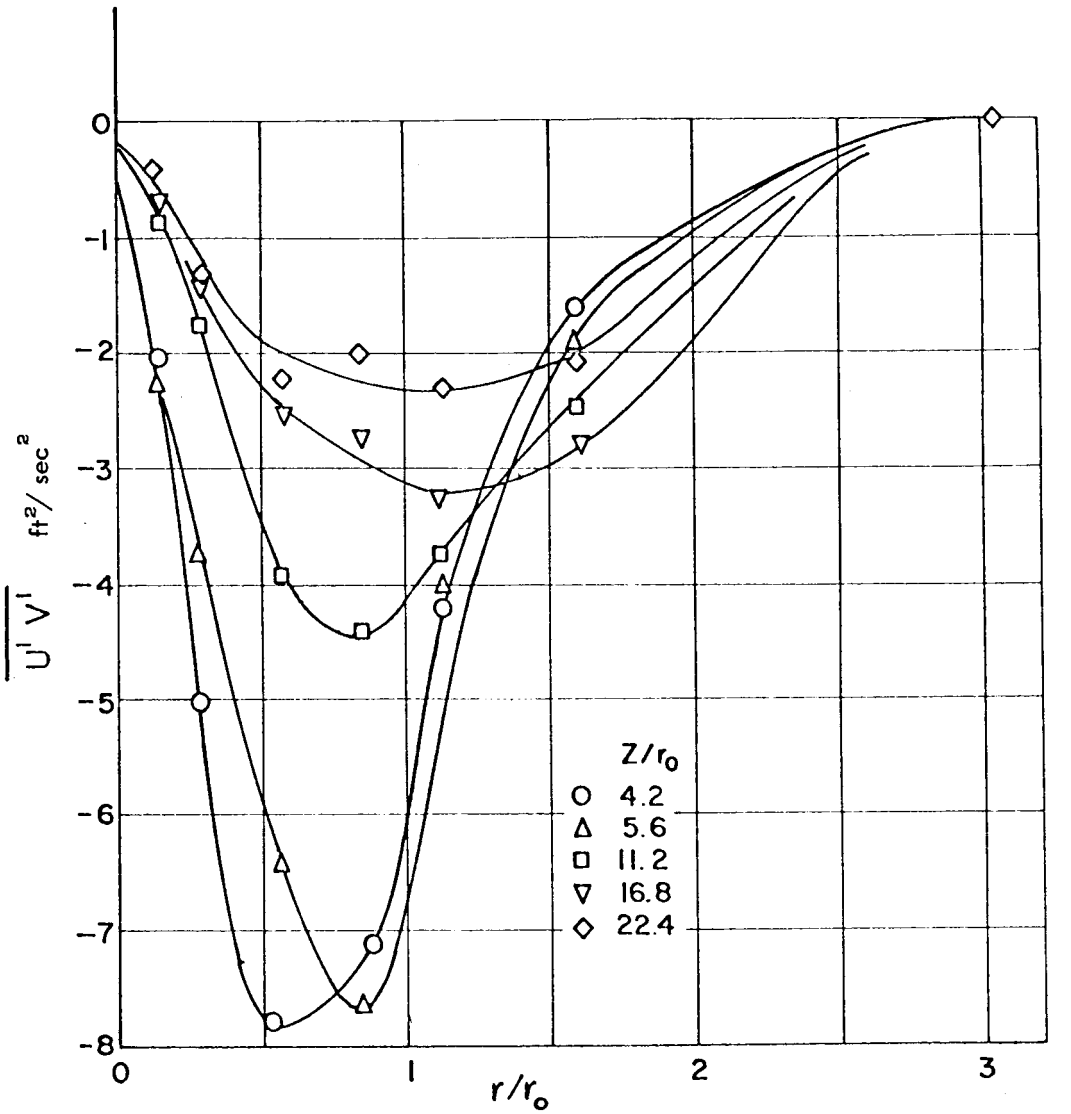

FIGURE V - 1 - 16

SHEAR STRESS DISTRIBUTION FOR $\frac{U_o}{U_i} = 28.5$

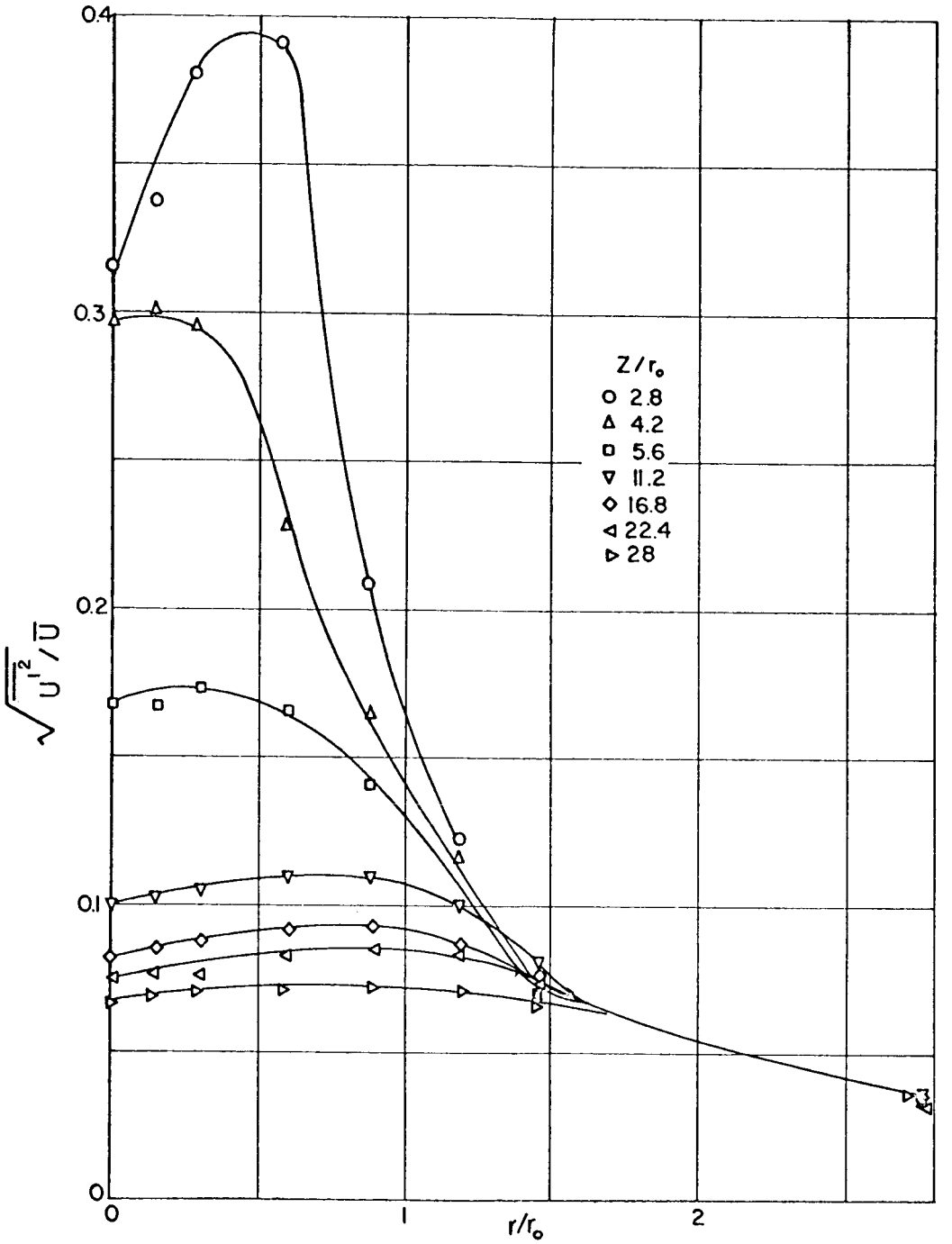

FIGURE V - 1 - 17

AXIAL TURBULENCE INTENSITY PROFILES FOR $\frac{\bar{U}_o}{\bar{U}_i} = 8$

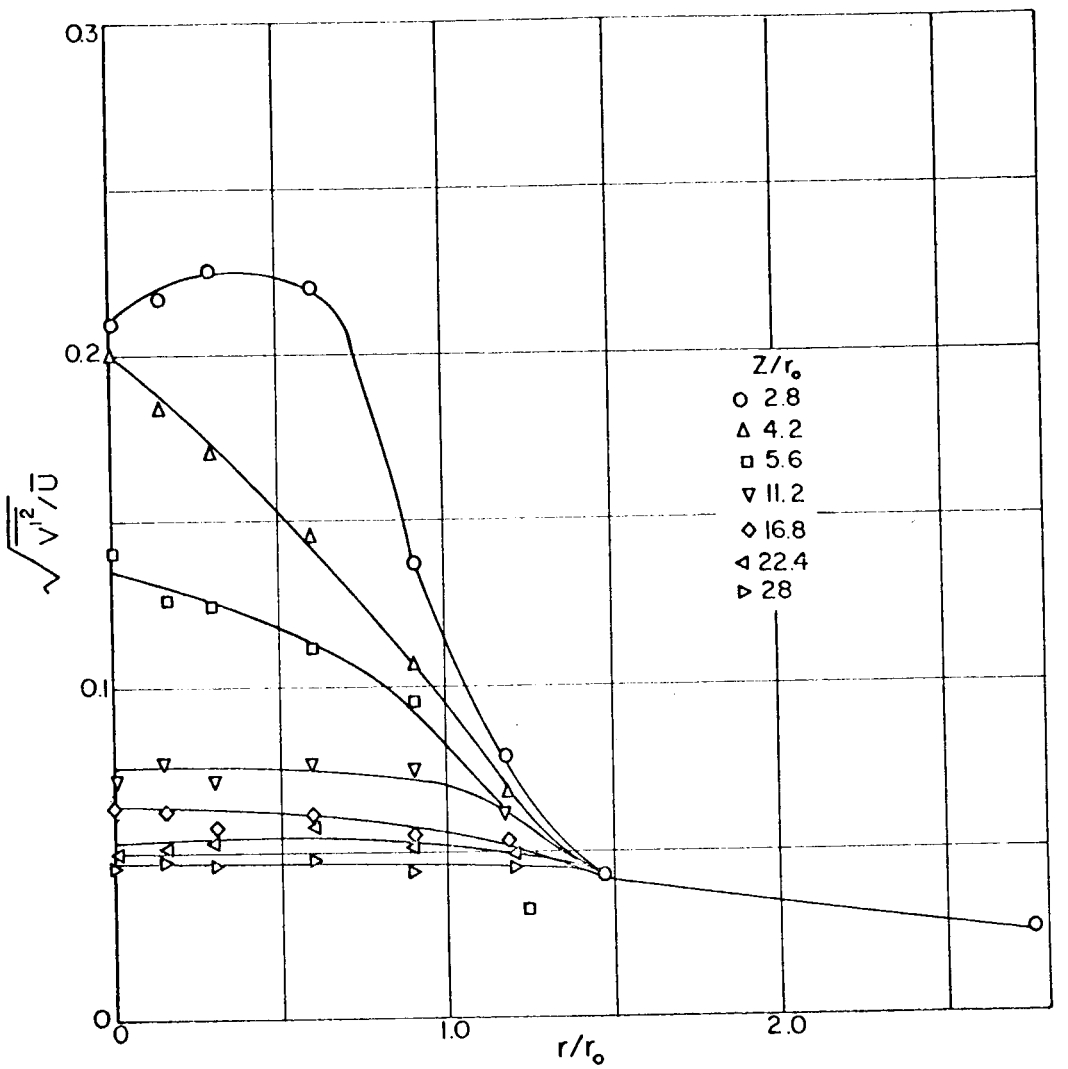

FIGURE V - 1 - 18

RADIAL TURBULENCE INTENSITY PROFILES FOR $\frac{\overline{U}_o}{\overline{U}_i} = 8$

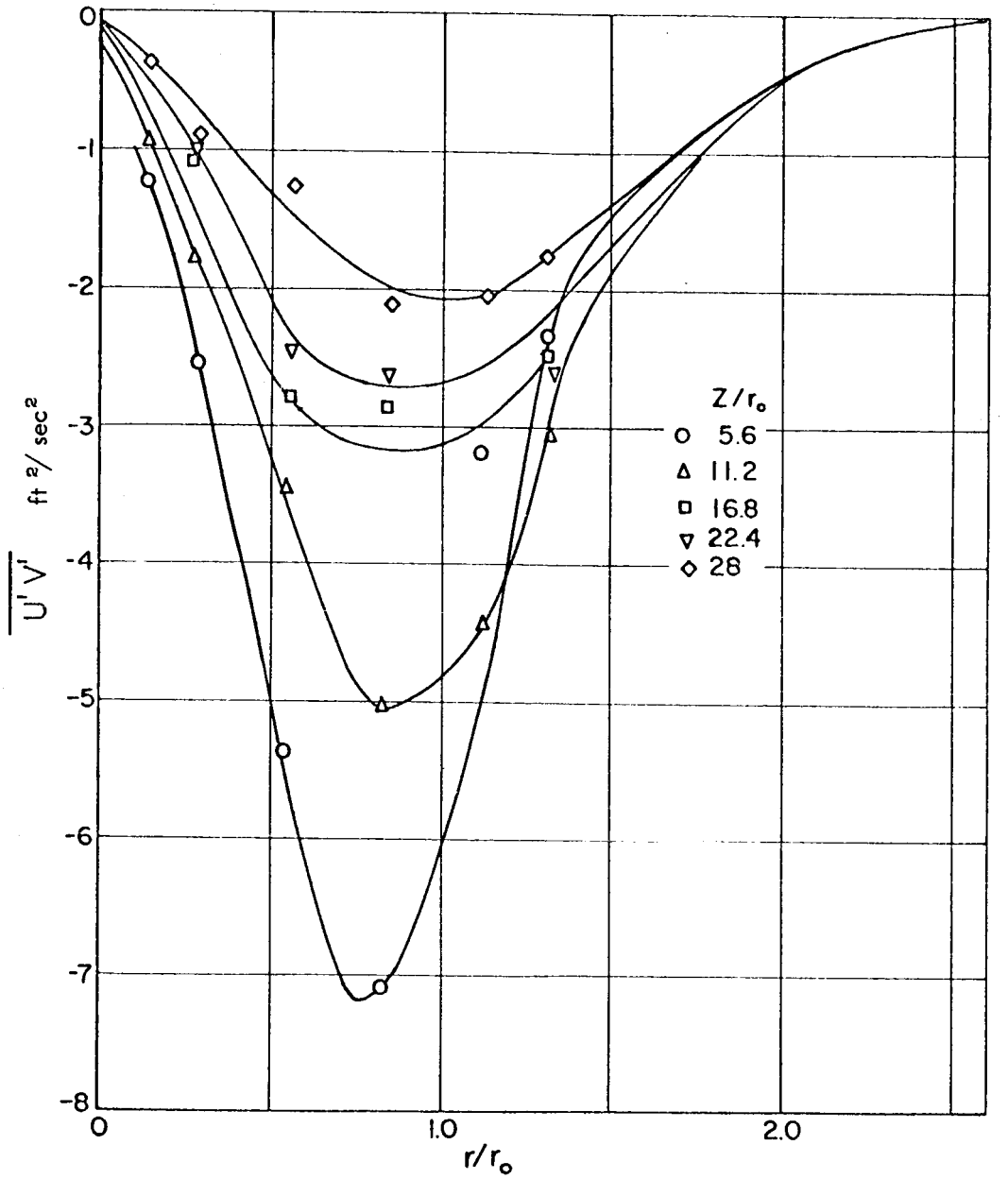

FIGURE V - 1 - 19

TURBULENT SHEAR STRESS PROFILES FOR $\frac{\overline{U}_o}{\overline{U}_i} = 8$

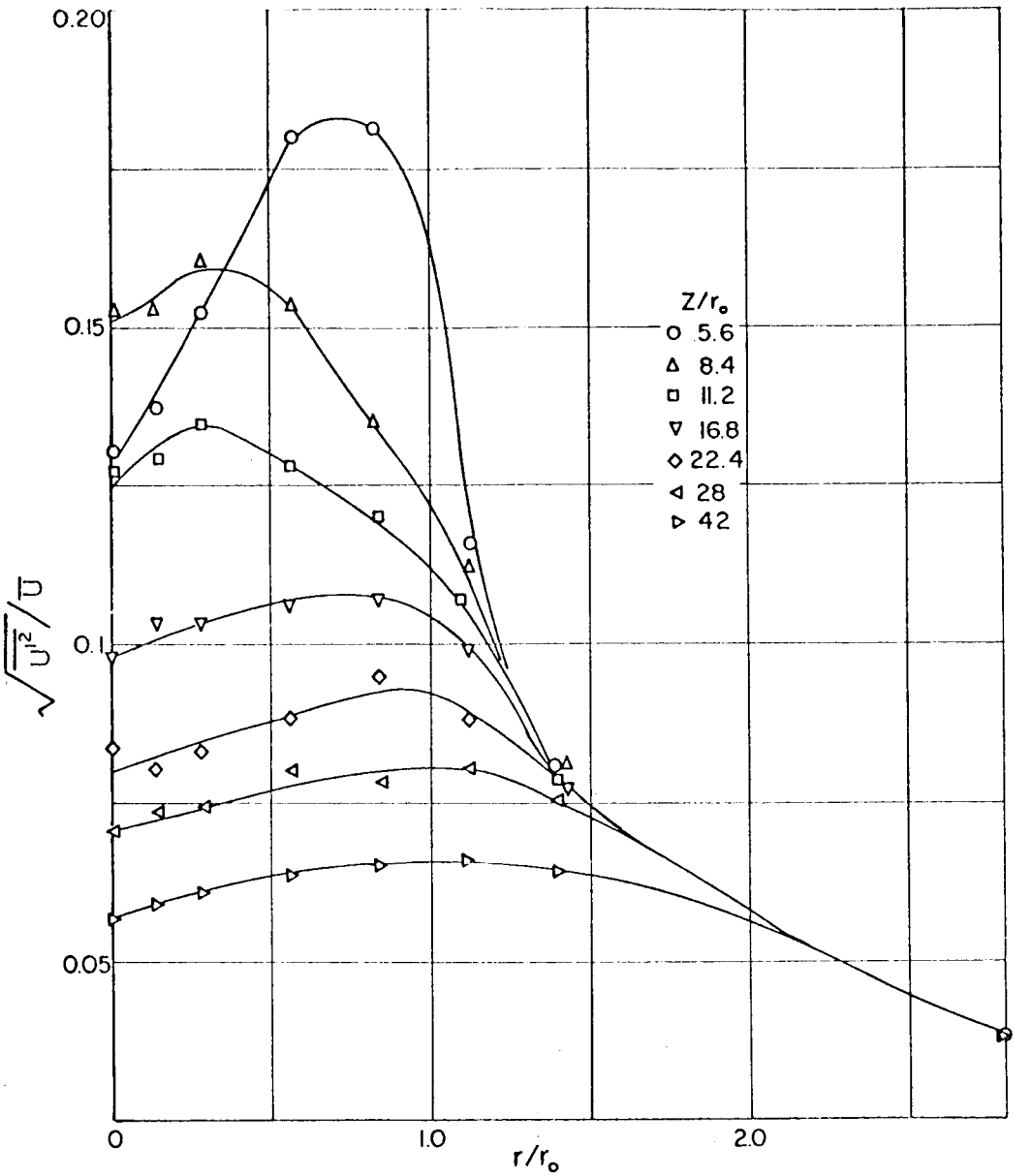

FIGURE V - 1 - 20

AXIAL TURBULENCE INTENSITY PROFILES FOR $\frac{\overline{U}_o}{\overline{U}_i} = 3.4$

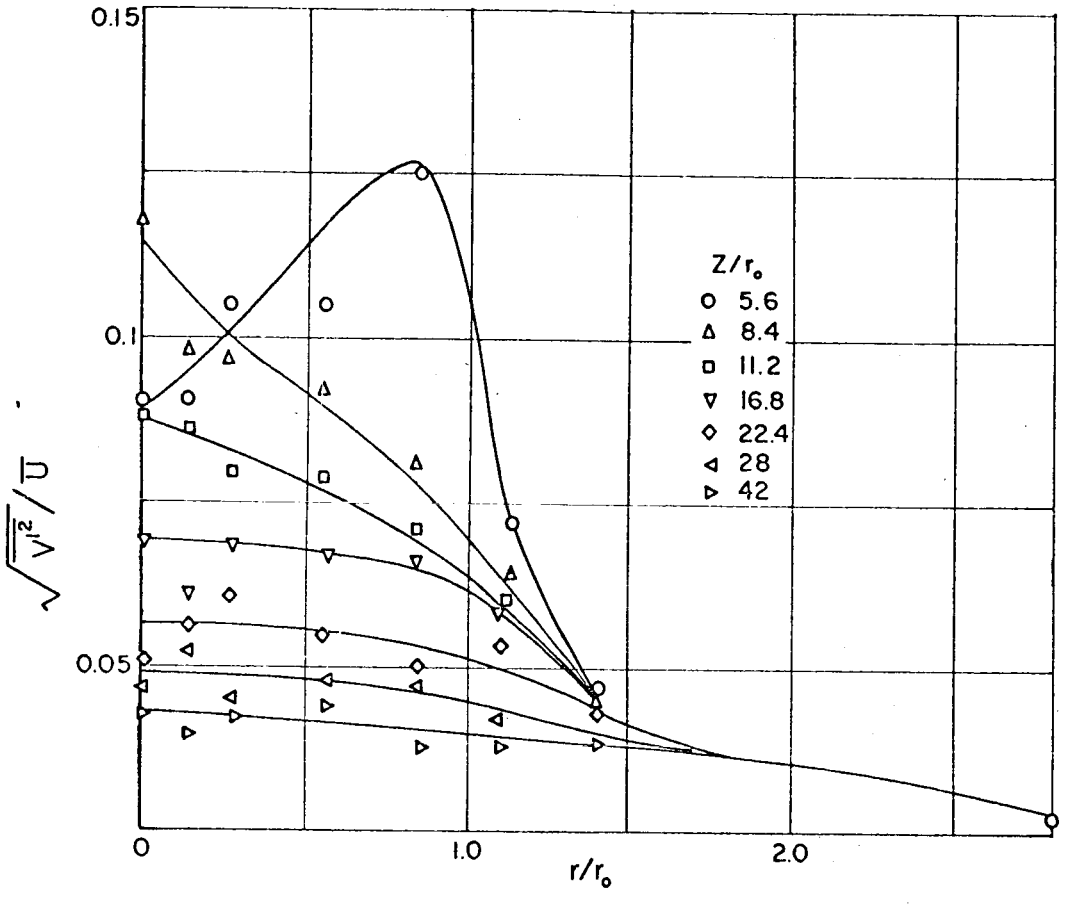

FIGURE V - 1 - 21

RADIAL TURBULENCE INTENSITY PROFILES FOR $\frac{U_o}{U_i} = 3.4$

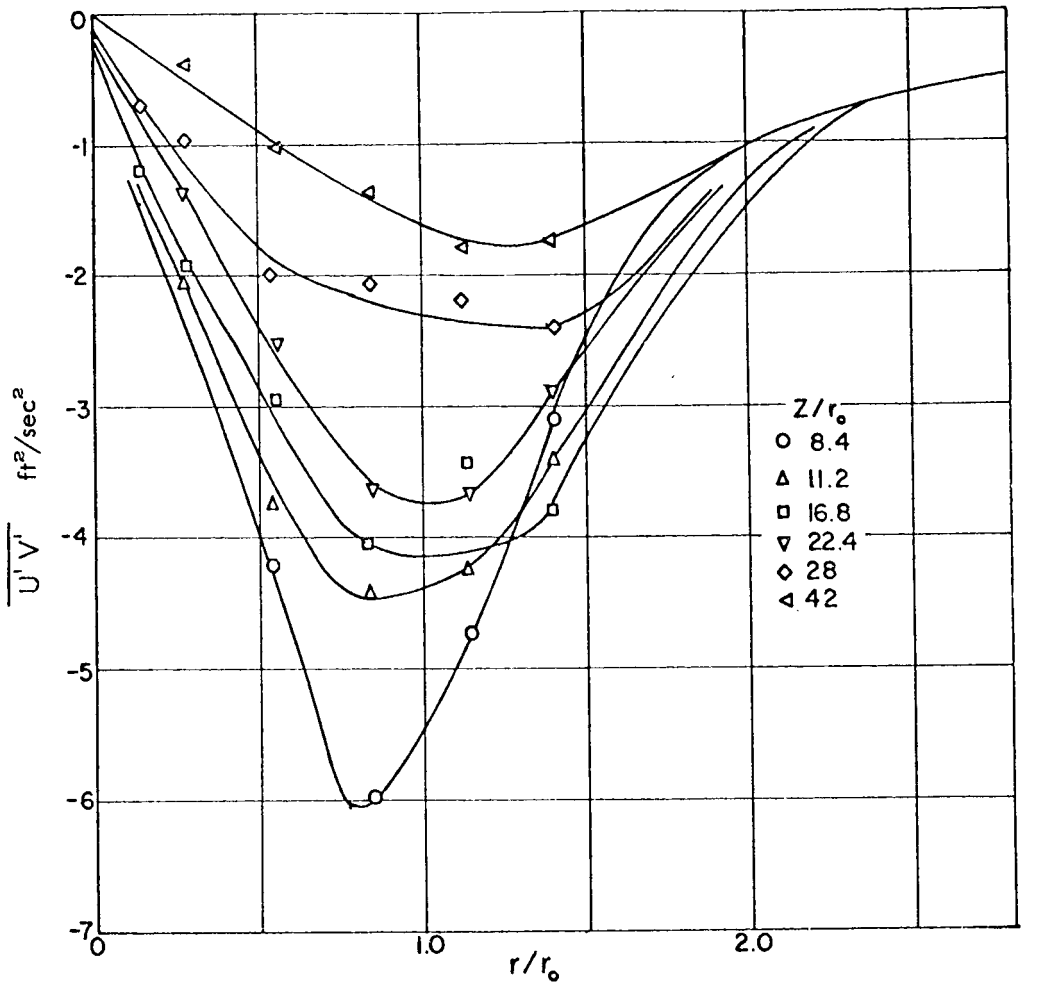

FIGURE V - 1 - 22

TURBULENT SHEAR STRESS PROFILES FOR $\frac{U_o}{U_i} = 3.4$

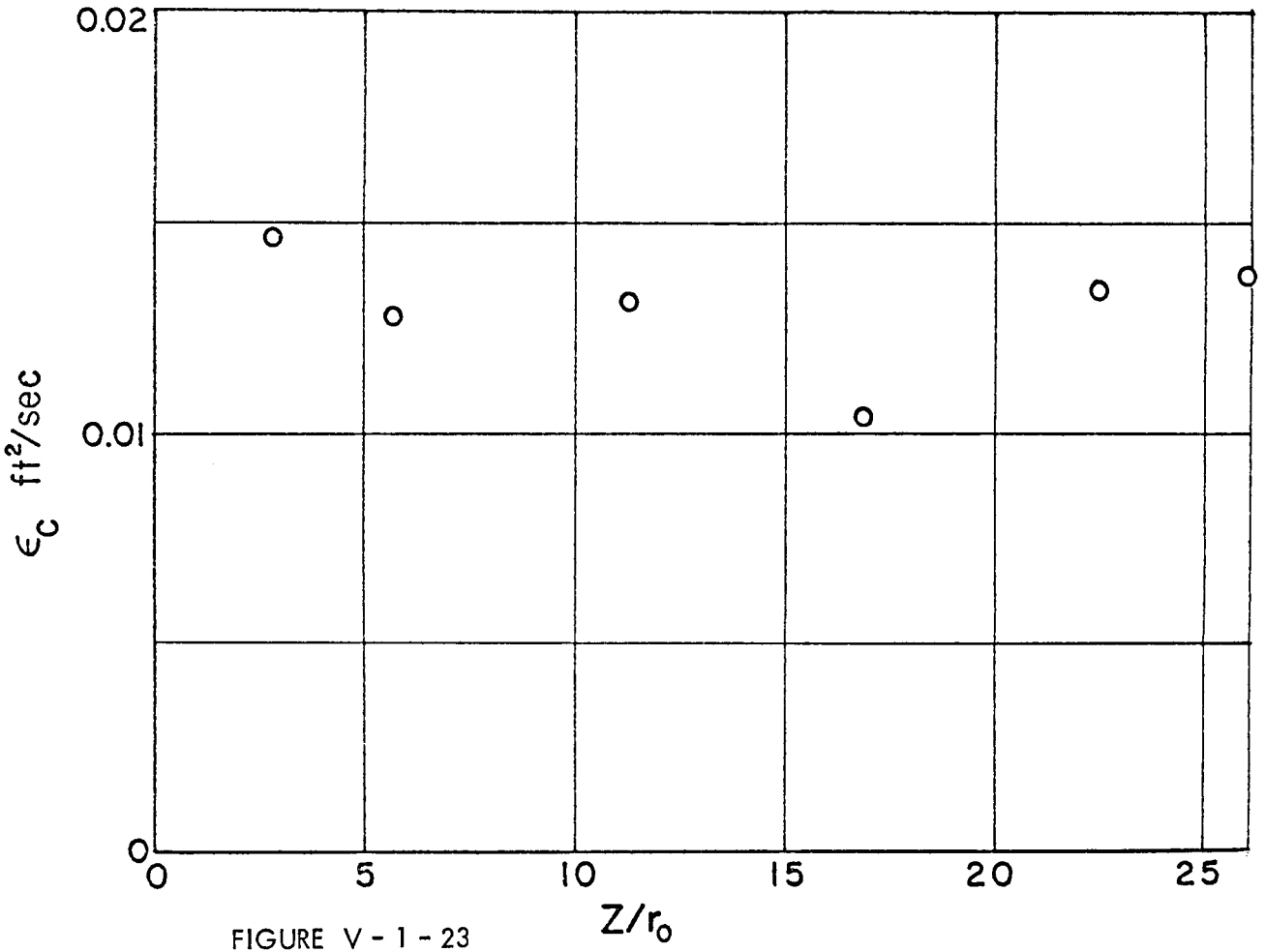

FIGURE V - 1 - 23

TYPICAL EDDY VISCOSITY DISTRIBUTION VERSUS DOWNSTREAM POSITION,

$\frac{U_o}{U_i} = 16$

V - 2 Heterogeneous Measurements

Eleven different outer stream to inner stream velocity ratios are presented for the Freon - 12 - air system. These runs are divided into two groups. The first group, a series of six runs, numbered 201F through 207F, have ratios of 20.3, 11.6, 9.2, 5.6, 5.4 and 3.6. The average velocity and density profiles are shown with the corresponding external stream velocity in figures V-2-1 through V-2-17. The second group of Freon 12-air cases, numbered 207F through 211F have velocity ratios of 36.8, 26.5, 0.2 and 5.4. The average velocity, density and the turbulence intensity of the velocity are shown in figures V-2-23 through V-2-34.

Three Freon C318-air system cases, having velocity ratios of 11.5, 5.8 and 9, are presented. The average velocity and density profiles are shown in figures V-2-15 through V-2-20.

The velocity and density profiles behave in the following manner. As an example, figure V-2-1, the velocity at the centerline decreases while the momentum trough caused by the boundary layers on the dividing tube, is being removed. Once the trough is removed, the centerline velocity increases rapidly. Figure V-2-9 is a representative example of density distribution. Unlike the velocity profile , the density profile has no boundary layer. After the entrance of the inner stream there is a region where the concentration is pure Freon-12. This region is usually termed the potential core region of concentration, and has a cone shape. From the figure it can be seen that as one proceeds from one axial position to the next, the outermost point of pure inner stream proceeds inward toward the centerline . The point where the Freon mole fraction is 1, only at the centerline, is about $\frac{z}{r_o} = 2.8$.

After the end the potential core region is reached, a sharp decline occurs in the concentration. As the velocity ratio is decreased the point at which the potential core for concentration ends increases. For example for the velocity ratio 3.6 the axial position where the core ends is $\frac{z}{r_o} = 8.4$. When the velocity of the inner stream is increased, the momentum of the stream is increased. The inner stream will then preserve itself longer, as indicated by the length of the potential core region of concentration.

The Freon C-318 air system profiles behave in the same manner as the Freon 12-air system. Run 202F and 301FC318 have nearly the same velocity ratio, and comparison of these two runs can be made regarding the spread of the density and momentum with respect to the density ratio. The gas with the higher molecular weight, Freon C-318, has a higher initial momentum than the Freon 12 gas with approximately the same initial velocity. Therefore the velocity field should not be accelerated as quickly for the Freon C-318 as for the Freon 12 case. Then for the density profile, the potential core region for the Freon C-318 would be longer than the core region for Freon 12.

Comparing figure V-2-2 to V-2-15, the centerline velocity ratio at an axial position $\frac{z}{r_o} = 2.8$ for the Freon C-318 case is 0.76, while at the same axial position for the Freon 12 case, the velocity ratio is 0.8. Thus the centerline value of the velocity ratio for the Freon 12 case has acce'erated faster than the centerline value of the Freon C-318 case. Comparison of figures V-2-9 and V-2-8 shows that the dimensionless density at a comparable axial position, is higher for the C-318 case than for the Freon 12 case.

Figures V-2-21 and V-2-22 are similarity plots of the velocity profiles

are similar far downstream of the initial mixing region. The velocity similarity figure is plotted as,

$$\frac{\overline{U} - \overline{U_o}}{\overline{U_c} - \overline{U_o}} \quad \text{versus} \quad \frac{r}{r_{1/2\,U}} \quad \text{where} \quad r_{1/2\,U}$$

is the half radius of velocity. The density similarity figure is plotted as

$$\frac{\overline{\rho} - \rho_o}{\overline{\rho_c} - \rho_o} \quad \text{versus} \quad \frac{r}{r_{1/2\,\rho}} \quad \text{where} \quad \rho$$

is the point density, ρ_o is the free stream density, $\overline{\rho_c}$ is the centerline density at the axial position the profile is being plotted, and $r_{1/2\,\rho}$ is the half radius of the density. Both the similarity plots for the velocity and density fall on the same curve. Also, comparing these figures to the similarity plot of the velocity profiles for the homogeneous case , figure V-1-7, the same curve that fits the heterogeneous profiles fits the homogeneous plot. Since the curves are all similar, the variables plotted in the curve must be functions of the initial velocity ratios and the initial density ratio. Because of errors in determining the half radius at large axial positions, the relationships of the variable $r_{1/2}$ to density and velocity ratio could not be obtained.

In section V-1, it was stated that when there was no flow in the inner stream, circulation patterns with large fluctuations were built up inside of the tube. These fluctuations were then observed for the cases where the flow rate was small in the inner tube. The same phenomenon occurs for the Freon 12-air system. For run 208F, having a velocity ratio of 36.8, the centerline velocity exhibits the characteristic of decreasing, increasing, decreasing again before finally increasing. The axial positions where the maximum and minimum velocities occur are $\frac{z}{r_o} = 1.4$,

and $\frac{z}{r_o} = 2.8$ respectively. The maximum and minimum velocity ratios occurred at the same axial positions for both the homogeneous and heterogeneous systems, but the velocity ratio was not as high for the heterogeneous case. For a comparable velocity ratio, the peak velocity ratio for the homogeneous case at $\frac{z}{r_o} = 1.4$ was 0.33, and for the heterogeneous case, the peak velocity ratio at the same axial position was 0.18.

The hot film is sensitive to flows normal to the wire, and therefore does not represent the axial direction alone. Therefore, care must be taken in analyzing the data presented in region close to the tube entrance, since for high velocity ratio flows there may be swirling, backflow, and a large radial component. The average component reported in the near region cannot be construed as a true axial velocity, but some average of all the components in that region. Once this region has been passed the axial average velocity can then be obtained from the hot film.

Figure V-2-24 shows the composition profile for the high velocity ratio case. The profile is unusual in that at an axial position $\frac{z}{r_o} = 0.3$, increases to a peak at $\frac{r}{r_o} = 0.6$, smaller than the centerline value, then rapidly decreases to the free stream. At the next axial position $\frac{z}{r_o} = 1.4$, the concentration increases from the centerline to a maximum at $\frac{r}{r_o} = 0.4$, then decreases to the free stream value.

The concentration was measured with the aspirating probe, and should represent the true value. The region of this unusual phenomenon takes place in the region of high fluctuations in the velocity. Somehow large eddies of air are entrapped in the near region of the jet, causing the humps in the composition profiles.

From the equations in section III, the fluctuations in the power dissapated from the hot film could be related to the time averaged fluctuations in the density $\overline{\rho'^2}$, the time averaged fluctuations in the velocity $\overline{u'^2}$, and the time averaged

cross term $\overline{\rho' u'}$. From the parallel film probe three r.m.s. voltages were obtained from the two films and the sum of the outputs of the films. The accuracy required in the data for a solution of the three simultaneous equations was unobtainable. Some other method had to be found to determine the fluctuations.

The correlation factor $\frac{\overline{\rho' u'}}{\sqrt{\overline{\rho'^2}}\sqrt{\overline{u'^2}}}$ represents the correlation between the velocity and the density. If the density and velocity are totally correlated, the absolute magnitude of the correlation factor will be one. If the density and velocity are not totally correlated, the absolute magnitude of the correlation factor will lie between zero and 1. Using this condition and only two equations it was found that the velocity fluctuatuons u'^2 were insensitive to changes in the density fluctuations in the region where the absolute magnitude of the correlation factor lies between 0 and 1. The velocity turbulence could be reported with fair accuracy, while the density fluctuations could not be reported at all.

Figure V-2-25 shows the turbulence intensity of velocity for the velocity ratio 36.8.

At an axial position $\frac{z}{r_o} = 0.7$, the turbulence intensity has a centerline value of 0.07, increases to a peak of 0.53 at an $\frac{r}{r_o} = 0.8$, then decreases to the free stream value. At the next axial position $\frac{z}{r_o} = 1.4$ the centerline intensity increases to a value of 0.35. The radial profile has a double hump at this position. However it is not known whether this is actually present in the flow field or whether it is due to an error in the data. At the next axial position $\frac{z}{r_o} = 5.6$ the turbulence has increased to a value of 0.7. The profile has a slight peak at $\frac{r}{r_o} = 0.2$, then decreases rapidly to the free value. In this near region the wire is subject to fluctuations in plane normal to the wire, and the turbulence intensity presented represents some average in the normal direction.

At the next axial position $\frac{z}{r_o} = 5.6$, the profile behaves in a regular

manner. The centerline value is 0.22 and the intensity increases slightly until the radial position $\frac{r}{r_o} = 0.6$, then decreases to the free stream value. At each succeeding profile the intensity decreases. It is not clear from the data whether the radial profiles are characterized by a slight hump, as was the case for the homogeneous system.

Referring back to figure V-1-11, the turbulence intensity profiles for the homogeneous case, having a velocity of 39.5, the heterogeneous and homogeneous systems can be compared. For the Freon 12-air case the maximum intensity reached was about 0.7 while for the homogeneous case, the maximim intensity obtained was 0.4. For each succeeding axial position the intensity for the heterogeneous system was higher than the intensity of the homogeneous system. Also for every other comparable velocity ratio the intensity of the Freon-12-air system is larger than that of the air system. The increase in momentum causes the turbulence to increase.

Figure V-2-35 shows the centerline turbulence intensity profile. For the cases where large fluctuations are present in the tube, runs 208F, and 209F, the maximum turbulence intensity occurs at an axial position of $\frac{z}{r_o} = 2.8$. This is the same axial position at which the maximum occurs for the homogeneous system. As the velocity ratio is decreased the point of maximum turbulence intensity moves further downstream. For run 210F, there is a dotted line drawn through the points for axial positions $\frac{z}{r_o} = 2.8$ and $\frac{z}{r_o} = 5.6$. Since no data was taken in this region it is not known whether the maximum turbulence occurred in the range.

The problem in both the homogeneous and heterogeneous systems is a combination jet and wake flow. As stated before the case with no flow in the inner stream (wake flow) large fluctuations were found in the inner tube. With high outer stream to inner stream velocity ratios the wake flow disturbance predominates. For both the homogeneous and heterogeneous the same type of average velocity profile was found. The centerline value decreased, increased, decreased before finally increasing.

The axial position for both the homogeneous and heterogeneous cases where the points of relative maximum $\frac{z}{r_o} = 1.4$ and $\frac{z}{r_o} = 2.8$ respectively and minimum velocities occurred were the same, indicating the same predominance of the wake. However, for the same velocity ratio, the peak velocity that occurred at an axial position $\frac{z}{r_o} = 1.4$ was greater for the homogeneous system than for the homogeneous system, indicating the effect of the increased momentum of the inner stream.

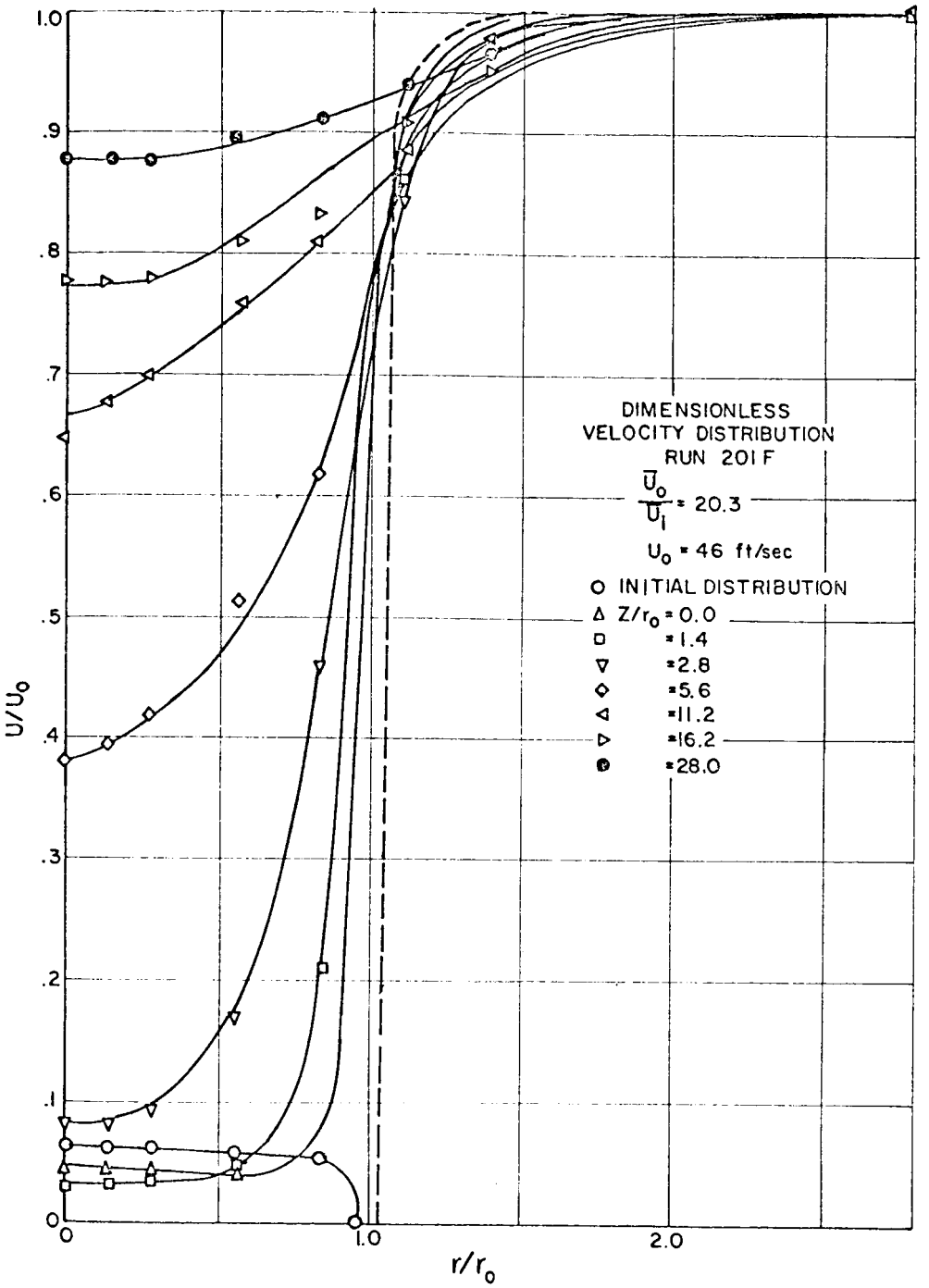

FIGURE V - 2 - 1

DIMENSIONLESS VELOCITY PROFILES, HETEROGENEOUS

$\frac{U_o}{\overline{U}_i}$ = 20.3, $\overline{U}_o$ = 46 ft/sec, $\frac{\rho_o}{\rho_i}$ = 0.25

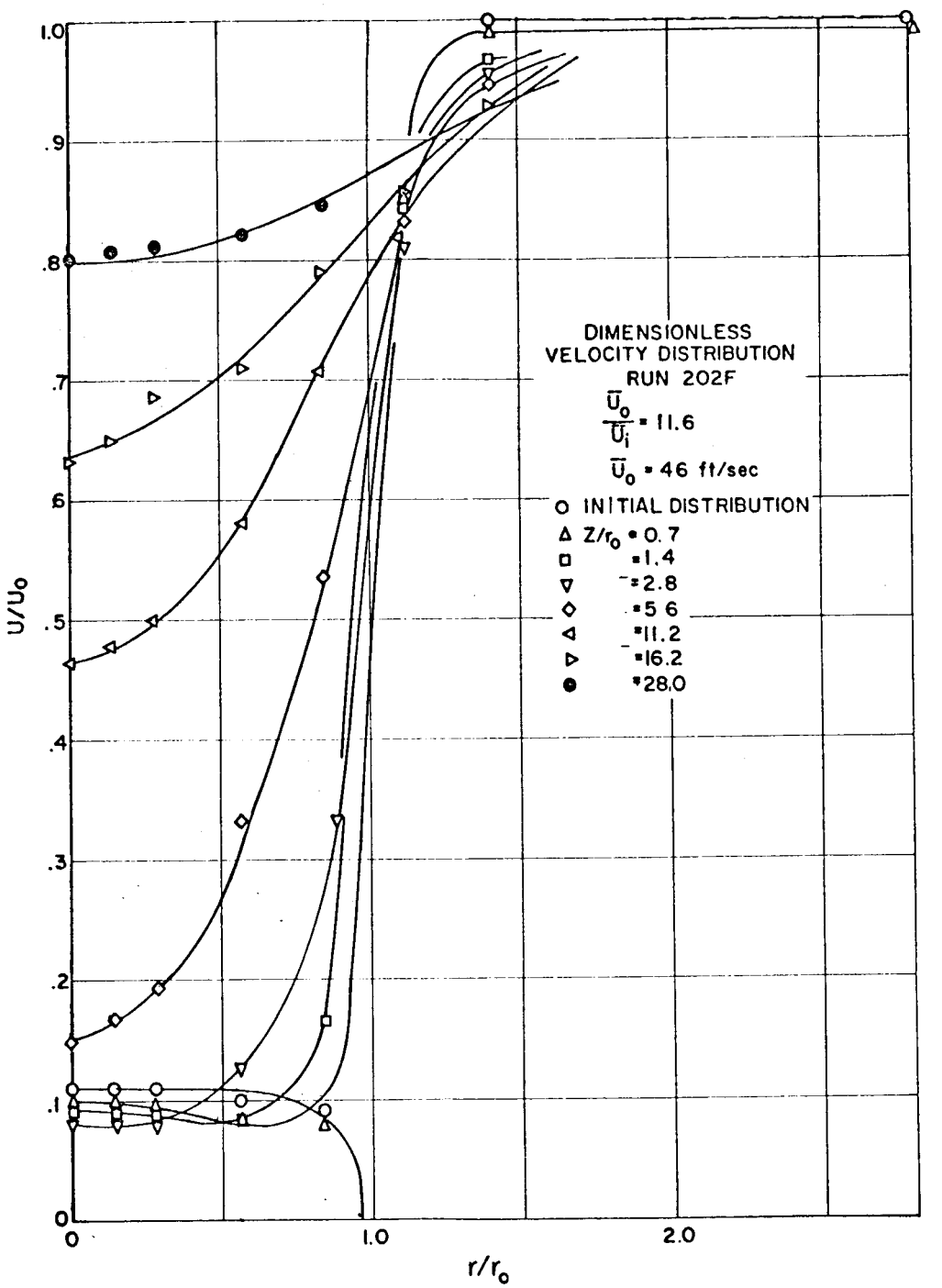

FIGURE V - 2 - 2

DIMENSIONLESS VELOCITY PROFILES, $\frac{U_o}{U_i}$ = 11.6

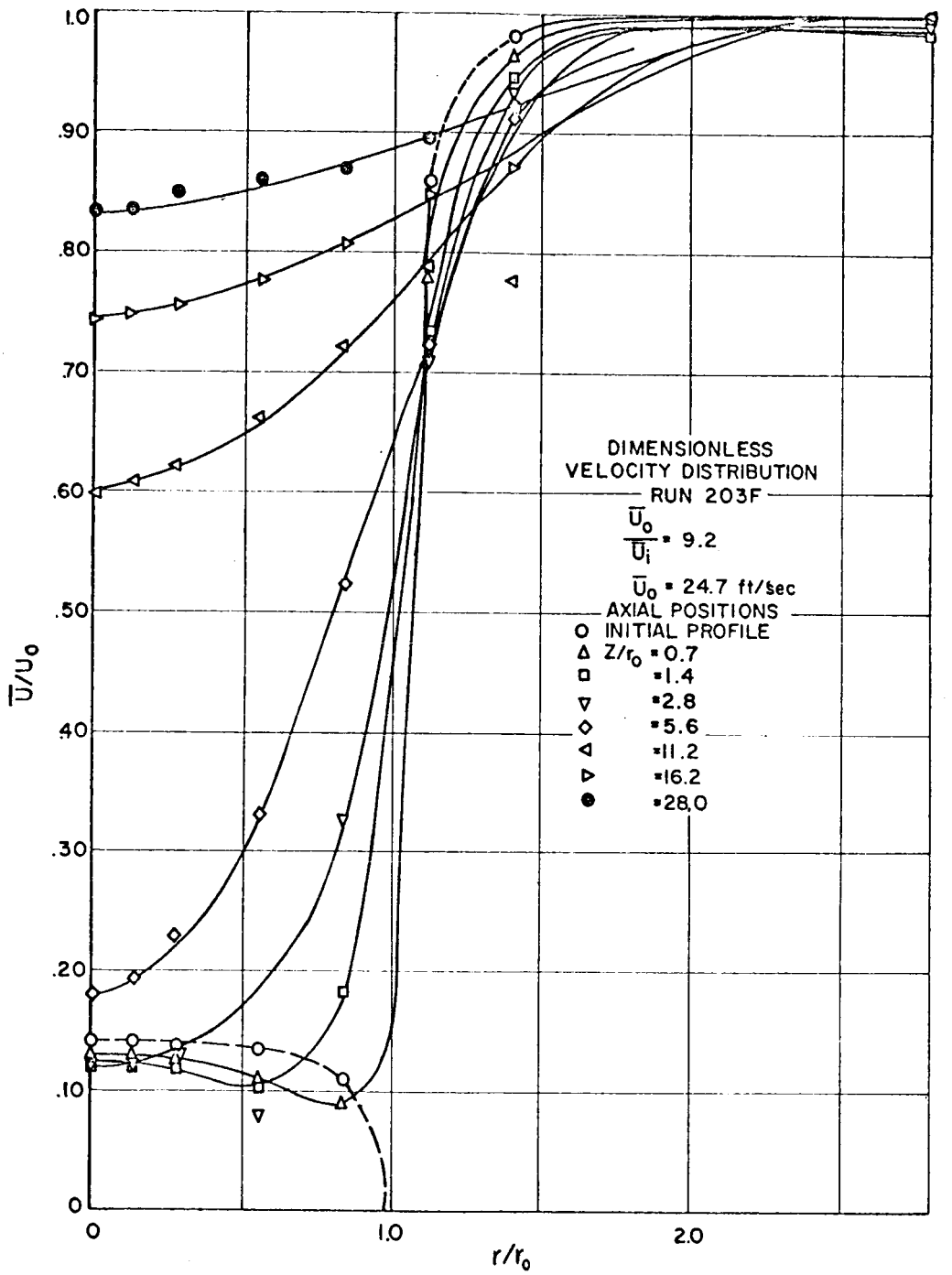

FIGURE V - 2 - 3

DIMENSIONLESS VELOCITY PROFILES, HETEROGENEOUS,

$$\frac{\bar{U}_o}{\bar{U}_i} = 9.2, \quad \bar{U}_o = 46 \text{ ft/sec}, \quad \frac{\rho_o}{\rho_i} = 0.25$$

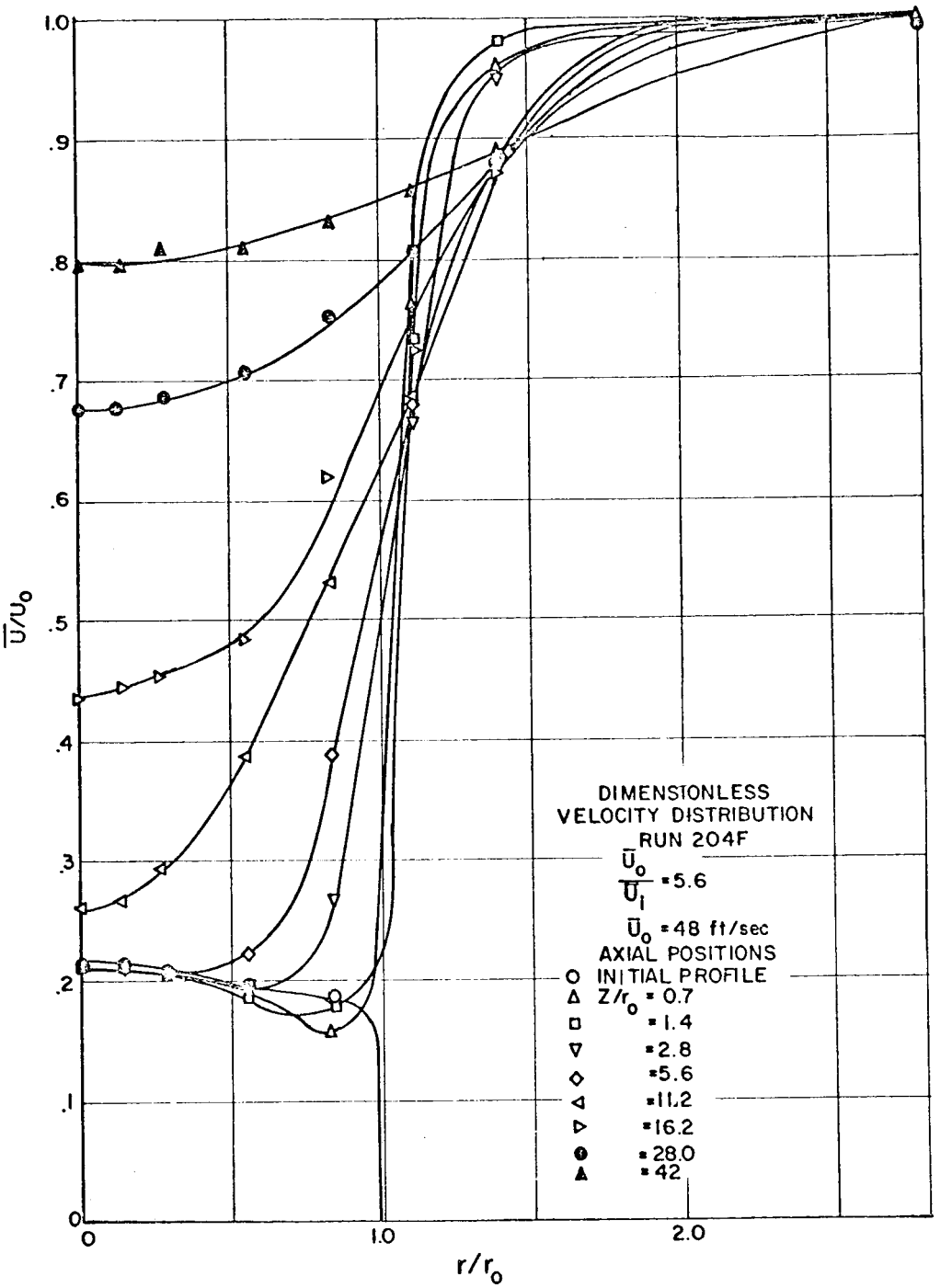

FIGURE V - 2 - 4

DIMENSIONLESS VELOCITY PROFILES, HETEROGENEOUS,

$\frac{\bar{U}_o}{\bar{U}_i} = 5.6$, $\bar{U}_o = 48$ ft/sec, $\frac{\rho_o}{\rho_i} = 0.25$

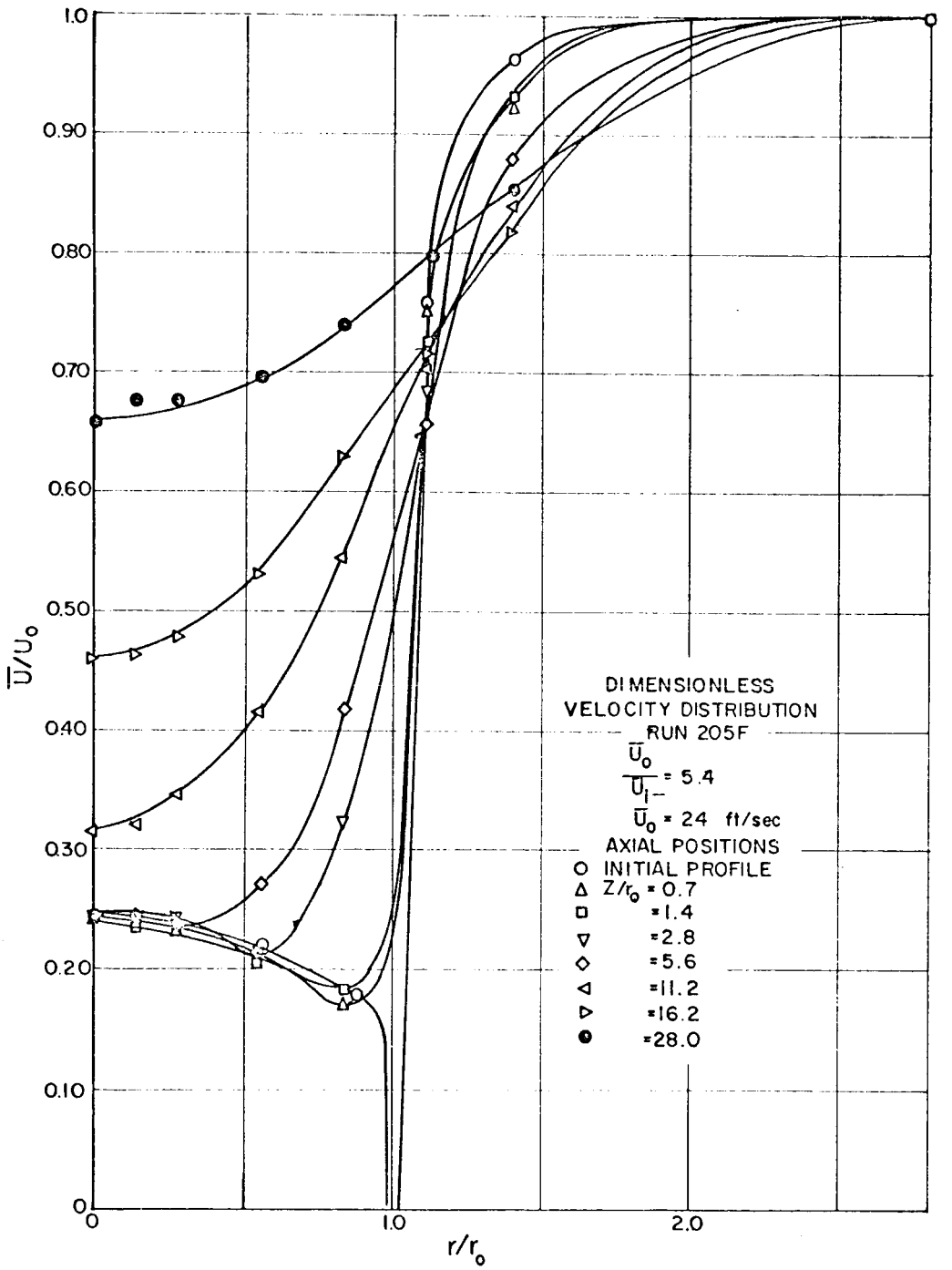

FIGURE V - 2 - 5

DIMENSIONLESS VELOCITY PROFILES, HETEROGENEOUS,

$\frac{\bar{U}_o}{\bar{U}_i} = 5.4$, $\bar{U}_o = 24$ ft/sec, $\frac{\rho_o}{\rho_i} = 0.25$

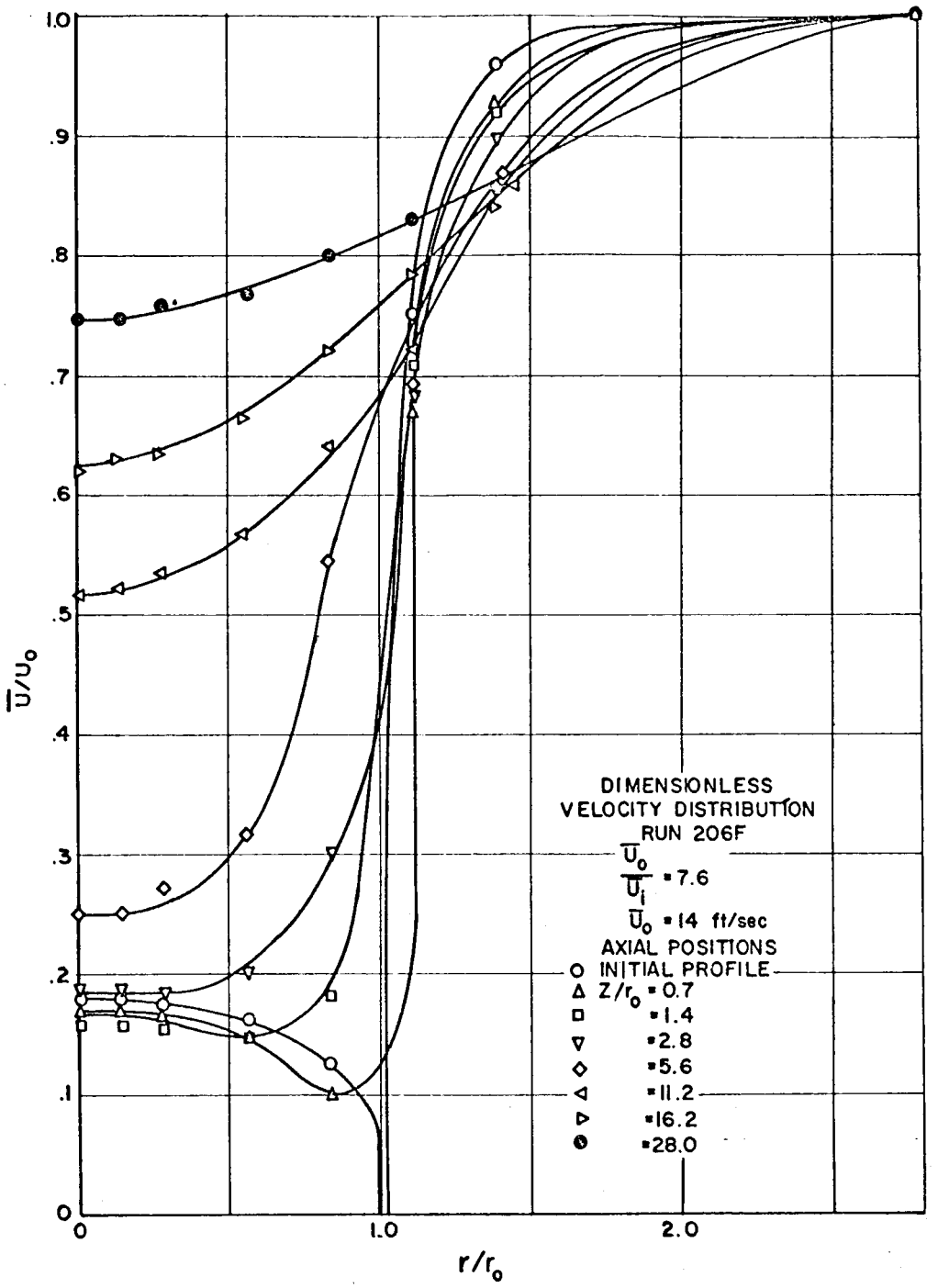

FIGURE V - 2 - 6

DIMENSIONLESS VELOCITY PROFILES, HETEROGENEOUS,

$\frac{\bar{U}_o}{\bar{U}_i} = 7.6$, $\bar{U}_o = 14$ ft/sec., $\frac{\rho_o}{\rho_i} = 0.25$

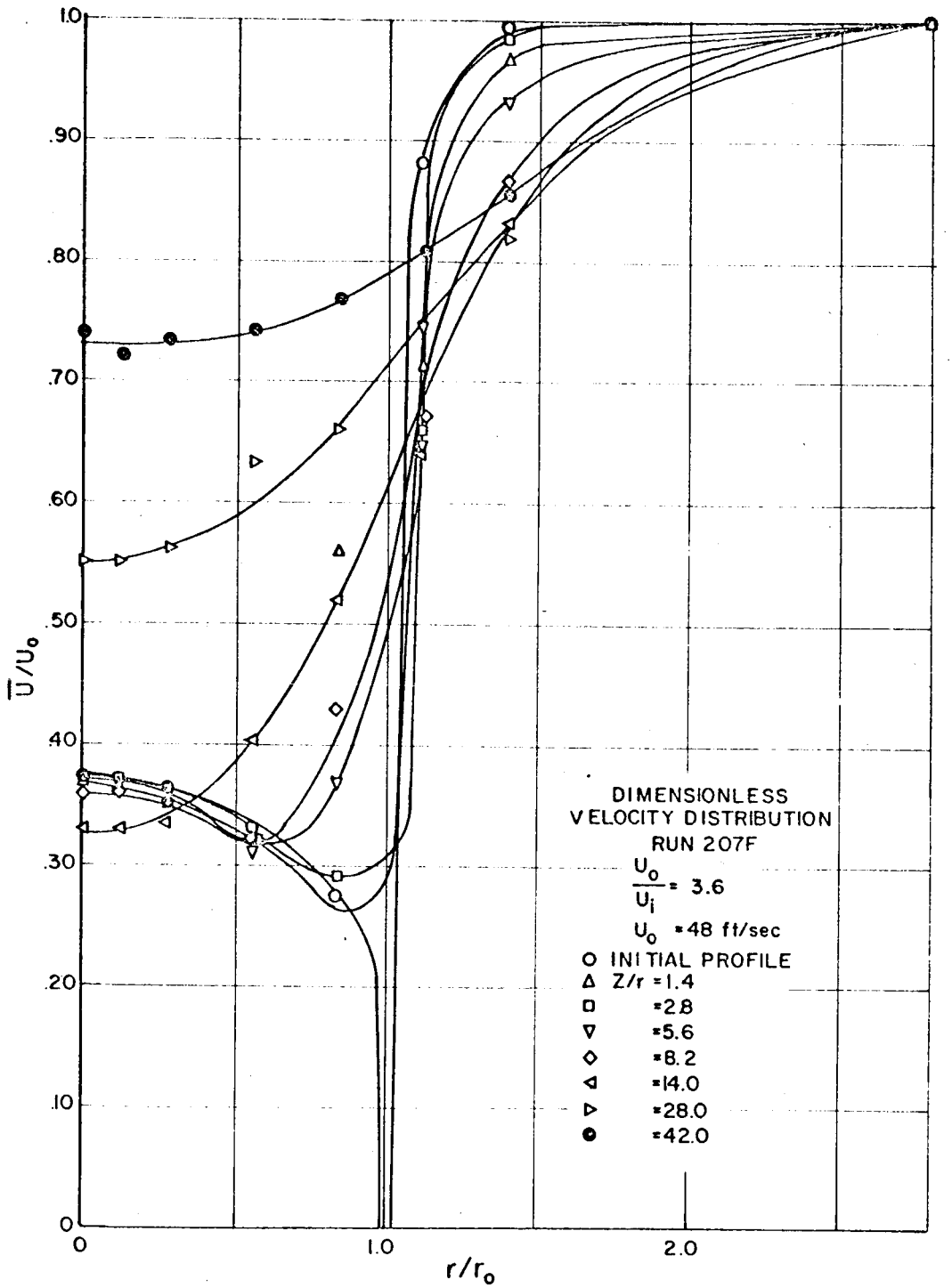

FIGURE V - 2 - 7

DIMENSIONLESS VELOCITY PROFILES, HETEROGENEOUS,

$\frac{\overline{U}_o}{\overline{U}_i}$ = 3.6, $\overline{U}_o$ - 48 ft /sec., $\frac{\rho_o}{\rho_i}$ = 0.25

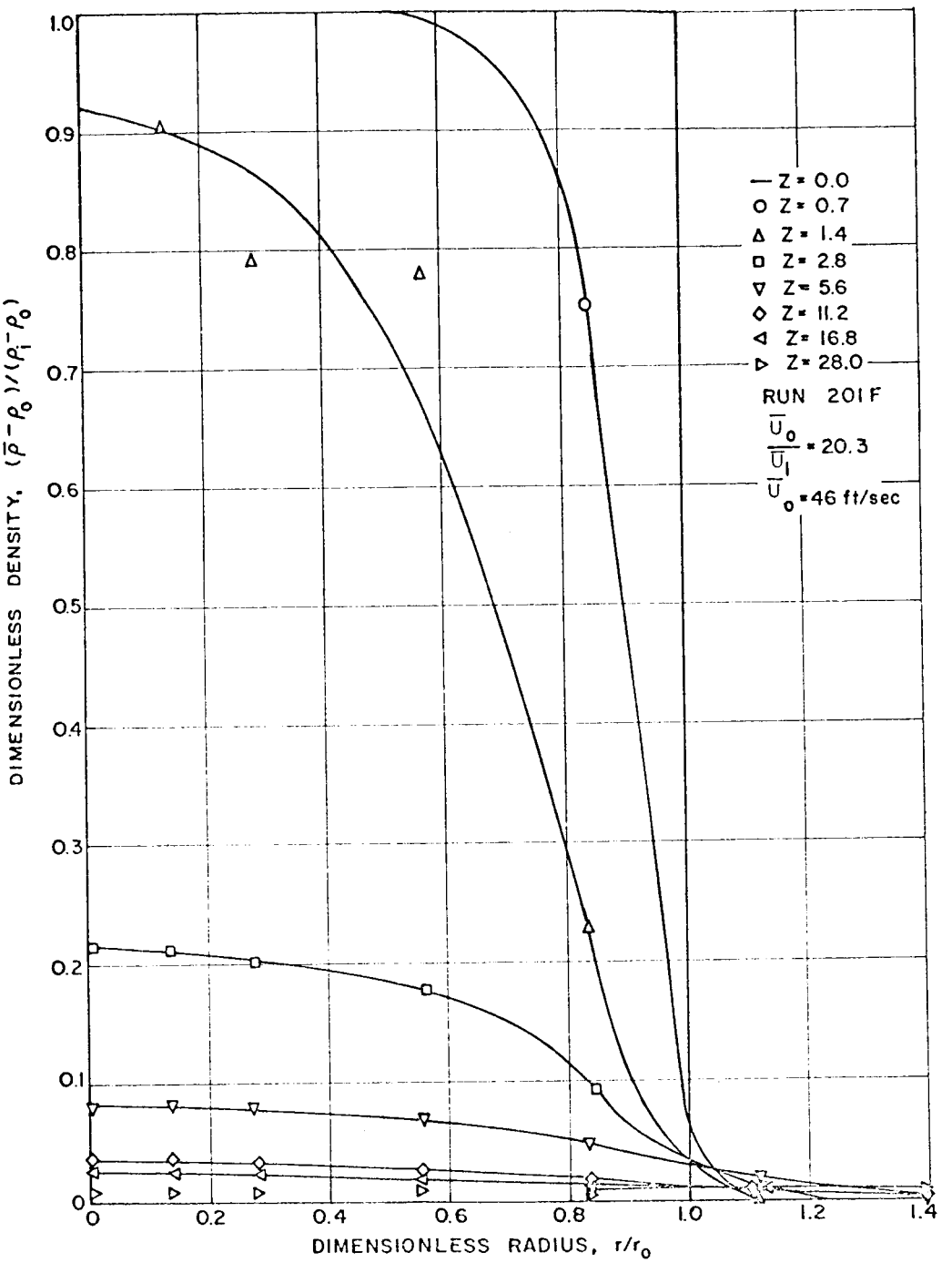

FIGURE V - 2 - 8

CONCENTRATION PROFILES, $\frac{U_o}{U_i} = 20.3$, $\frac{\rho_i}{\rho_i} = 0.25$

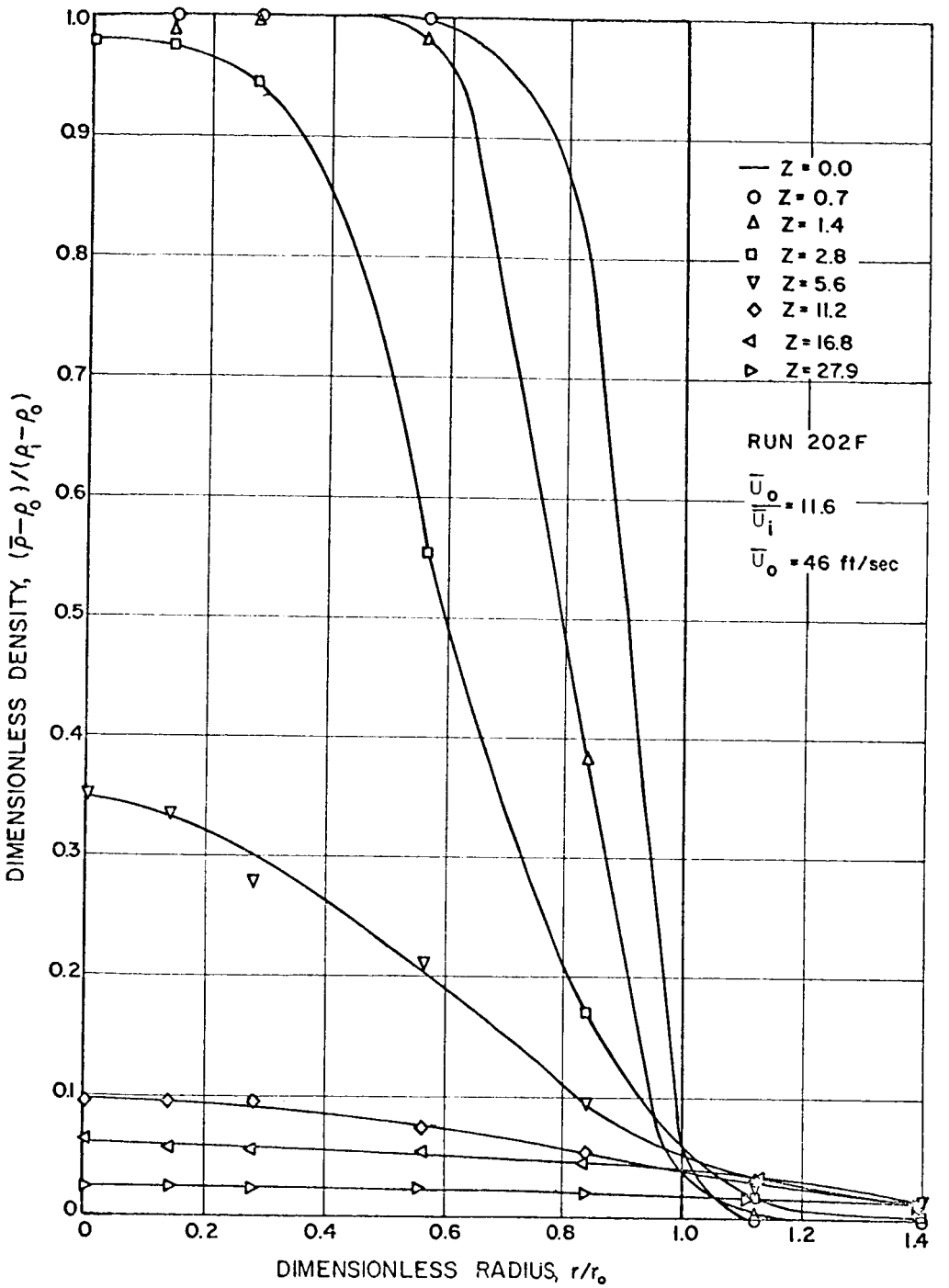

FIGURE V - 2- 9

CONCENTRATION PROFILES, $\frac{U_o}{U_i} = 11.6$, $\frac{c_o}{\rho_i} = 0.25$

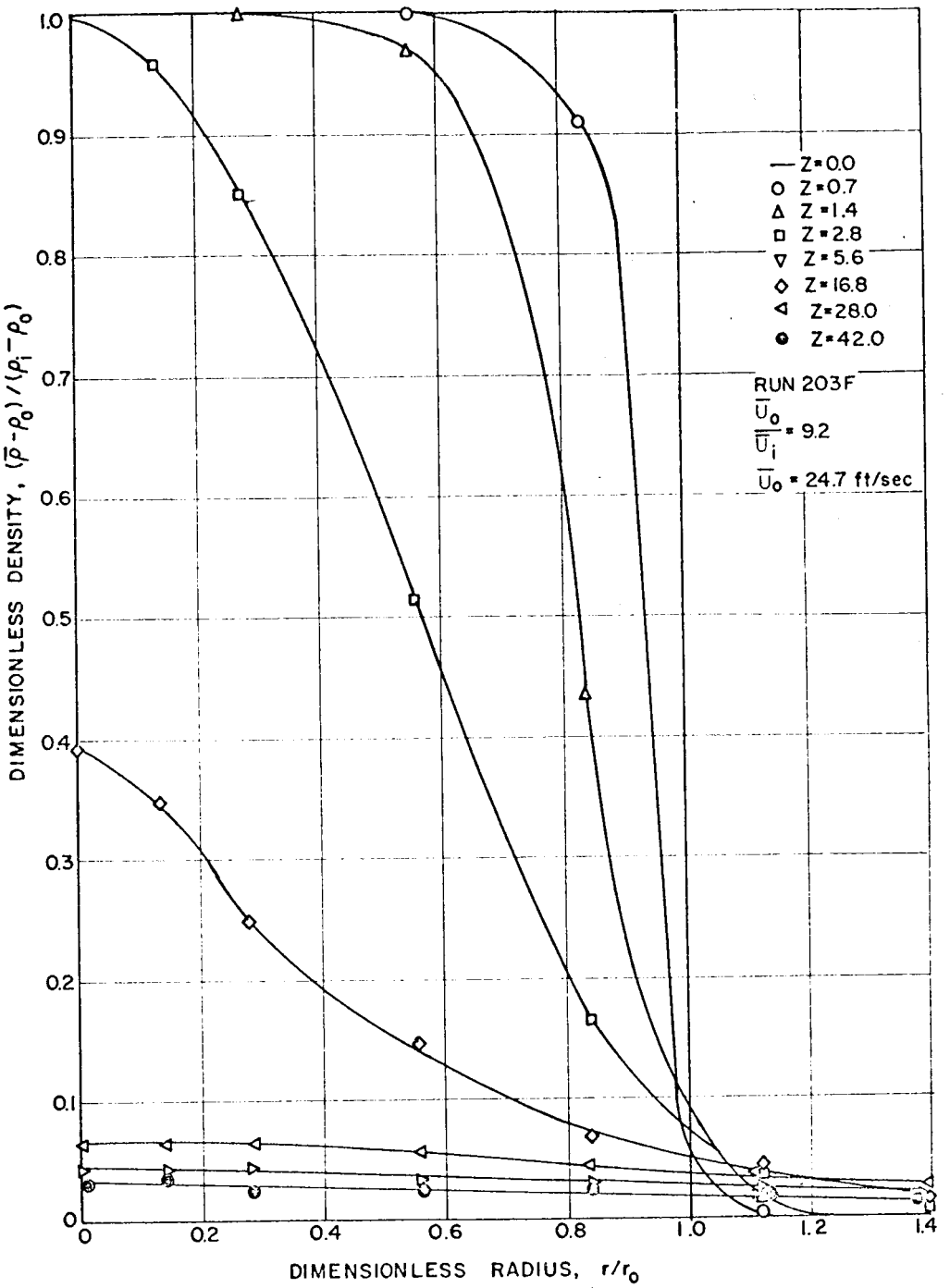

FIGURE V - 2 - 10

CONCENTRATION PROFILES, $\frac{U_o}{U_i} = 9.2$, $\frac{\rho_o}{\rho_i} = 0.25$

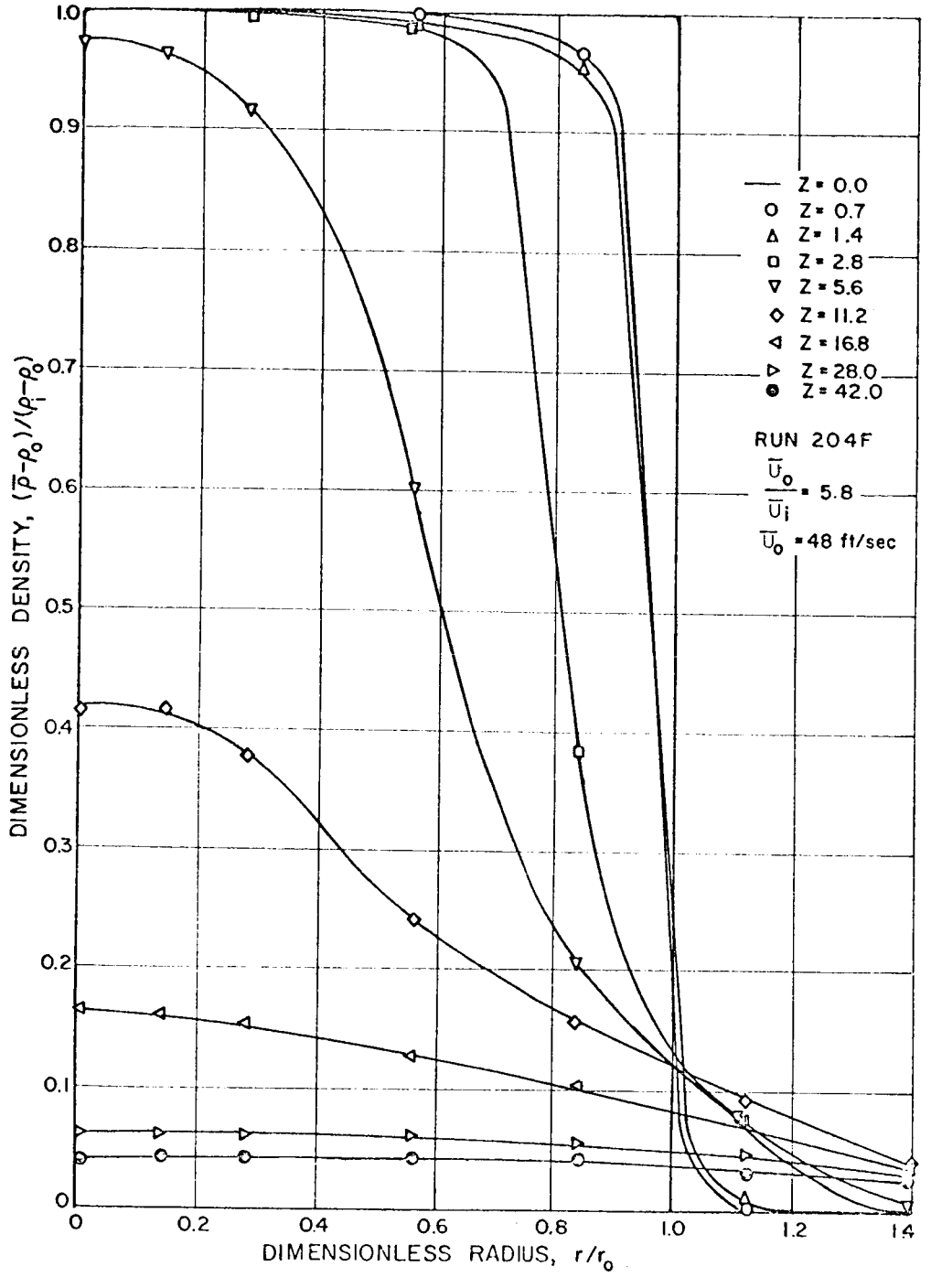

FIGURE V - 2 - 11

CONCENTRATION PROFILES, $\frac{U_o}{U_i} = 5.8$, $\frac{\rho_i}{\rho_i} = 0.25$

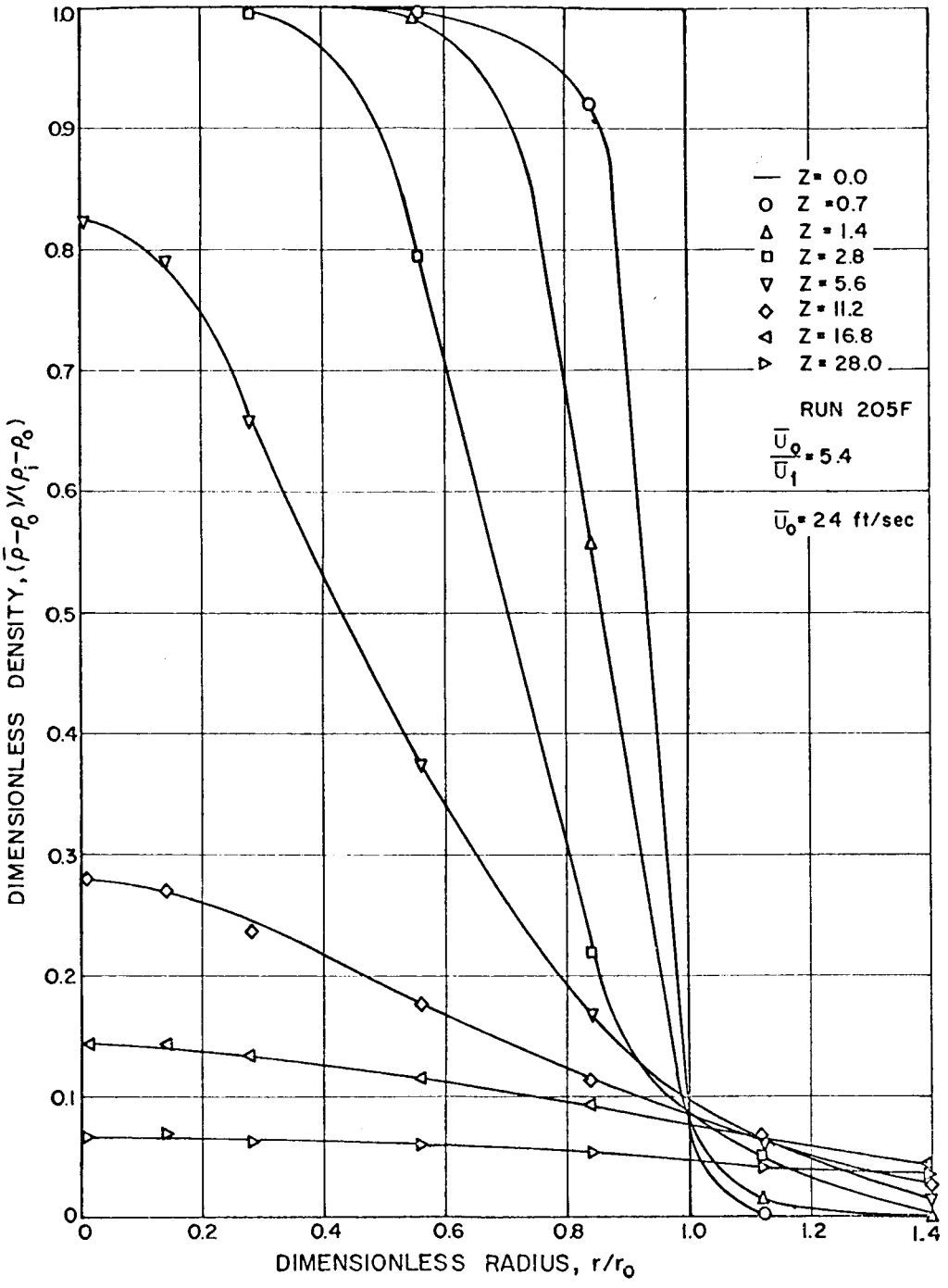

FIGURE V - 2 - 12

CONCENTRATION PROFILES, $\frac{U_o}{U_i} = 5.4$, $\frac{\rho_o}{\rho_i} = 0.25$

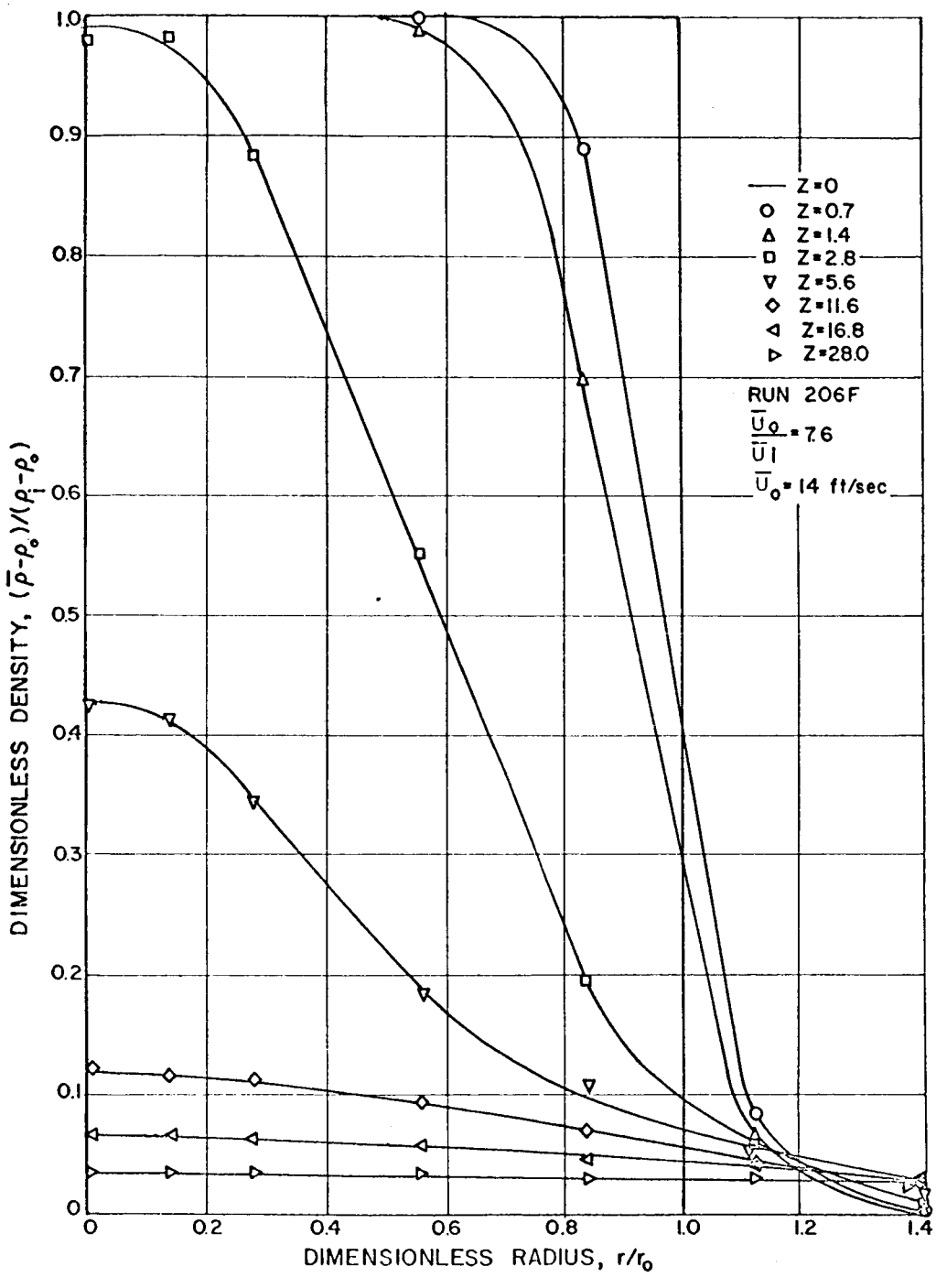

FIGURE V - 2 - 13

CONCENTRATION PROFILES, $\frac{U_o}{U_i} = 7.6$, $\frac{\rho_o}{\rho_i} = 0.25$

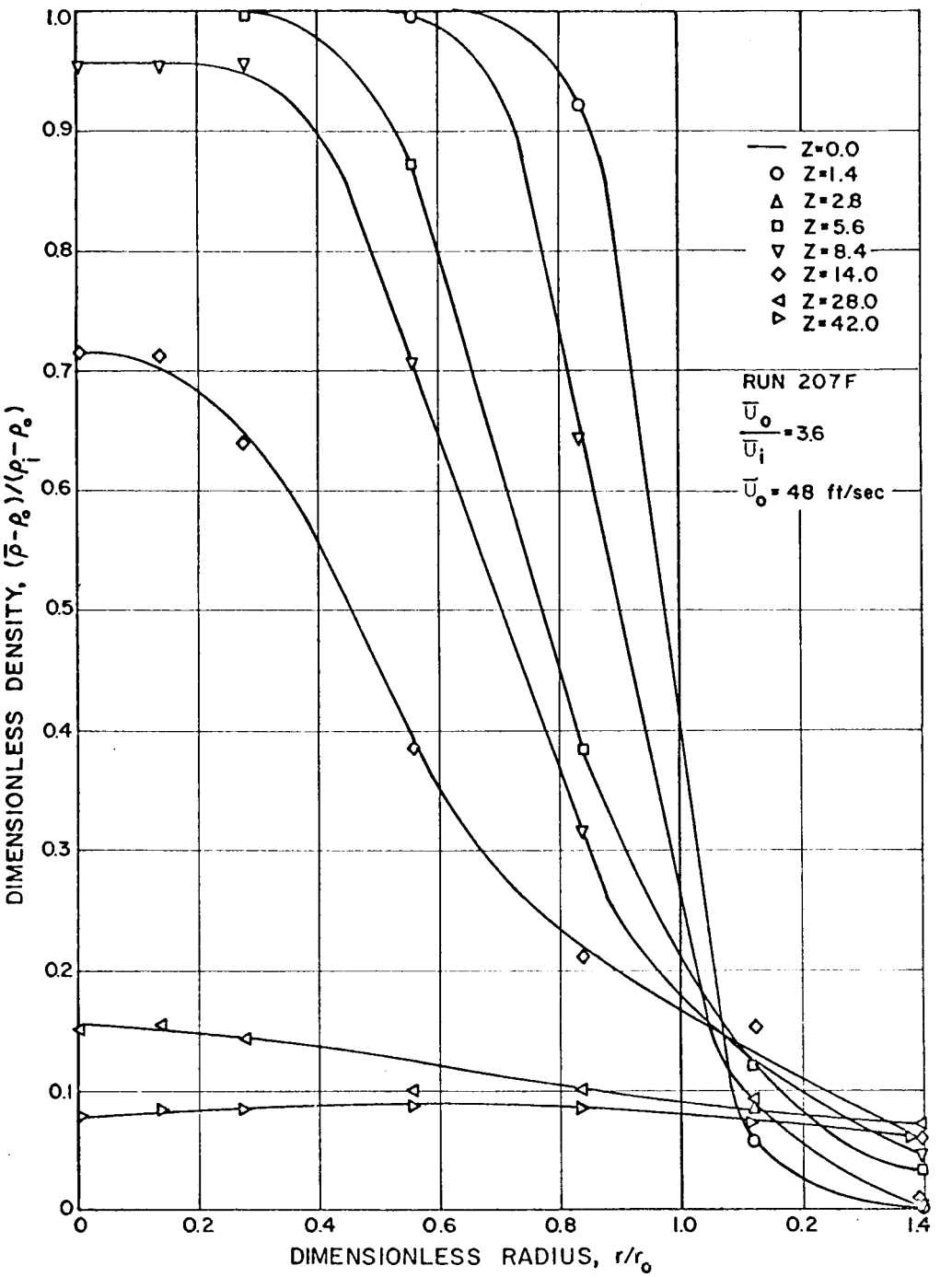

FIGURE V - 2 - 14

CONCENTRATION PROFILES, $\frac{U_o}{U_i} = 3.6, \frac{\rho_o}{\rho_i} = 0.25$

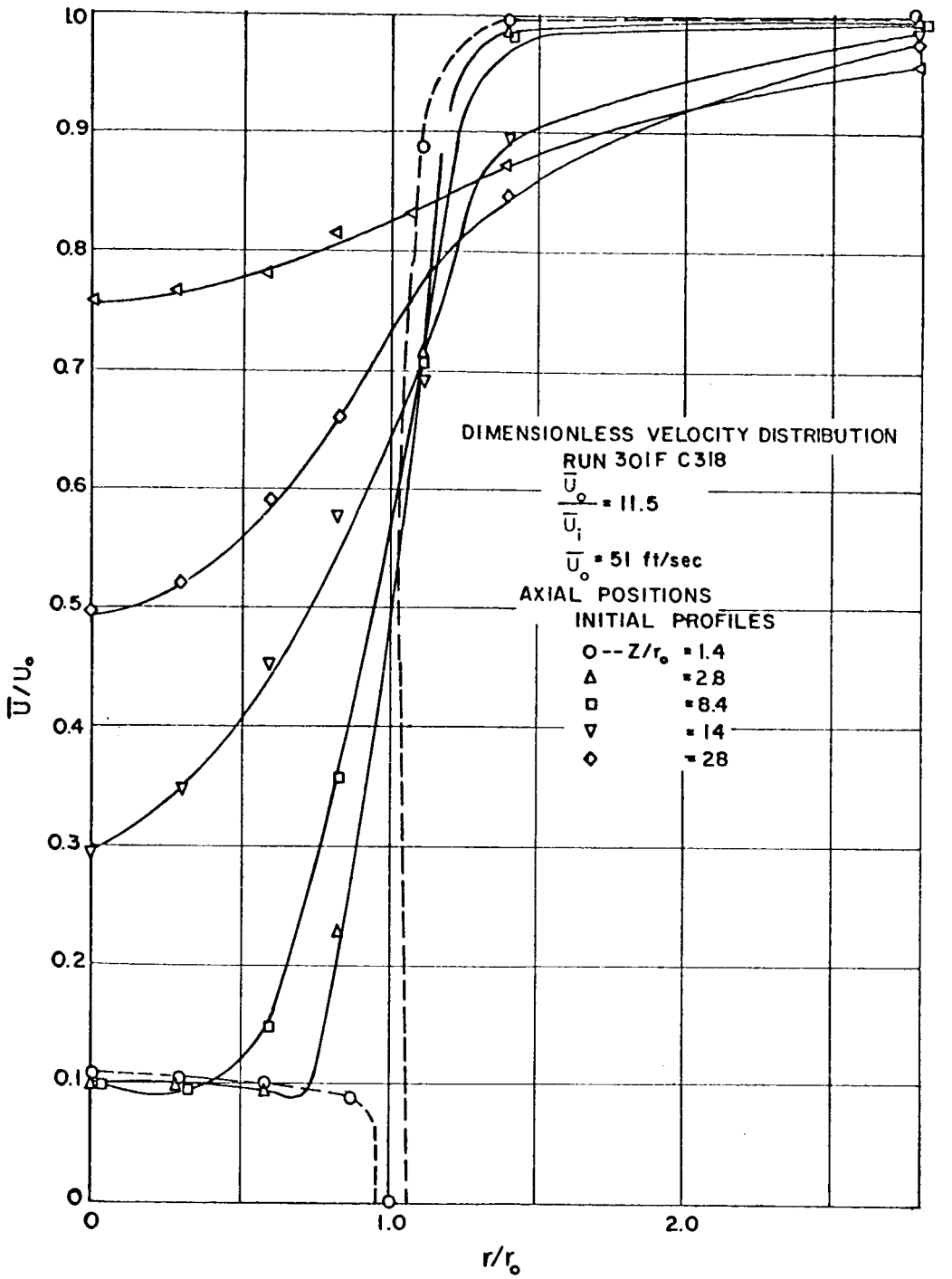

FIGURE V - 2 - 15

DIMENSIONLESS VELOCITY PROFILES, $\frac{U_o}{U_i}$ = 11.5,

U_o = 51 ft/sec, $\frac{\rho_o}{\rho_i}$ = 0.143

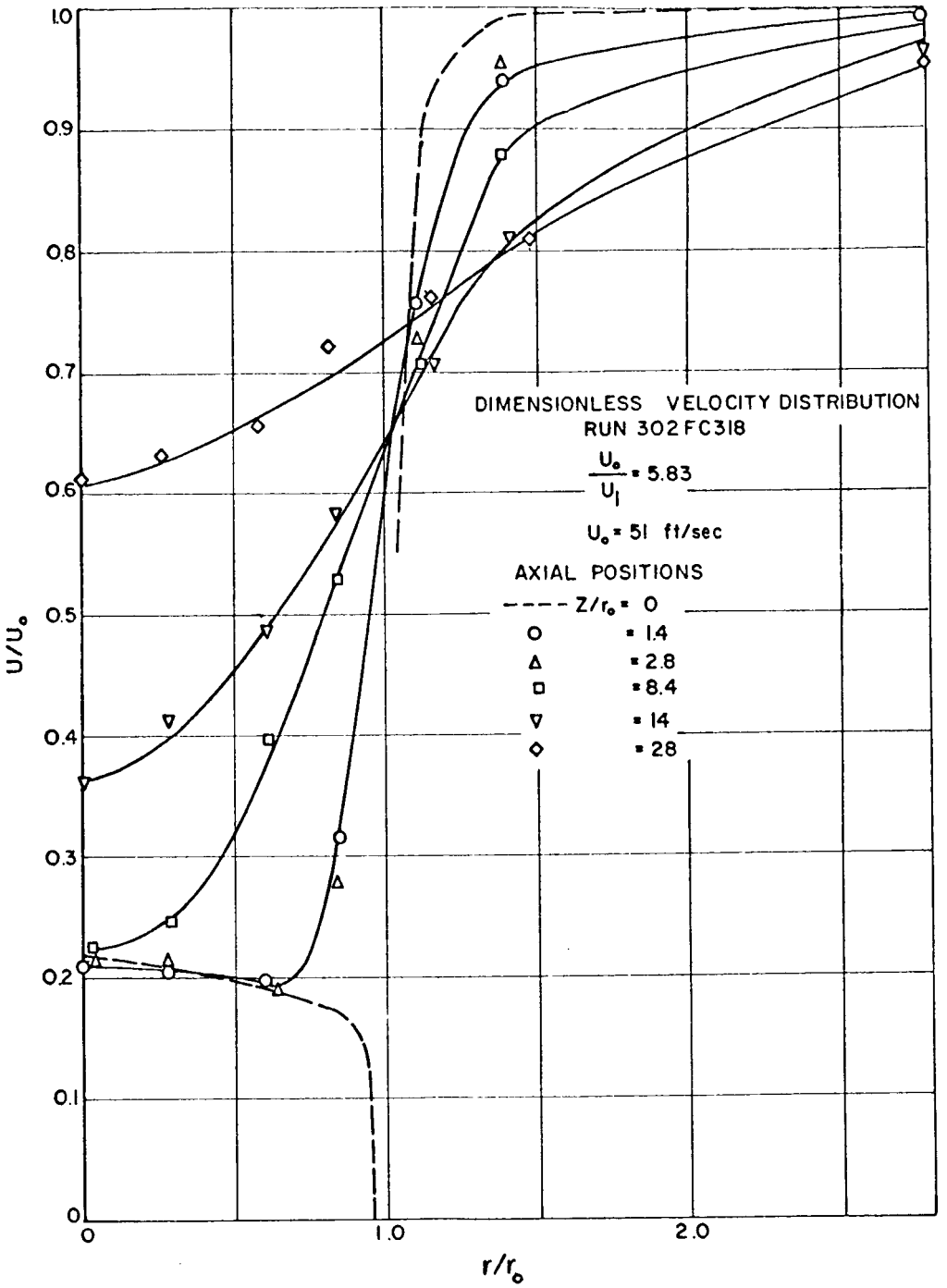

FIGURE V - 2 - 16

DIMENSIONLESS VELOCITY PROFILES $\frac{U_o}{U_i}$ = 5.8, U_o = 51 ft/sec

$\frac{\rho_o}{\rho_i}$ = 0/143

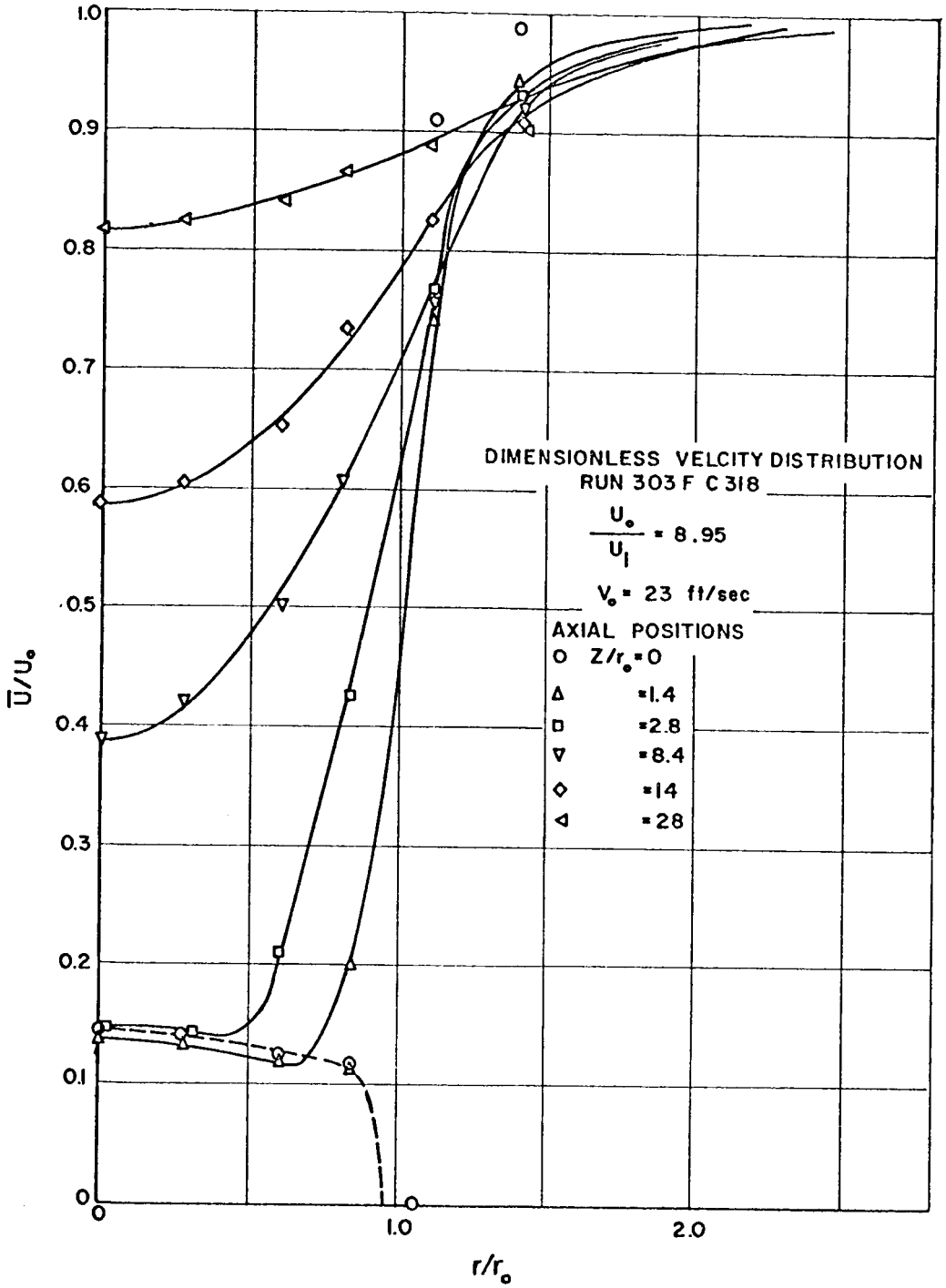

FIGURE V - 2 - 17

DIMENSIONLESS VELOCITY PROFILES, $\frac{U_o}{U_i}$ = 8.9,

U_o = 23 ft/sec $\frac{\rho_o}{\rho_i}$ = 0.143

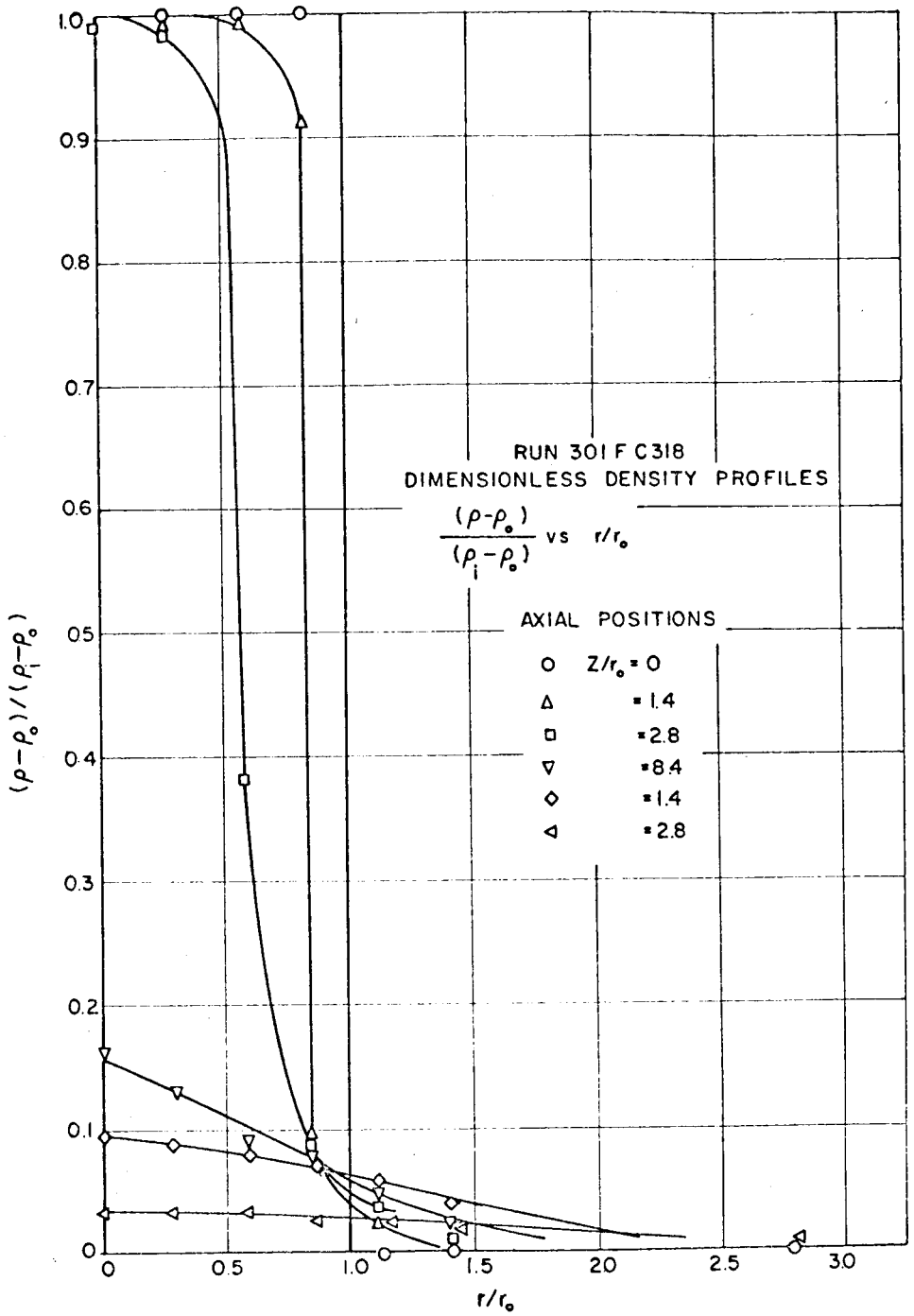

FIGURE V - 2 - 18

CONCENTRATION PROFILES, $\frac{U_o}{U_i} = 11.5$ $\frac{\rho_o}{\rho_i} = 0.143$

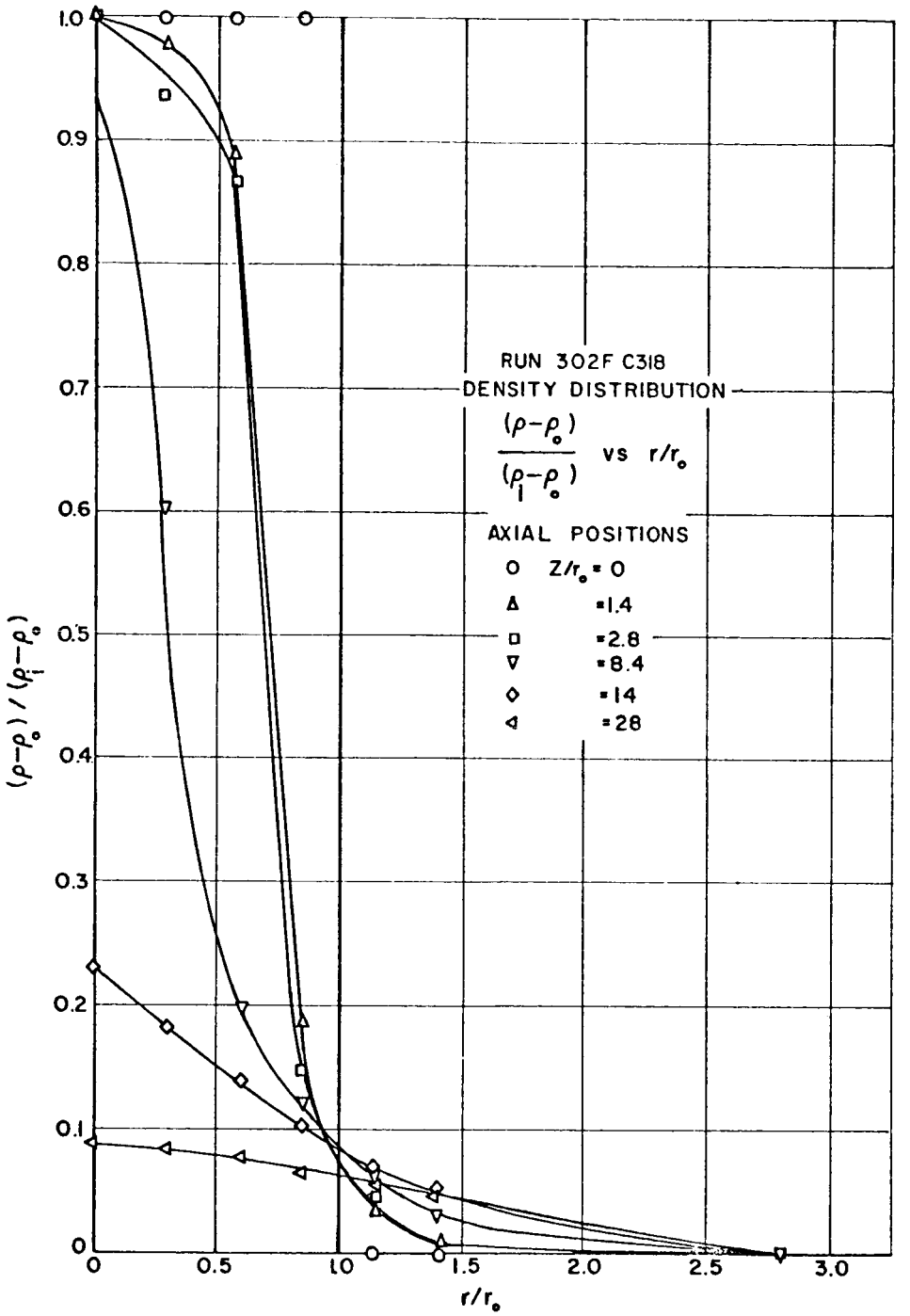

FIGURE V - 2 - 19

CONCENTRATION PROFILES, $\frac{U_o}{U_i} = 5.8$, $\frac{\rho_o}{\rho_i} = 0.143$

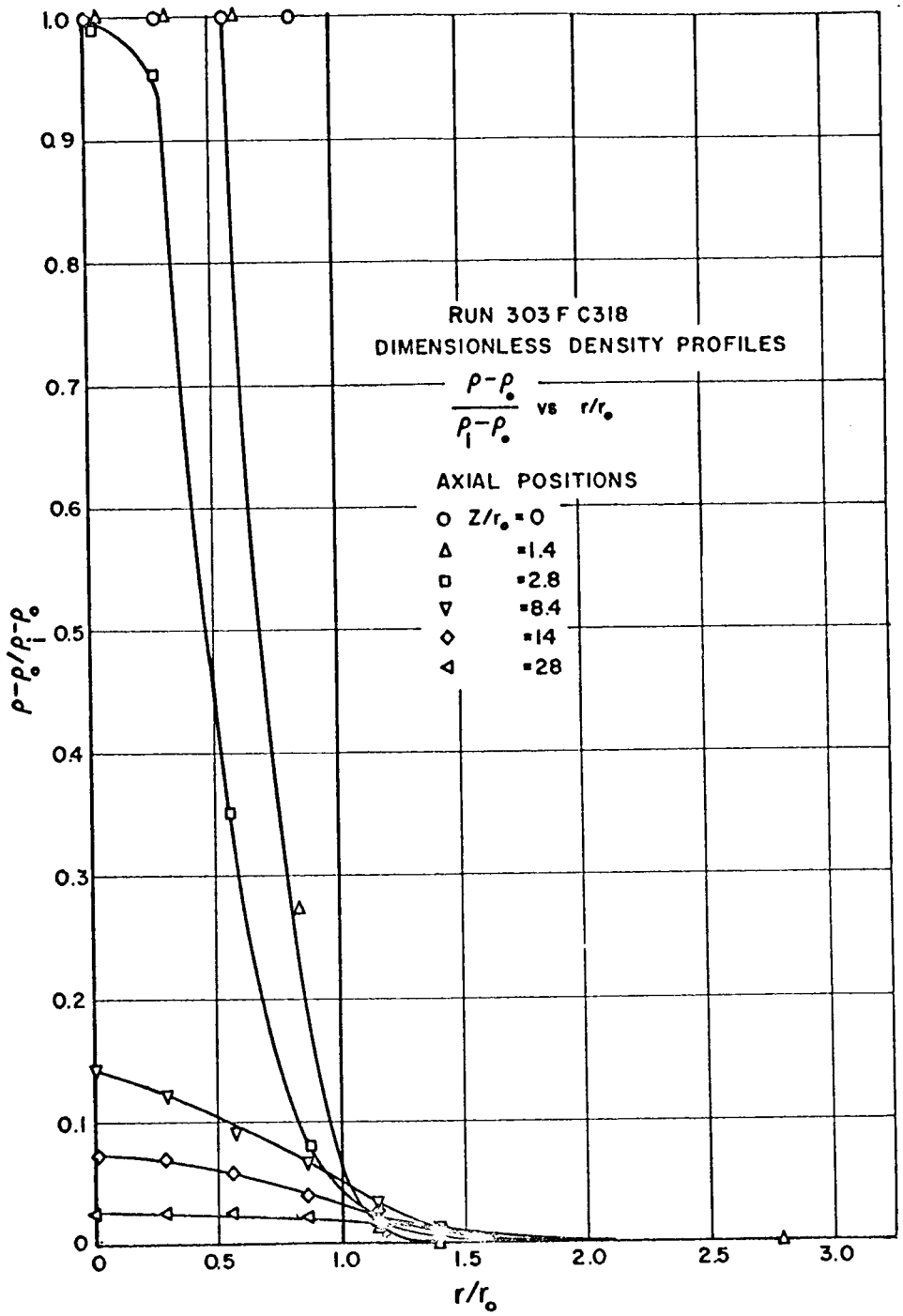

FIGURE V - 2 - 20

CONCENTRATION PROFILES, $\frac{U_o}{U_i} = 8.9$, $\frac{\rho_o}{\rho_i} = 0.143$

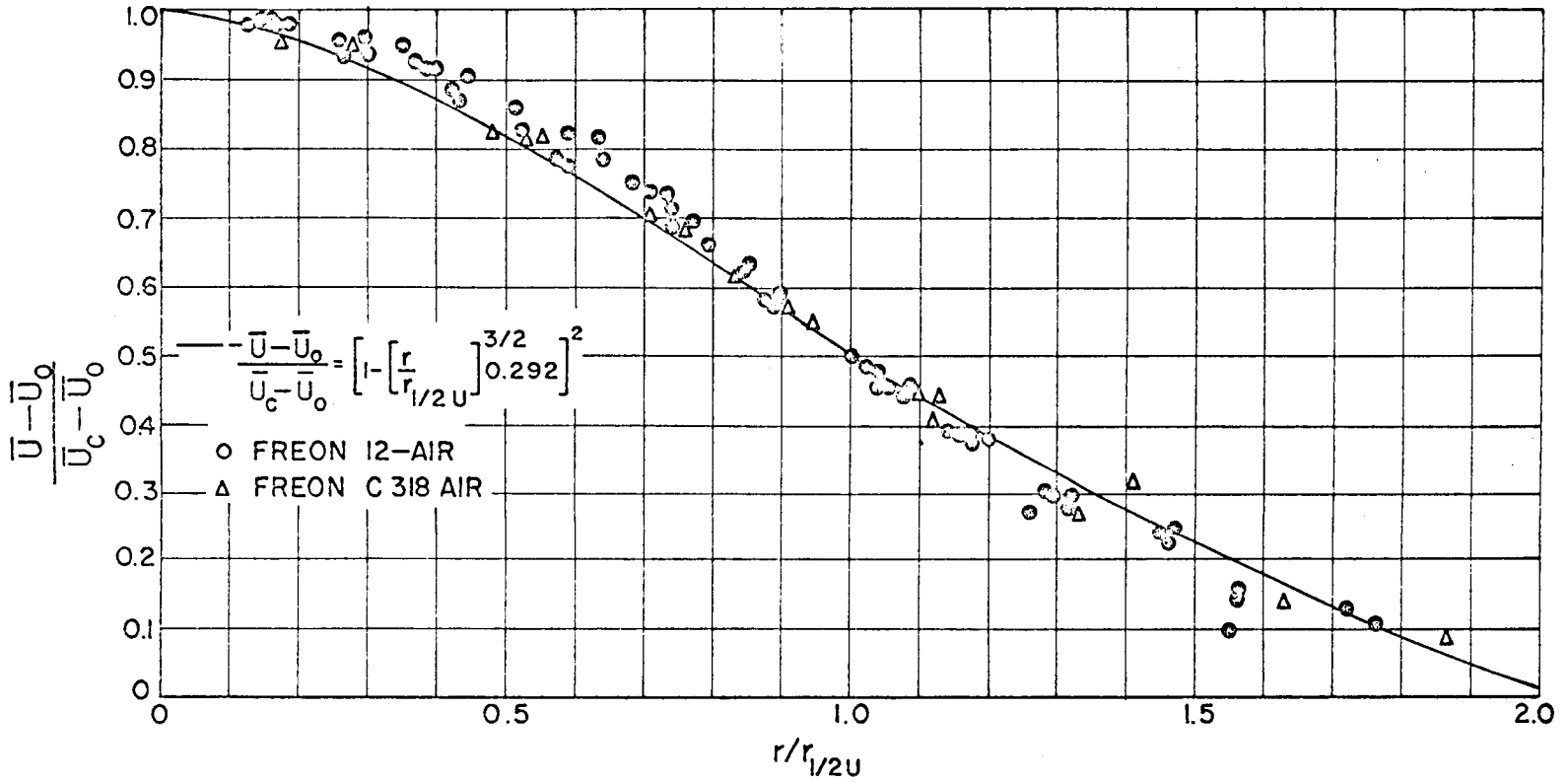

FIGURE V - 2- 21

SIMILARITY PLOT OF VELOCITY PROFILES FOR ALL HETEROGENEOUS CASES

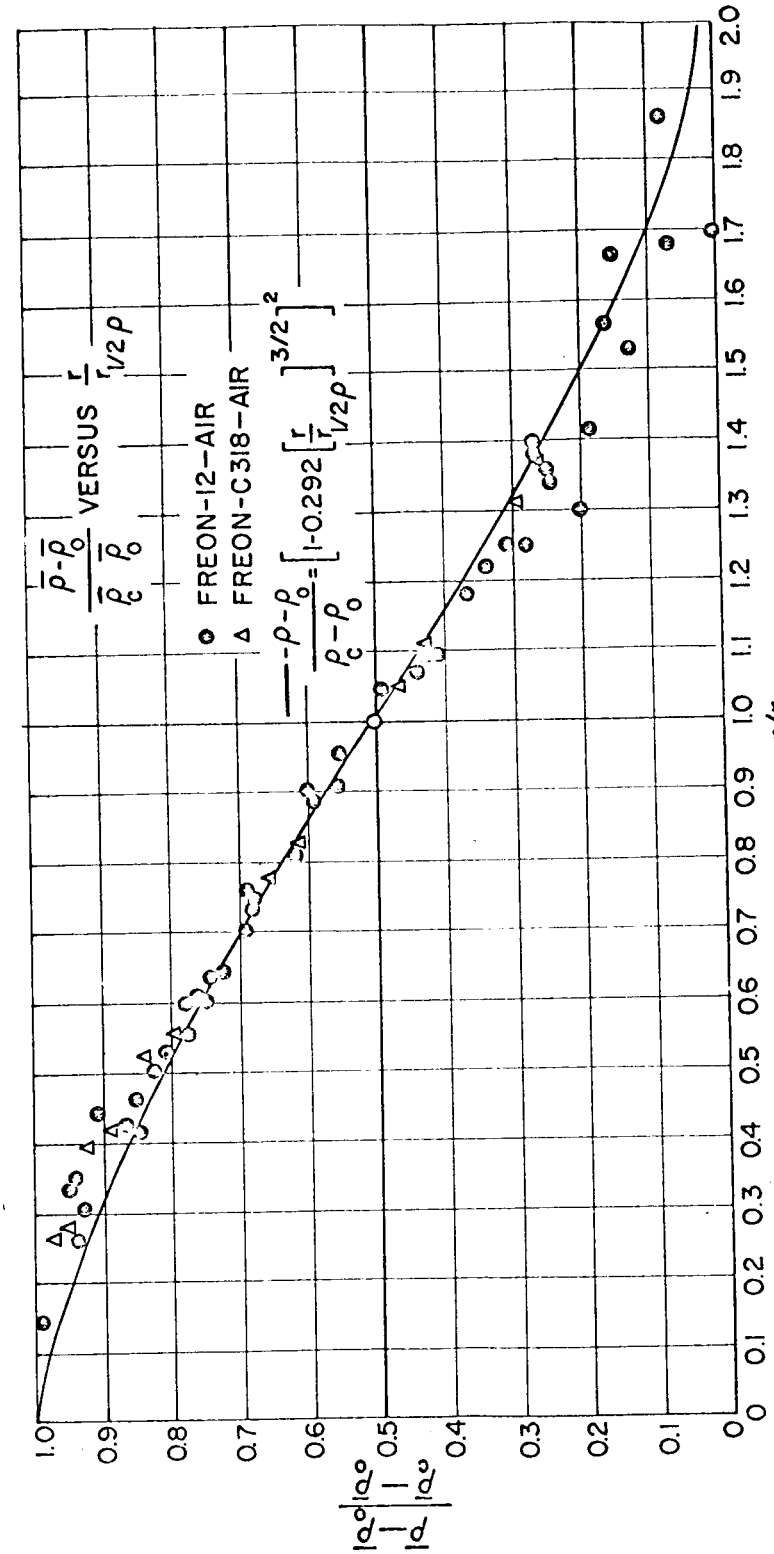

FIGURE V - 2 - 22

SIMILARITY PLOT OF THE DENSITY PROFILES $\frac{r}{r_{1/2\rho}}$

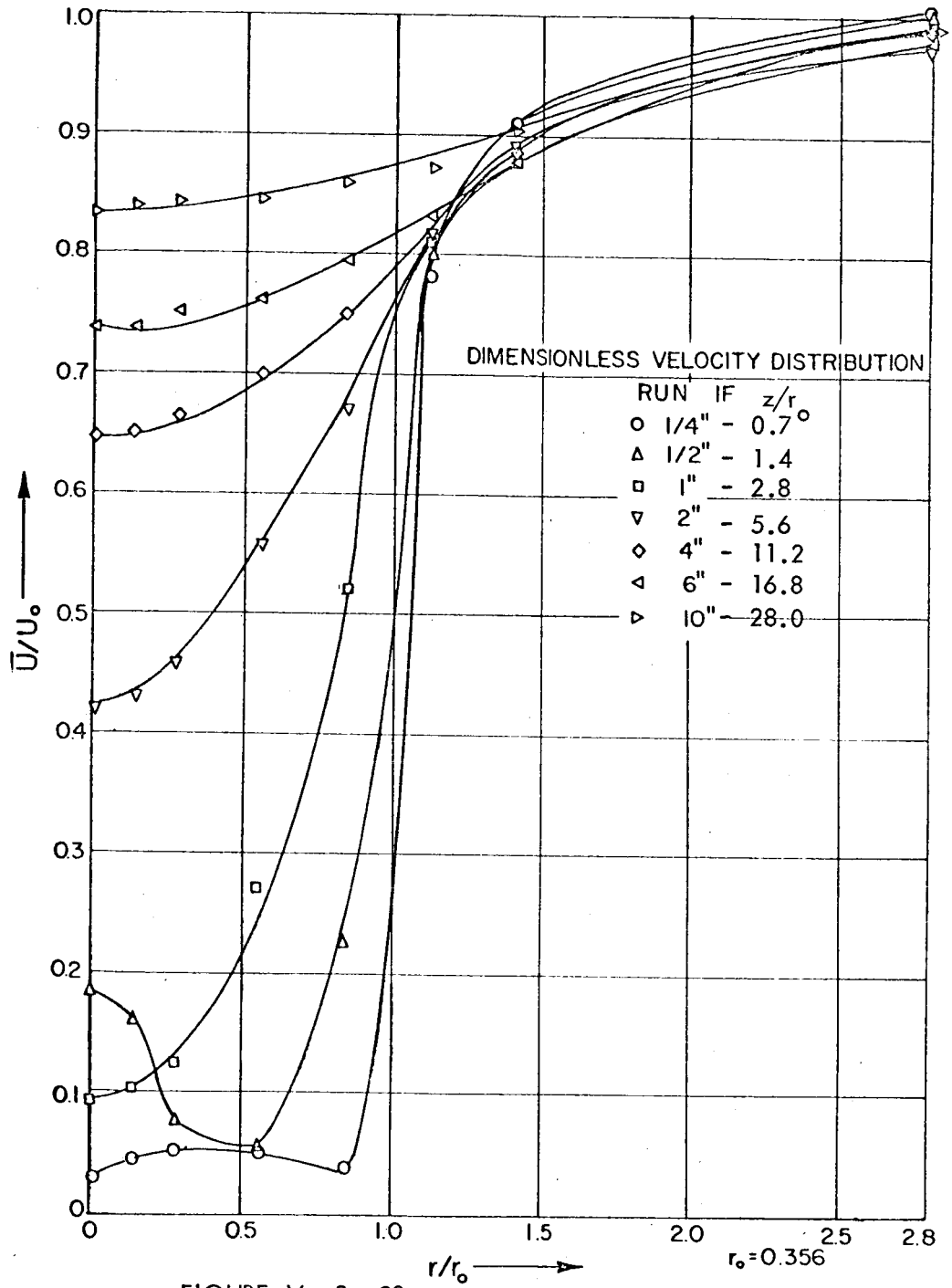

FIGURE V - 2 - 23

DIMENSIONLESS VELOCITY PROFILES, HETEROGENEOUS,

$\frac{U_o}{U_i} = 36.8, \quad U_o = 51.1$ ft/sec, $\frac{\rho_o}{\rho_i} = 0.25.$

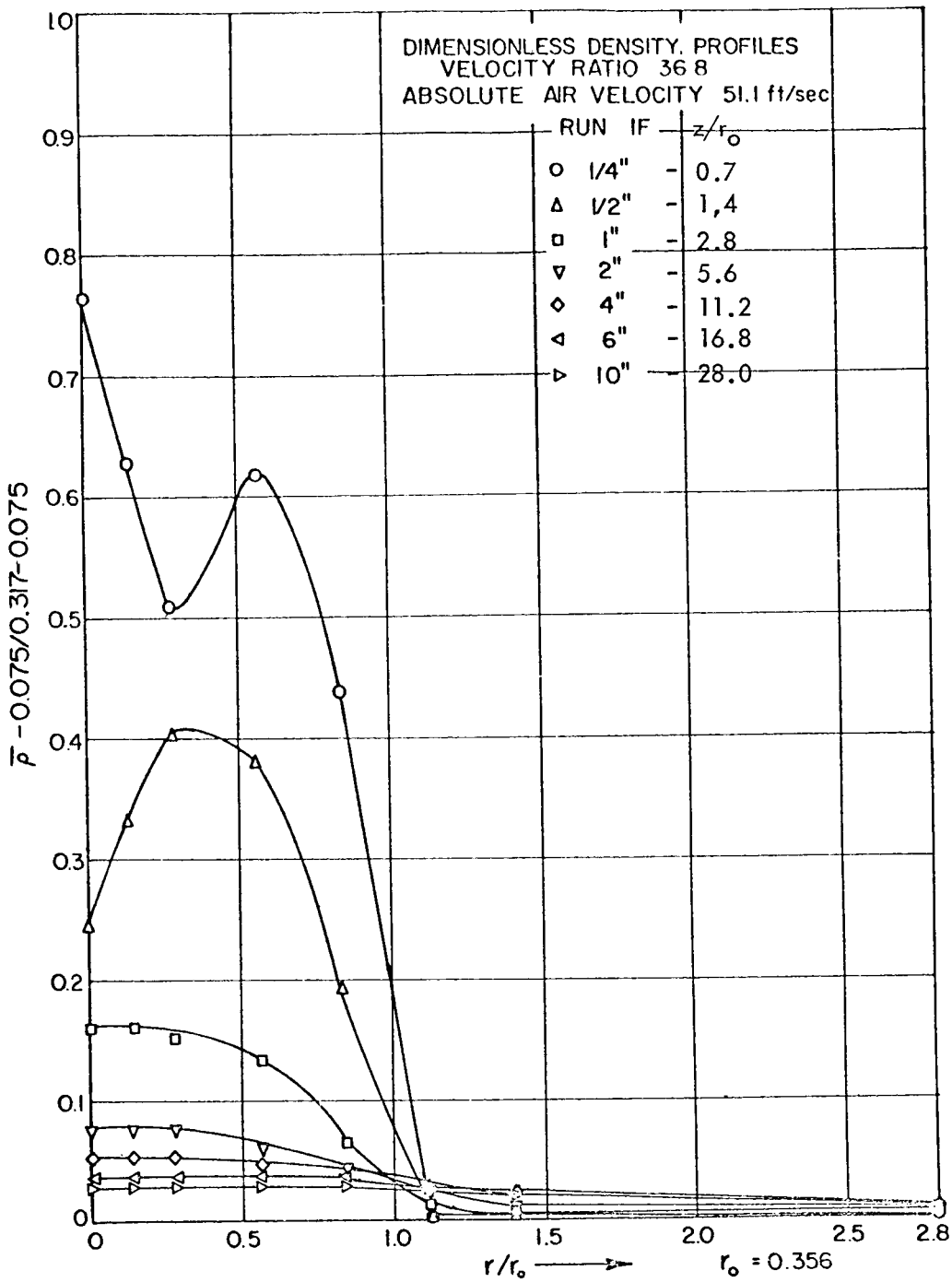

FIGURE V - 2 - 24

CONCENTRATION PROFILES, $\frac{U_o}{U_i} = 36.8$, $\frac{\rho_o}{\rho_i} = 0.25$

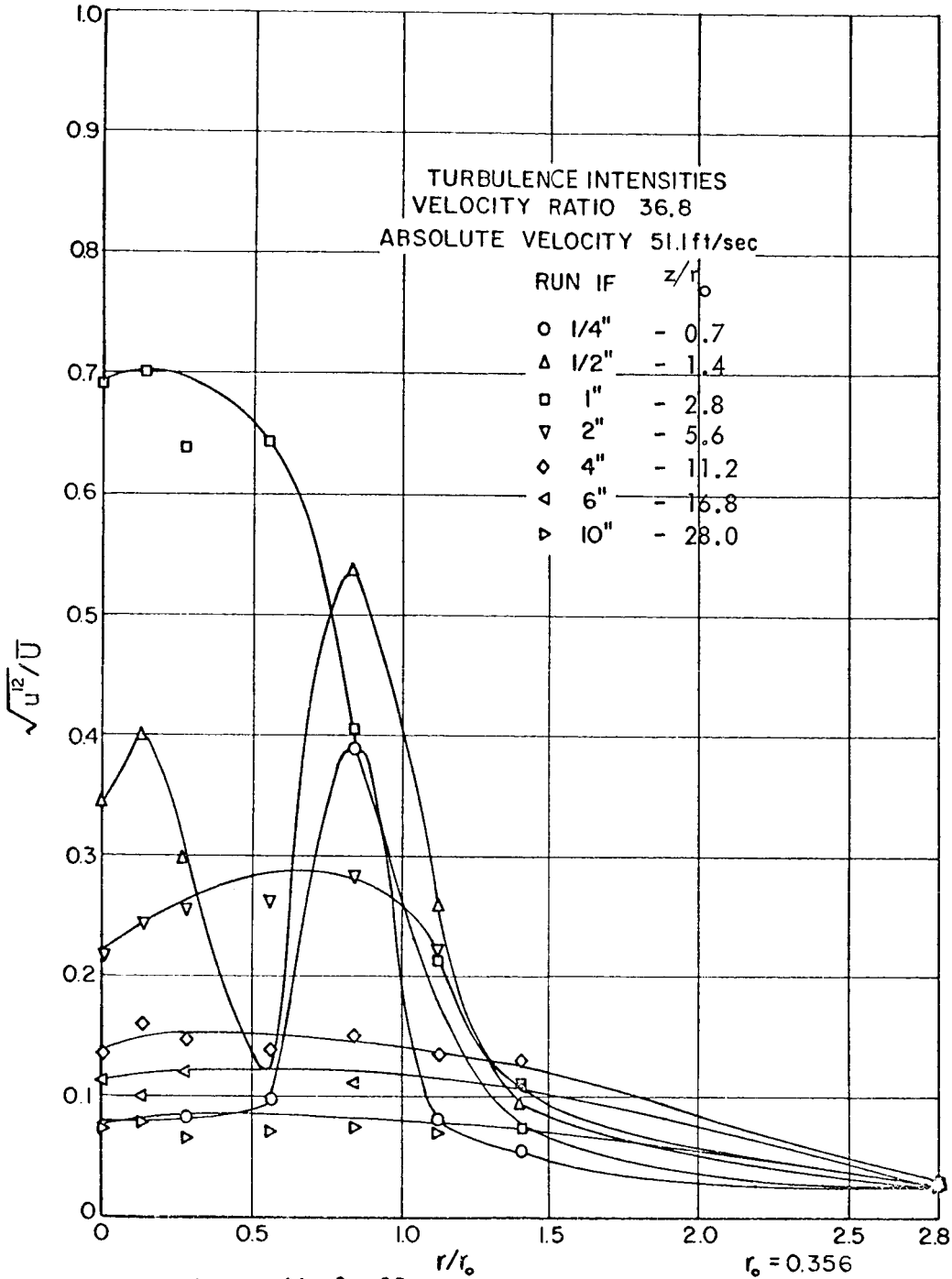

FIGURE V - 2 - 25

VELOCITY TURBULENCE INTENSITY PROFILES, HETEROGENEOUS,

$\frac{U_o}{U_i} = 36.8, \quad \frac{\rho_o}{\rho_i} = 0.25$

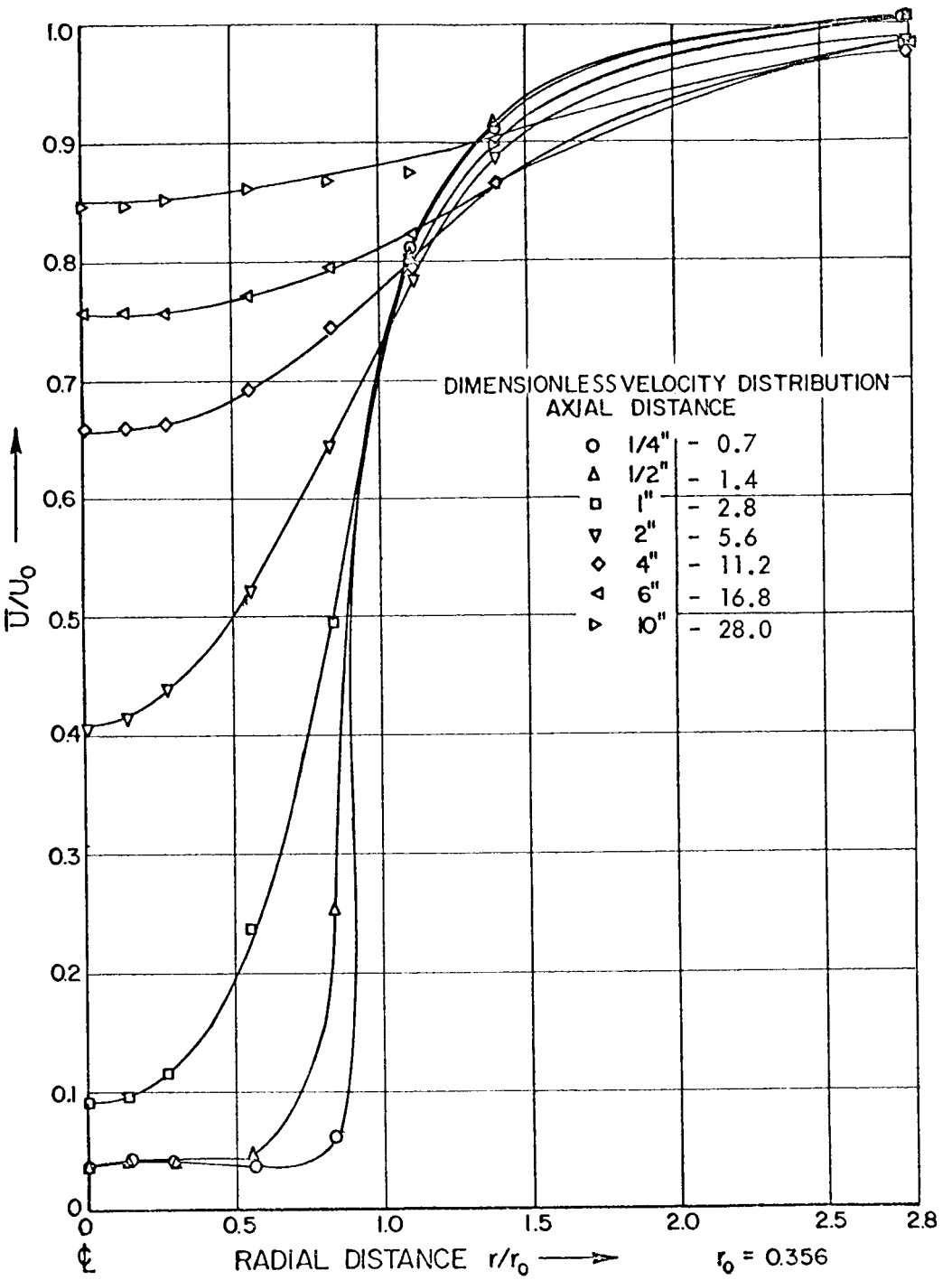

FIGURE V - 2 - 26

DIMENSIONLESS VELOCITY PROFILES, HETEROGENEOUS,

$\frac{U_o}{U_i} = 26.5 \quad U_o = 49$ ft/sec, $\frac{\rho_o}{\rho_i} = 0.25$

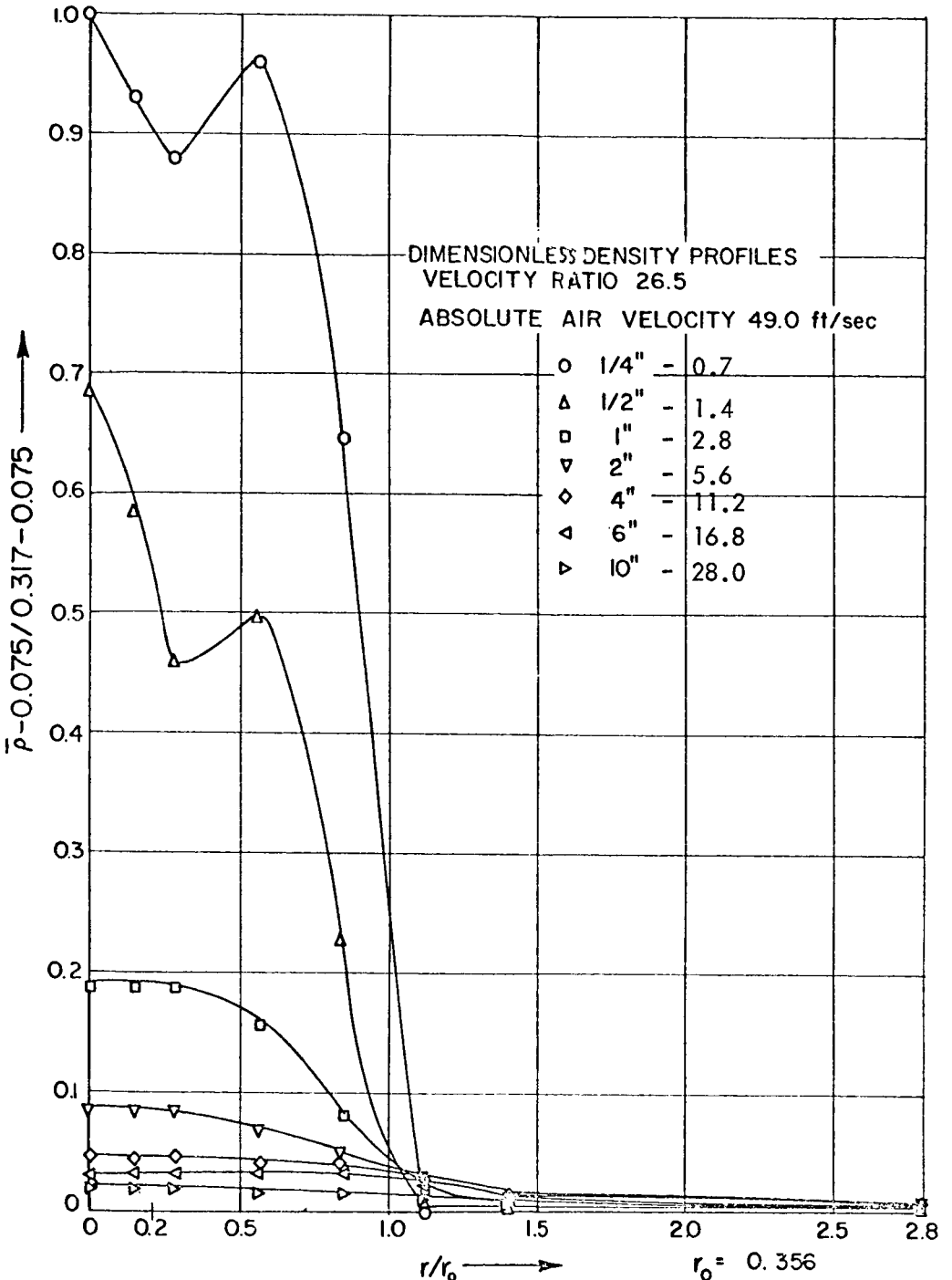

FIGURE V - 2 - 27

CONCENTRATION PROFILES, $\frac{U_o}{U_i} = 26.5$, $\frac{\rho_o}{\rho_i} = 0.25$

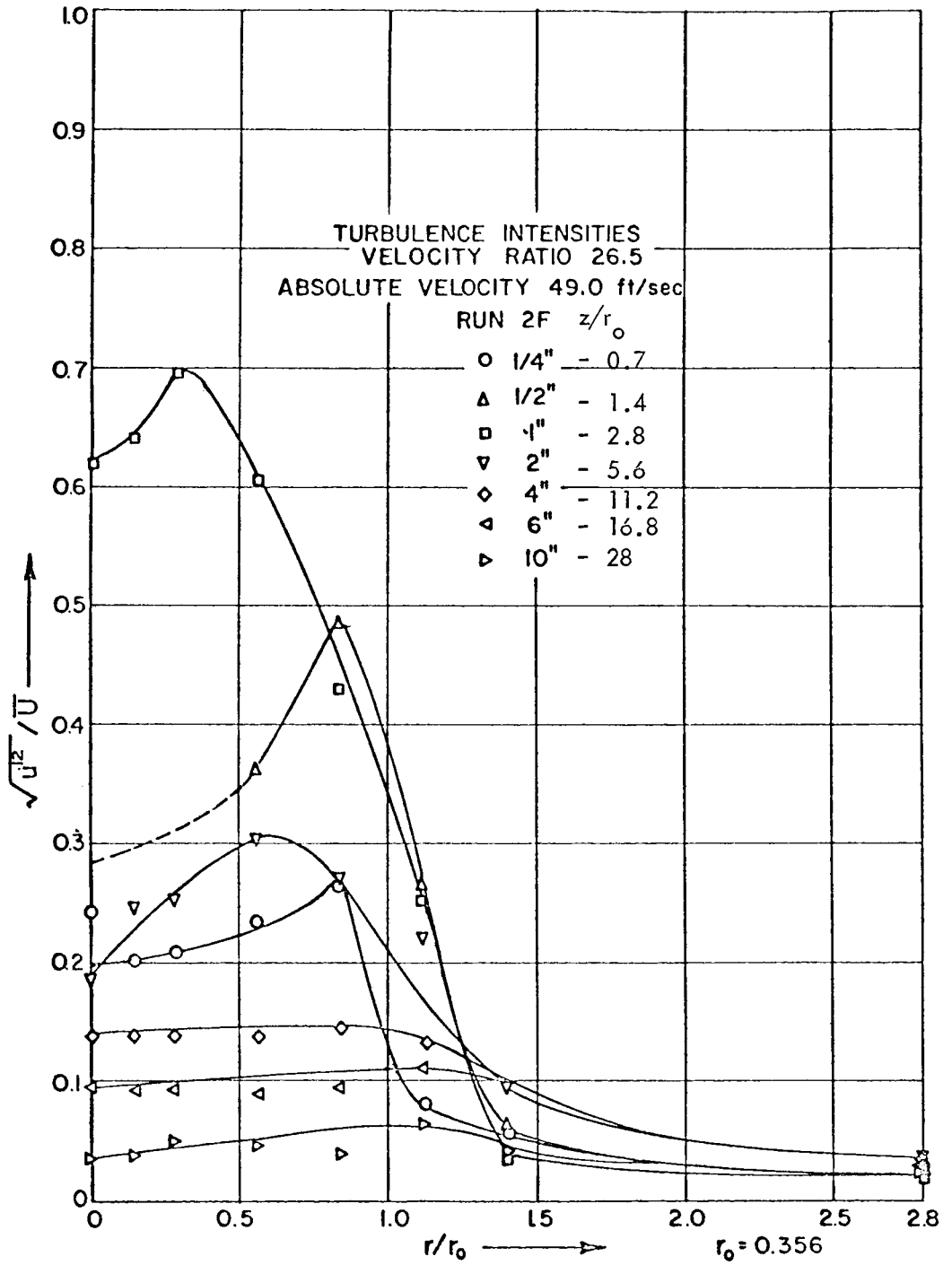

FIGURE V -2-28

VELOCITY TURBULENCE INTENSITY PROFILES,
HETEROGENEOUS, $\frac{U_o}{U_i} = 26.5$, $\frac{\rho_o}{\rho_i} = 0.25$

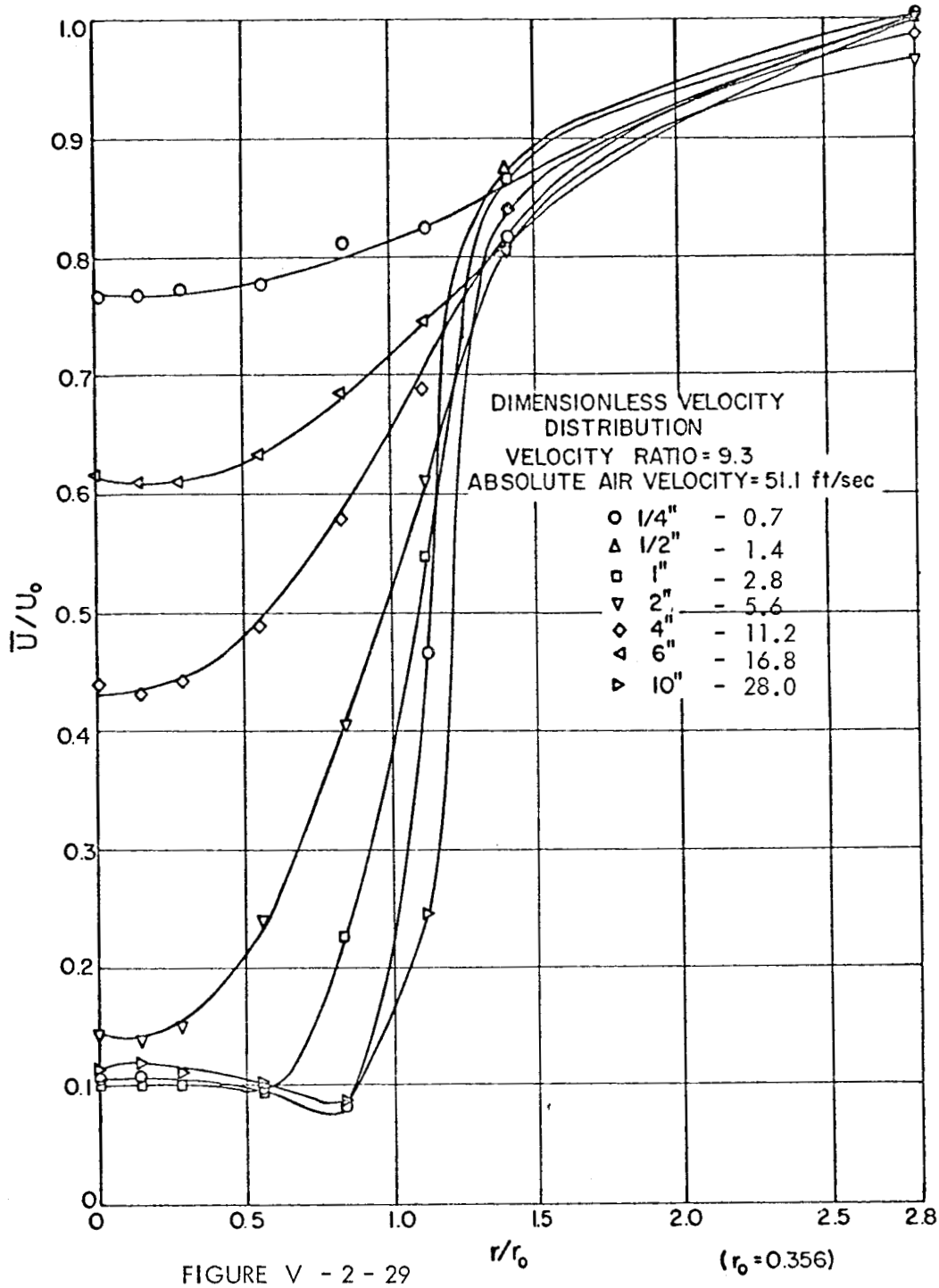

FIGURE V - 2 - 29

DIMENSIONLESS VELOCITY DISTRIBUTION, HETEROGENEOUS,

$\frac{U_o}{U_i} = 9.3, \quad \frac{\rho_o}{\rho_i} = 0.25$

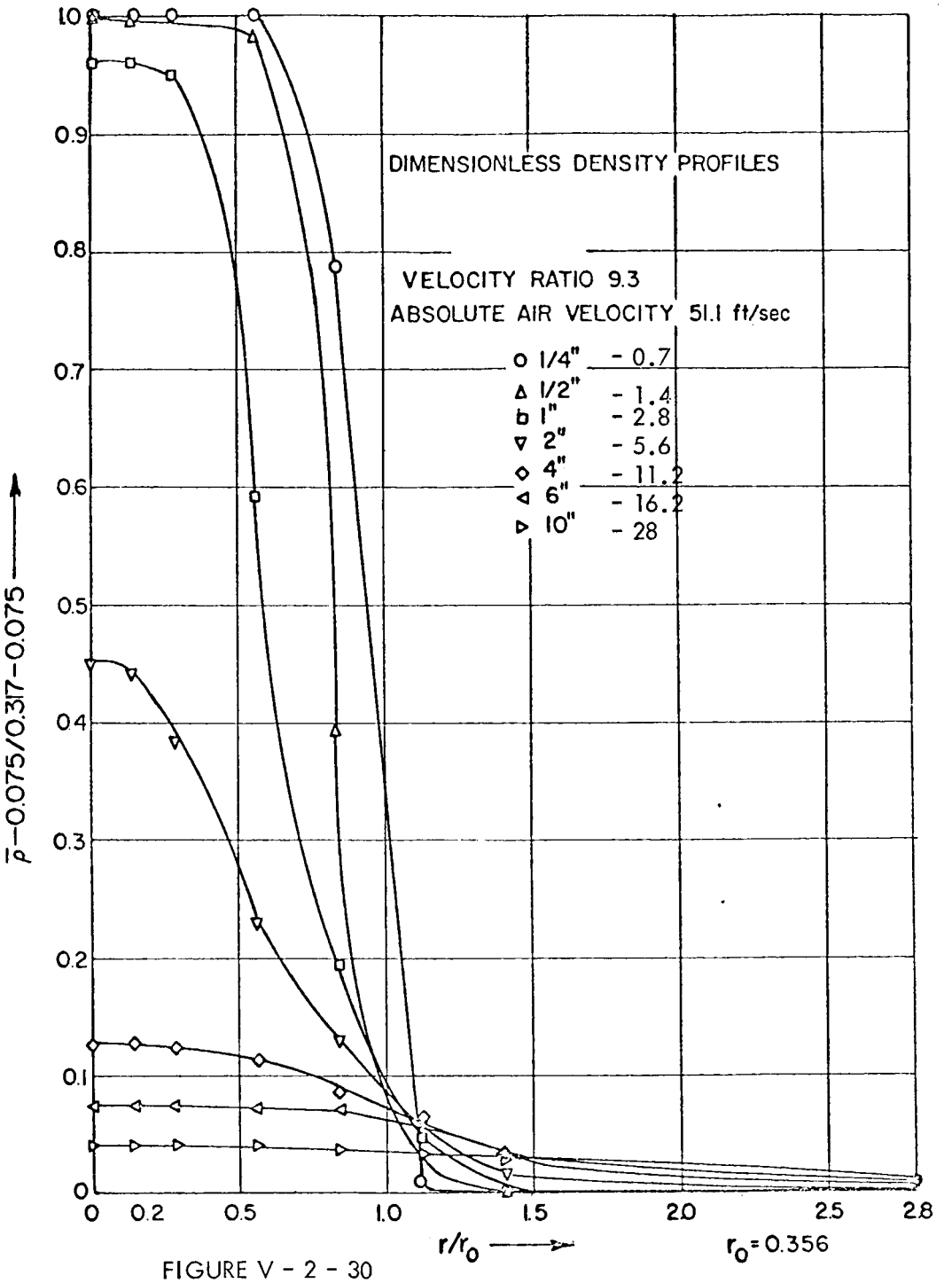

FIGURE V - 2 - 30

CONCENTRATION PROFILES, $\frac{U_o}{U_i} = 9.3$, $\frac{\rho_o}{\rho_i} = 0.25$

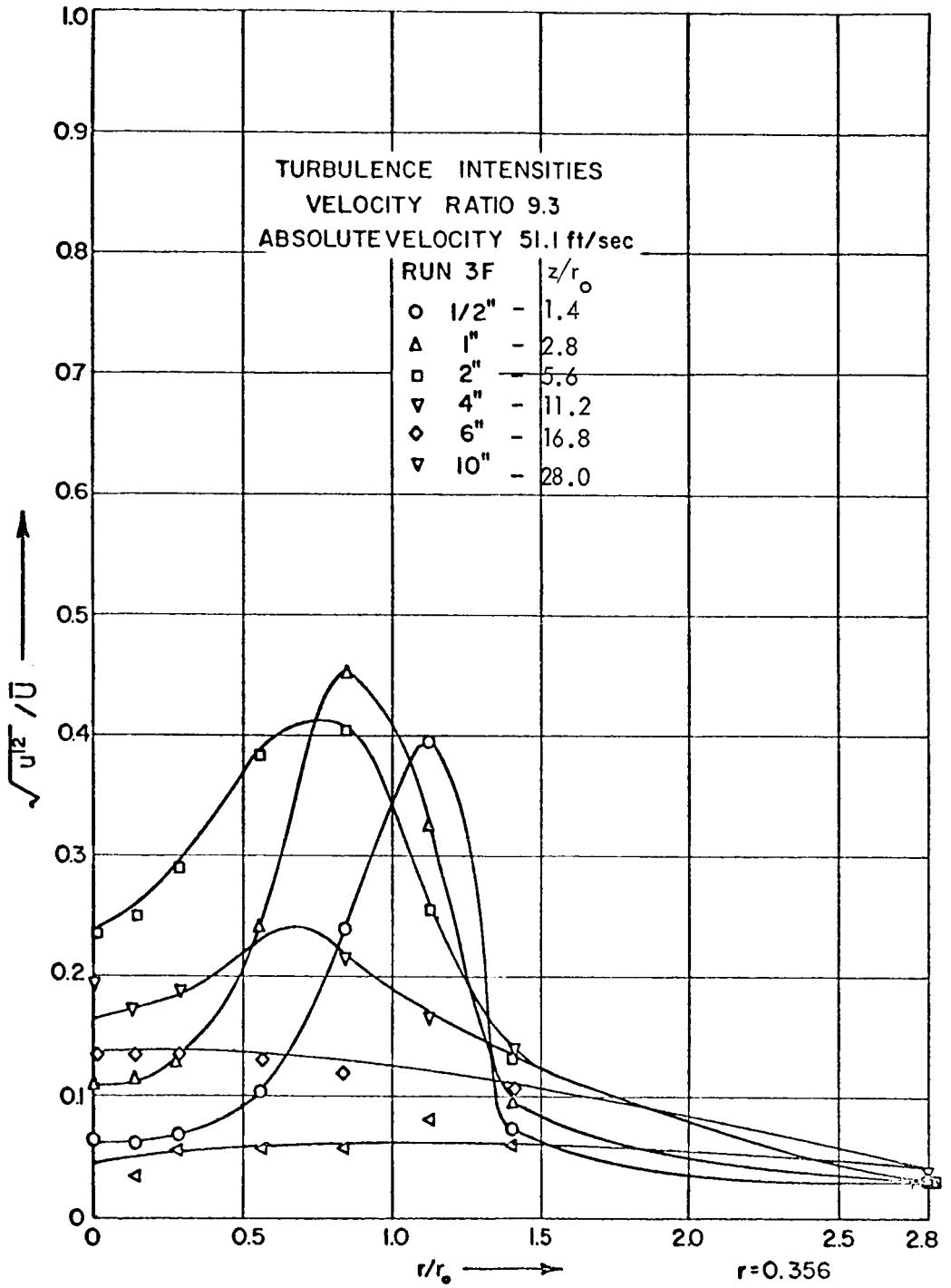

FIGURE V - 2 - 31

CONCENTRATION PROFILES, $\frac{U_o}{U_i} = 9.3$, $\frac{\rho_o}{\rho_i} = 0.25$

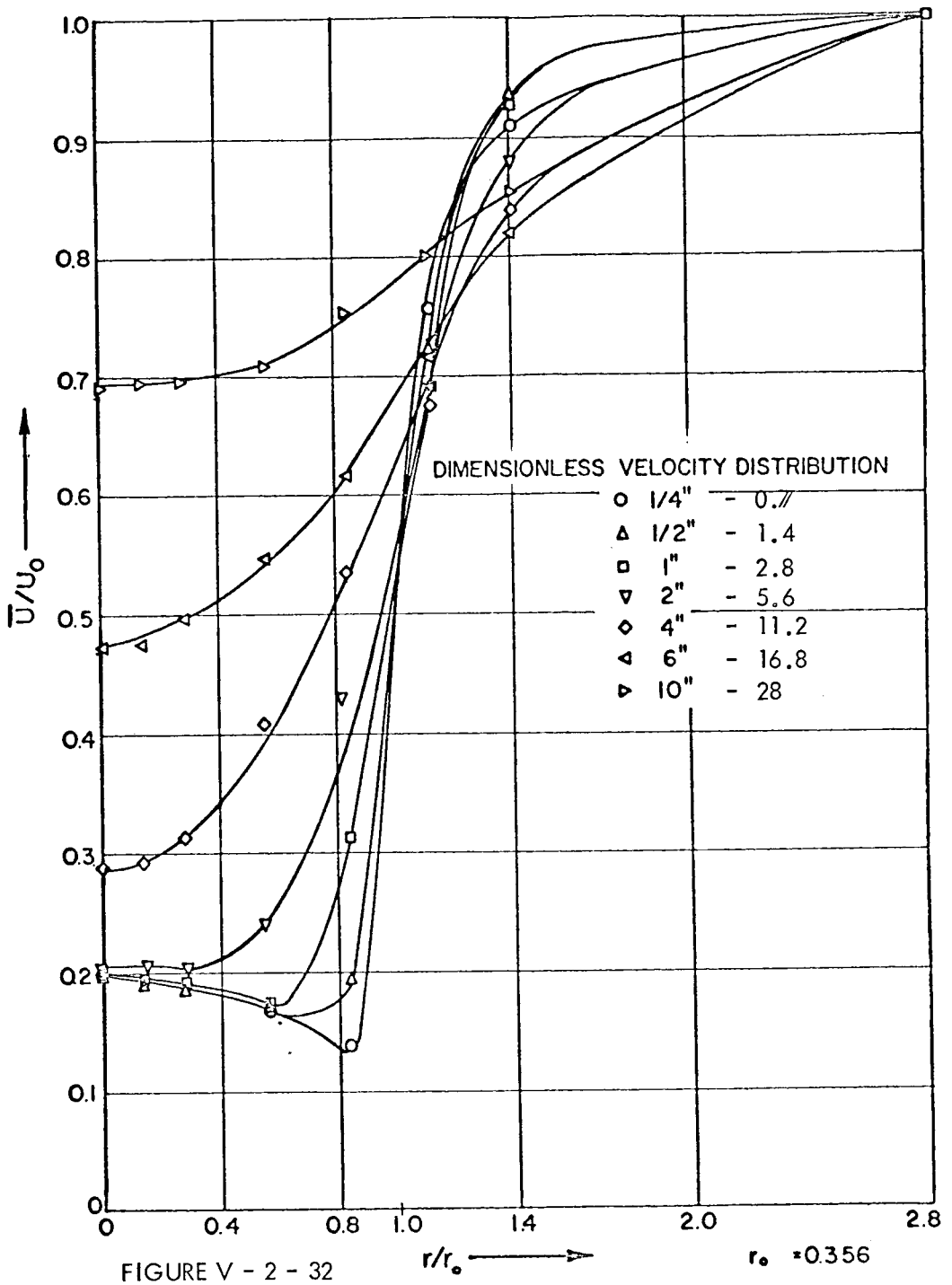

FIGURE V - 2 - 32

DIMENSIONLESS VELOCITY PROFILES, HETEROGENEOUS,

$\frac{U_o}{U_i} = 5.4$, $U_o = 5.4$ ft/sec, $\frac{\rho_o}{\rho_i} = 0.25$

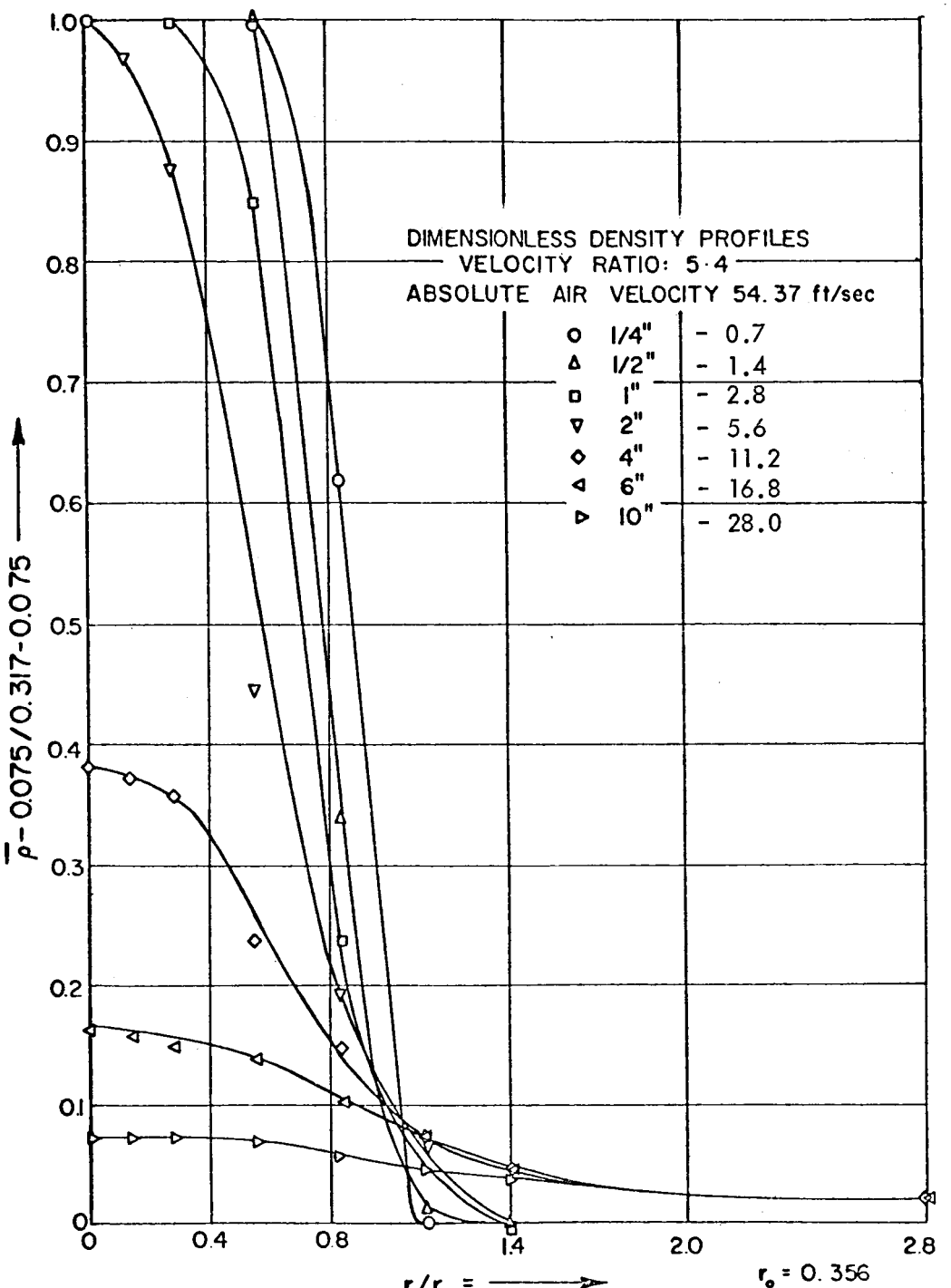

FIGURE V - 2 - 33

CONCENTRATION PROFILES, $\frac{U_o}{U_i} = 5.4$, $\frac{\rho_o}{\rho_i} = 0.25$

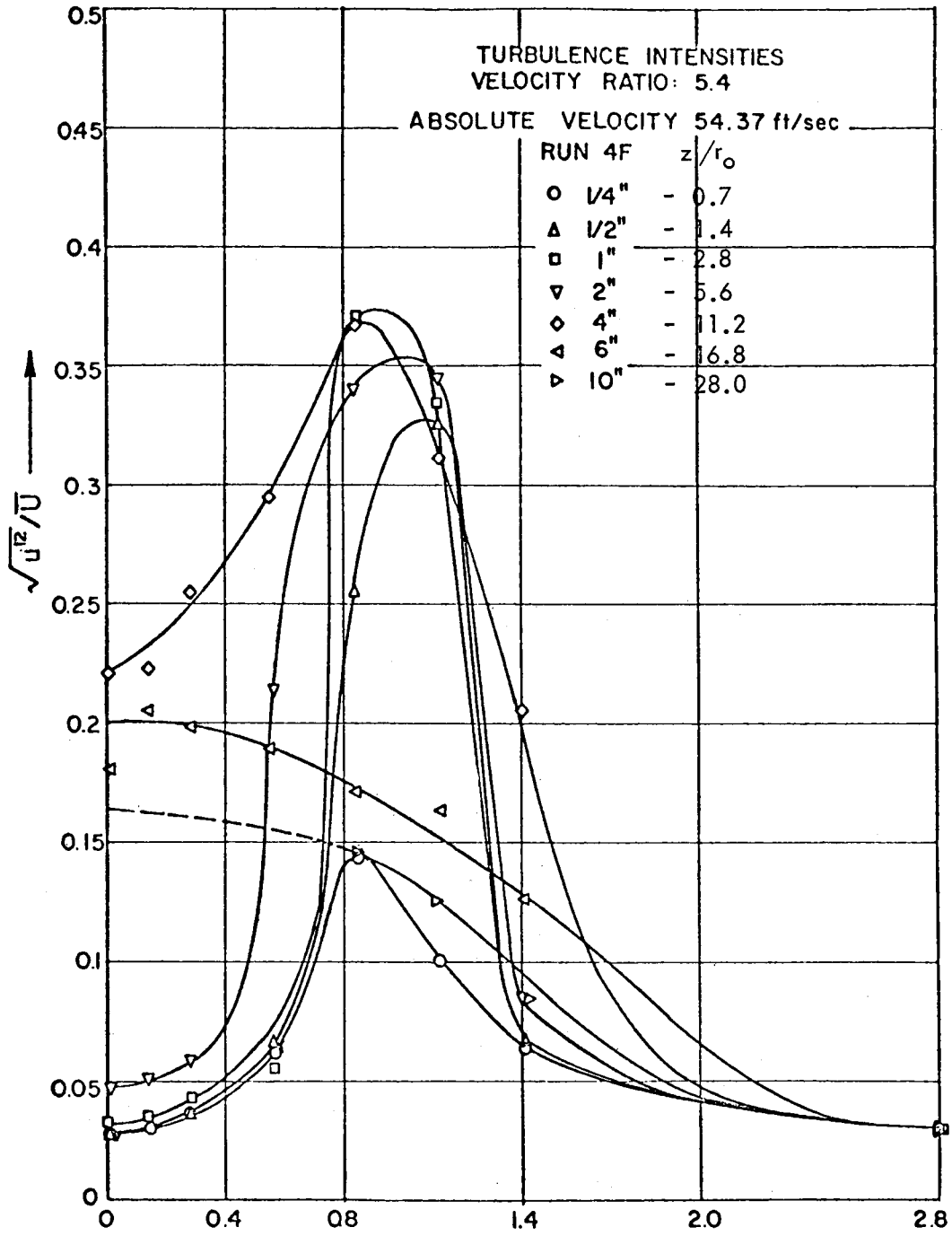

FIGURE V - 2 - 34

VELOCITY TURBULENCE INTENSITY, $\frac{U_o}{U_i} = 5.4 \frac{\rho_o}{\rho_i} = 0.25$

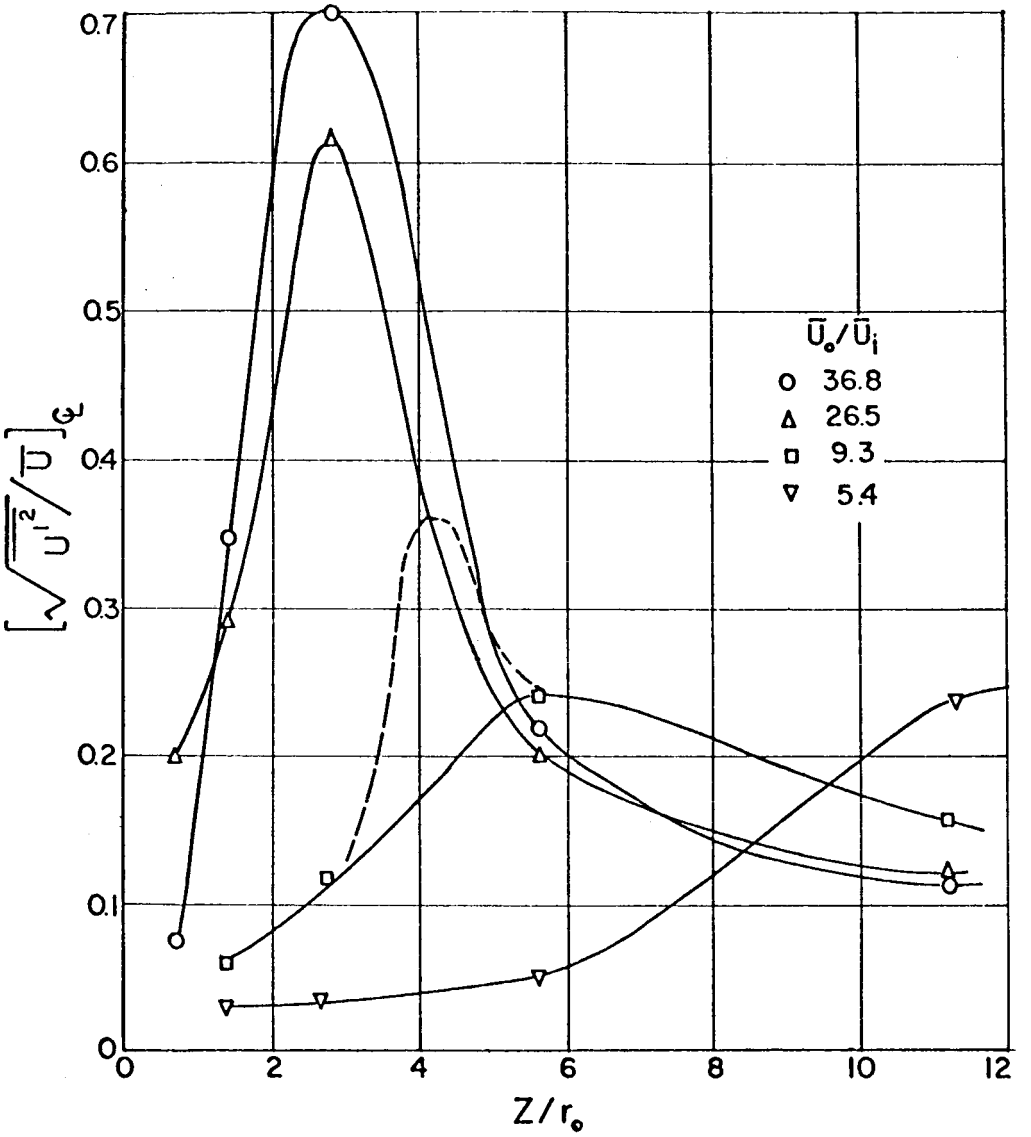

FIGURE V - 2 - 35

CENTERLINE TURBULENCE INTENSITY VERSUS DOWNSTREAM POSITION

VI CONCLUSIONS

Homogeneous System.

1. It has been demonstrated that the problem is one of a combined wake-coaxial flow system. For the wake flow (no inner stream flow), the sudden expansion of the outer stream around the end of the inner stream tube causes large fluctuations at the entrance of and inside of the tube. At high outer stream to inner stream velocity ratios, the wake flow predominates with the fluctuations superimposed on the mean flow in the entrance region. Characteristicly the measured average centerline velocity will decrease from the entrance of the tube, increase to a maximum at $z/r_o = 1.4$, decrease to a minimum at $z/r_o = 2.8$, and then will increase, becoming asymptotic to the free stream value. At velocity ratios $\overline{U}_o / \overline{U}_i \leq 8$ this secondary flow is no longer observed, and the coaxial flow case predominates.

2. The turbulence intensity at the center line was coupled to the secondary flow in the high velocity ratio cases. The intensity exhibited a maximum value at the point where the velocity displayed a minimum valve ($z/r_o = 2.8$). When the mass flow in the inner stream became sufficient to remove the secondary flow, the point of maximum turbulence, on the centerline, moves further downstream .

3. The maximum valves for the spatial turbulence intensities decreased as the velocity ratio was decreased.

4. The wake effects were confined to the region between, $z/r_o = 0$ and $z/r_o = 5.6$ for all velocity ratios.

5. At axial stations downstream of $z/r_o > 5.6$, the velocity profiles fit the

similarity analyses of Tollmien and the cosine or 3/2 power similarity profiles used by Squire and Trouncer and Keuthe.

6. Measured values of the eddy kinematic viscosity ϵ, $\left(\frac{\overline{u'v'}}{\partial \overline{U}/\partial r} \right)$ were essentially constant in the similarity region.

Heterogoneous System

1. For high outer stream to inner stream velocity ratios, the problem is again one of a combined wake-coaxial flow with secondary flow. As in the homogeneous case, the measured centerline velocity decreased from the tube entrance, increased to a maximum at $z/r_o = 1.4$, decreased to a minimum at $z/r_o = 2.8$, before asymptotically approaching the free stream value. This shows the wake predominance for the heterogeneous system for $\overline{U}_o/\overline{U}_i > 9.3$. For a comparable initial velocity ratio, the minimum centerline velocity obtained was lower for the heterogeneous case than for the homogeneous.

2. It was shown that the centerline turbulence intensity for the heterogeneous system exhibited the same characteristic as the homogeneous system of reaching a maximum at $z/r_o = 2.8$, for the cases with secondary flow.

3. For all comparable velocity ratios, it was shown that the heterogeneous system produced larger values of the relative turbulence intensity than the homogeneous system.

4. At axial stations downstream of $z/r_o > 11.2$, universal profile laws were established for both velocity and density. The parameters used in making

the individual profiles fit the universal profile were the half radius with respect to velocity $r_{1/2\ u}$ for the velocity profiles, and the half radius with respect to density $r_{1/2\ \rho}$ for the density profiles.

BIBLIOGRAPHY

1. Prandtl, L. Bericht über Untersuchunger zur ausgebildeten Turbulenz, ZAMM 5, 136 (1925).

2. Taylor, G. I., "The Transport of Vorticity and Heat Through Fluids in Turbulent Motion", Proc. Roy. Soc., (London), A135, 685 (1932).

3. Prandtl, L., "Bemerkung zur Theories der Freien Turbulenz", ZAMM 22, 5 (1942)

4. Reichardt, H., "Gesetzmässigkeiten der Freinen Turbulenz", VDI - Forschungsh, 414 (1951).

5. Görtler, H., "Berechnung von Auggaben der Freien Turbulenz auf Grund eines neuen Naherungsansatzes", ZAMM 22, 5 (1942).

6. Abramovich, G. N., The Theory of Turbulent Jets. M. I. T. Press, 1963.

7. Tollmien, W., "Berechnung turbulenter Ausbreitungsvorgange", ZAMM 6, 458-478 (1926), NACA TM1085 (1945)

8. Trüpel, T., "Über die Einwirkung eines Luftstrahles auf die umgebende Luft", Zeitschrift für das gesammte Turbinenwesen, 5-6 (1915).

9. Zimm, W., "Uber die Stromungsvorgange in Freien Luftstrahl", Forsch. Gebiete Ingenierw, 234 (1921).

10. Syrkin, A. N., and Laykhovskiy, D. N., "Aerodynamics of an Elementary Flame", Soobshch. Tsentr. Nauchn-Issled. Kotloturvinnyi Inst. (1936).

11. Pai, S. I., Fluid Dynamics of Jets, D. van Norstrand Company, Princeton, New Jersey, 1954.

12. Schlichting, H., Boundary Layer Theory 4th ed., Mc Graw-Hill, New York, 1960.

13. Keuthe, A.M., "Investigation of the Turbulent Region Formed by Jets", Journal of Applied Mechanics, Trans. ASME, Vol. 57, 4-87 (1935).

14. Squire, H. B., and Trouncer, J. "Round Jets in a General Stream", Aeronautical Research Committee Technical Report R and M No. 1974, 1944.

15. Torda, T. P., Thompson, W. J. and Genetti, B. K., "Laminar Incompressible Mixing of Two-Dimensional and Axially Symmetric Jets", Proceedings of the Second U. S. Congress of Applied Mechanics, 715 (1954).

16. Kobashi, Y. and Tani, I., "Experimental Studies on Compound Jets", Proceedings of the Second Japan National Congress for Applied Mechanics, 465-468 (1951).

17. Kobashi, Y., "Experimental Studies on Compound Jets", Proceedings of the Second Japan National Congress for Applied Mechanics, 223-236 (1952).

18. Forstall, W. Jr., and Shapiro, A. H., "Momentum and Mass Transfer in Coaxial Jets", Journal of Applied Mechanics, Vol. 17 No. 12, 399-408 (1950)

19. Macynski, J. F. J., "A Round Jet in an Ambient Coaxial Stream, Journal of Fluid Mechanics, Vol. 13, Part 4, 597-608 (1962).

20. Alpinieri, L. J., "An Experimental Investigation of the Turbulent Mixing of Non-Homogeneous Coaxial Jets", Polytechnic Institute of Brooklyn, PIBAL Rept. 789, (1963); "Turbulent Mixing of Coaxial Jets", AIAA Journal, Vol. w, 1560-1568 (1964).

21. Libby, P. A., "Theoretical Analysis of Turbulent Mixing of Reactive Gases with Application to Supersonic Combustion of Hydrogen", ARS Journal 388-396 (1962).

22. Ferri, A., Libby, P. A., and Zakkay, V., "Theoretical and Experimental Investigation of Supersonic Combustion", Third Congress, International Council of the Aeronautical Sciences (Spartan Books Baltimore, Maryland (1964)).

23. Zakkay, V., Krause, E., "The Radial Variation of the Eddy Viscosity in Compressible Turbulent Jet Flows", International Journal of Heat and Mass Transfer, Vol. 8, No. 7, 1047-1050 (1965).

24. Zakkay, V., Krause, E. and Woo, S.D.L., "Turbulent Transport Properties for Axisymmetric Heterogeneous Mixing", AIAA Journal, Vol. 2, No. 11, 1939-1947 (1964).

25. Hinze, J. O., Turbulence, McGraw-Hill Company, (1959).

26. Kramers, H., Phsyca, 12, 61 (1946).

27. King, L. V., Phil. Trans. Roy. Soc. London, 214A, 373 (1914).

28. Corrsin , S., "Extended Applications of Hot Wire Annemometry", NACA TN 1864 , (1949).

29. Thermo Systems Inc. Technical Bulletin No. 4, "Applications of the Heat Flux System in Low Temperature Gases and Liquids.

30. Boehman, L. "Mass and Momentum Transport Properties in Isoenergetic Coaxial Flows", Ph. D. Thesis, Illinois Institute of Technology, (1967).

31. Conger, W. L. "Measurement of Concentration Fluctuations in the Mixing of Two Gases by Hot Wire Anemometer Techniques", Ph. D. Thesis, University of Pennsylvania, (1965).

32. Collis, D. C. and Williams, M. J., "Two-dimensional Convection from Heated Wires t Low Reynolds Numbers", J. Fluid Mechanics, Vol. 6, 357,(1959).

33. Baid, M., "Measurement of Velocity in Gaseous Mixtures", M. S. Thesis, Illinois Institute of Technology, (1967).